Quantum Phase of Bose-Einstein Condensates

JACOB ANDREW DUNNINGHAM

A thesis submitted in partial fulfilment of
the requirements for the degree of
Doctor of Philosophy at the University of Oxford

St John's College
University of Oxford
Hilary Term 2001

Abstract

Quantum Phase of Bose-Einstein Condensates

Jacob Dunningham, St John's College

DPhil thesis, Hilary Term 2001

The quantum phase of a Bose-Einstein condensate has long been a subject fraught with misunderstanding and confusion. In this thesis we provide a consistent description of this phenomenon and, in particular, discuss how phase may be defined, created, manipulated, and controlled.

We begin by describing how it is possible to set up a reference condensate against which the phase of other condensates can be compared. This allows us to think of relative phases as if they were absolute and gives a clear and precise definition to 'the phase of a condensate'. A relative phase may also be established by coupling condensates and we show how this can be controlled. We then extend this model to explain how the phase along a chain of coupled condensates can lock naturally without the need for any measurements.

The second part of the thesis deals primarily with the link between entanglement and phase. We show that, in general, the more entangled a state is, the better its phase resolution. This leads us to consider schemes by which maximally entangled states may be able to be created since these should give the best practical advantages over their classical counterparts. We consider two such states: a number correlated pair of condensates and a Schrödinger cat state. Both schemes are shown to be remarkably robust to loss.

A comparison of the merits of these two states, as the inputs to an interferometer, reveals very different behaviours. In particular, the number correlated state performs significantly better than the cat state in the presence of loss, which means that it might be useful in interferometry and frequency standard schemes where phase resolution is of the utmost importance.

Finally, we propose a scheme for concentrating the entanglement between condensates, which is an important step in quantum communication protocols. This, along with the ability to manipulate phase and entanglement, suggests that the future for condensates holds not only academic interest but great potential for practical applications.

Sometimes a scream is better than a thesis

Ralph Waldo Emerson

ACKNOWLEDGEMENTS

I have had a wonderful time in Oxford and this has been largely due to the kindness of many people. Firstly, I would like to thank Keith Burnett for providing me with a fascinating problem, for his inspiring insight whenever I was stuck, and for his continual encouragement and generosity in many ways. But perhaps, above all, I thank him for creating such a fun and friendly environment to work in.

I am very grateful to all the members of the Burnett theory group: David, Sam, Stephen, Martin, Matt, Mark, David, Thomas, Vicki, Thorsten, David, Alex, Peter, and Karen for many invigorating discussions and help with countless matters where my understanding fell short of the mark. It has been a great pleasure and privilege to be part of such a talented and fun group. Special thanks are due to Matt for patiently dealing with my computing problems and for generously providing me with a quiet place to write up. Also to Martin who, though many others came and went, steadfastly put up with sharing an office with me.

I would like to thank Mark Edwards for being the first to spot the phenomenon of number squeezing that is discussed in Chapter 6 and for generously allowing me to work on it. I have benefited from many helpful discussions with members of the experimental groups and the CQC, especially Vlatko Vedral, Sougato Bose, and Leah Henderson, with whom I collaborated for Chapter 9.

This work would not have been possible without the generous financial support of the British Council through the Commonwealth Scholarship scheme, the L. B. Wood trust, and St John's College. I am also grateful to the Clarendon Laboratory for use of their facilities.

I would like to thank Catherine for her selflessness and encouragement and for making sure I ate properly, especially during the write up stage. I am always very aware of the many opportunities my family have given me, and of their love and support in countless ways. Thanks also for providing a warm retreat from the Oxford winter!

Finally, I dedicate this thesis to my brother Sam, who always showed great interest in my work.

Contents

CHAPTER 1

BOSE-EINSTEIN CONDENSATION

1.1 Introduction

In 1924, Bose derived the Planck distribution by developing a new statistical description of a collection of photons as identical particles [1]. The following year, Einstein extended this description to ideal gases of material bosons [2] and realised that when the particle number is conserved, these statistics could force a macroscopic number of the particles to occupy a single quantum state. This effect, now known as Bose-Einstein condensation (BEC), is one of the most startling predictions of quantum-statistical mechanics.

In the decade following its prediction, the properties of BEC were extensively studied, but it was still not clear whether the effect was real. Einstein himself commented, "The theory is pretty, but is there also some truth to it?". It was London who first found this 'truth' when in 1938 he made the ground-breaking step of conceptually linking the properties of liquid ^{4}He with BEC [3, 4]. Since then BEC has been widely associated with the macroscopic quantum phenomena of superfluidity and superconductivity [5]. The theoretical description of both these systems, however, is clouded by the presence of strong interactions and so there has been intense interest in achieving BEC in a weakly interacting gas, since this would allow for a detailed quantitative comparison with theory.

The quest began in the 1970s with work on spin polarised hydrogen [6, 7], but proved to be very difficult. Direct experimental observation of BEC in a weakly interacting system continued to elude experimentalists up until 1995, when a remarkable series of experiments was carried out in dilute vapours of rubidium

[8, 9], lithium [10], and sodium [11]. This marked the end of a search that spanned two decades and, more excitingly, heralded a golden era in coherent matter wave physics. Since these first experiments, numerous groups around the world have observed BEC, techniques in cooling and trapping atoms continue to be improved, and many exciting new phenomena have been revealed. The spectacular success of these experiments has also triggered a renaissance in theoretical interest.

In this chapter we develop the subject of Bose-Einstein condensation, we summarise some of the main results, provide a brief discussion of how they are made, and conclude with an overview of this thesis.

1.2 BEC in an Ideal Gas

The fact that identical particles are fundamentally indistinguishable has a profound effect on their statistical properties. If particles cannot be distinguished, the exchange of two of them in a many body system must leave all observables unchanged. This means that such a process can at most introduce an overall global phase shift to the wave function. Furthermore, repeating the exchange must return the original state, which means that the process of swapping two particles can only introduce a phase factor of either $+1$ or -1.

All fundamental particles can therefore be divided into two categories depending on their behaviour under the exchange of particles. Particles for which the wave function is antisymmetric (i.e. the phase factor is -1) are called *fermions*, and particles for which the wave function is symmetric are called *bosons*. Remarkably, this property is related by the spin statistics theorem of quantum field theory to the intrinsic angular momentum or spin of the particles [12]. All particles with a spin that is an integer multiple of the reduced Planck constant, $\hbar$, are bosons, and all particles with half integer units of spin are fermions.

This classification of particles is not merely book-keeping: the simple fact that particles have wave functions that are either symmetric or antisymmetric gives rise to very different behaviours. A direct consequence of this for fermions, is the Pauli Exclusion Principle which states that no two particles can occupy identical quantum states. Bosons, on the other hand, are not restrained by the same law and, in fact, like to occupy the same state. Under certain specific conditions all the bosons of a system may crowd into a single state and form a Bose-Einstein condensate.

The formation of a BEC is closely related to laser action. In a laser, a macro-

scopic population is built up in a single mode of the radiation field due to stimulated emissions. Photons are more likely to be emitted into modes that already have a large population. A similar stimulated transition takes place for bosons. We can see this by considering the transition rate for the scattering of two bosons,

$$\Gamma_{(1,2)\to(3,4)} \propto N_1 N_2 (1+N_3)(1+N_4). \tag{1.1}$$

This depends on the population not only of the initial states, $N_{1,2}$, but also of the final states, $N_{3,4}$, and so a boson is more likely to end up in a state that is already occupied. For classical particles, the transition rate would be completely independent of the populations of the final modes. The so-called Bose enhancement factors, $(1+N_3)(1+N_4)$, play a critical role in the formation of a condensate [13, 14] since they 'coax' atoms into the same state.

The equilibrium distribution for a collection of bosons can be found by applying detailed balance to the scattering rates given in (1.1). The result is

$$N_i(\epsilon_i, T) = \frac{1}{e^{(\epsilon_i-\mu)/k_B T} - 1}, \tag{1.2}$$

where $N_i(\epsilon_i, T)$ is the population of a state with energy ϵ_i at temperature, T, k_B is Boltzmann's constant, and μ is the chemical potential. The chemical potential is the energy required to add a particle to the system while keeping the entropy and volume fixed. It is determined by the constraint that the total number of atoms in the system is fixed,

$$N = \sum_{\epsilon_i} \frac{1}{e^{(\epsilon_i-\mu)/k_B T} - 1}. \tag{1.3}$$

From Equation (1.2), we see that μ must be smaller than the lowest energy, ϵ_0, otherwise the population of that energy level would be negative. If we set the ground state to be $\epsilon_0 = 0$, we require that $\mu < 0$.

For homogeneous systems, the spacing between energy levels scales inversely with the volume of the system, V. If V is large, the energy spacing is small and the distribution varies slowly between energy levels, which allows us to replace the sum in (1.3) with an integral. For the lowest energy level, this may not be a good approximation, since we see from (1.2) that as $\mu \to 0$, the population of the ground state can become macroscopically large. Furthermore, this level is actually neglected by the density of states (see Equation (1.5)) and so this is not a good description. To overcome this, it is common to remove the lowest energy level from

the integral and to treat it separately. This allows us to write (1.3) as

$$N = N_0 + \int \mathrm{d}\epsilon \; g(\epsilon) N_i(\epsilon_i, T), \tag{1.4}$$

where $N_0 = \left[\mathrm{e}^{-\mu/k_B T} - 1\right]^{-1}$ is the condensate population and the integral gives the total number of atoms in excited states, N_{ex}. The density of states, $g(\epsilon)$, for free particles in 3-dimensions is [15],

$$g(\epsilon) = \frac{V}{4\pi^2}\left(\frac{2m}{\hbar^2}\right)^{3/2} \epsilon^{1/2}. \tag{1.5}$$

The population of each energy level, given by (1.2), increases with an increase of μ or T. This means that, in order to keep the total number of particles in the system constant, a decrease in temperature must be accompanied by an increase in μ. However, μ must be negative, which gives an upper limit to the number of atoms that can be in the excited states of the system. This can be found by evaluating the integral in (1.4) with $\mu = 0$, and gives

$$N_{ex}^{max} = V\zeta(3/2)\left(\frac{mk_BT}{2\pi\hbar^2}\right)^{3/2} \tag{1.6}$$

where $\zeta(x)$ is the Riemann zeta function [16] and $\zeta(3/2) \approx 2.612$.

As the temperature is decreased, μ approaches zero and the number of atoms that can be populated in the excited states decreases. Eventually we will reach a point where the maximum number of atoms that can be in excited states is equal to the total number of atoms in the system. If we were to cool further, the only place for atoms to go is into the ground state, which leads to a macroscopic build up of population in this mode. We can calculate the so-called critical temperature, T_c, at which this transition takes place, simply by setting $N_{ex}^{max} = N$ in (1.6) and solving for temperature. This gives,

$$T_c = \frac{2\pi\hbar^2}{mk_B}\left(\frac{N}{\zeta(3/2)V}\right)^{2/3}. \tag{1.7}$$

The proportion of atoms in the condensate mode for $T < T_c$ follows directly, and is given by

$$\frac{N_0}{N} = 1 - \left(\frac{T}{T_c}\right)^{3/2}. \tag{1.8}$$

A useful way to reformulate the condition for BEC is in terms of the length

scales of the system: the interparticle spacing, $(N/V)^{1/3}$ and the de Broglie wavelength of the particles, λ_{dB}, defined by

$$\lambda_{dB} = \left(\frac{2\pi\hbar^2}{mk_BT}\right)^{1/2}. \tag{1.9}$$

Substituting this into (1.7) allows us to rewrite $T \leq T_c$ as

$$\frac{N}{V}\lambda_{dB}^3 \geq 2.612, \tag{1.10}$$

which is the most commonly quoted criterion for BEC. It tells us that BEC occurs when the de Broglie wavelength of the particles is comparable to their separation, or equivalently, when there is a significant overlap of the de Broglie wavelengths of the particles.

So far, we have discussed only the case of an homogeneous condensate. All current experiments, however, are performed on trapped condensates which are spatially localised and so have inhomogeneous densities. The traps used in experiments are very well approximated by harmonic potentials. For noninteracting atoms in a spherically symmetric harmonic trap with angular frequency ω, the critical temperature is given - in the thermodynamic limit - by [17]

$$\frac{k_BT_c}{\hbar\omega} = \left(\frac{N}{\zeta(3)}\right)^{1/3}, \tag{1.11}$$

where $\zeta(3) \approx 1.202$. Since N can be very large, we see that the energy at the critical temperature may be much larger than the spacing between energy levels of the system. This highlights an important point about the nature of the transition: BEC does occur because the particles are energetically forced to occupy the lowest energy state and simply don't have the energy to be in higher levels. Rather they are encouraged into it by the Bose enhancement factors, in much the same way that stimulated transitions take place in a laser. For $T < T_c$, the number of condensate atoms is given by,

$$\frac{N_0}{N} = 1 - \left(\frac{T}{T_c}\right)^3. \tag{1.12}$$

This has the same form as for the homogeneous case (1.8), but differs in the value of the exponent.

1.3 Interacting gases

Although the theory of BEC does not rely on interactions, they form an important part of any realistic system. Bogoliubov showed in 1947 [18] how interactions do not significantly alter a BEC in a weakly interacting gas and so can be perturbatively included in the ideal gas theory. The advantage of such a system is that it allows for an accurate quantitative comparison between experiment and theory.

The measure of diluteness of the gas is expressed as the ratio of the scattering length, a, to the mean interparticle separation, r, a/r. For ratios near 1, as is the case for liquid ^{4}He, the simple theory of BEC fails. The interactions are so strong in this case that it is estimated that fewer than 10% of the atoms are in the condensate [19]. Remarkably, however, the observed transition temperature of $T_c \sim 2.2$K is very close to the temperature calculated by assuming that it is an ideal gas BEC, $T_c \sim 3.2$K.

The conditions for BEC in a weakly interacting dilute gas can be written as

$$\lambda_{dB}/r > 1 \qquad \text{and} \qquad a/r \ll 1. \tag{1.13}$$

The first condition is simply a reformulation of the BEC criterion (1.10) and the second inequality is the diluteness condition. These can be combined to write, $a \ll r < \lambda_{dB}$. For current experiments in alkali gases $a/r \sim 0.01$, and so these systems can justifiably be considered to be weakly interacting.

Although the interactions are weak, they can have a major impact on the behaviour of the system. For example, an homogeneous condensate with attractive interactions is unstable whereas one with repulsive interactions is stable. The collective excitation spectrum of an interacting gas also differs significantly from that of a non-interacting ideal gas. The effect of the interactions can be seen from energetic considerations: even for condensates of only a few thousand atoms, the total energy of the condensate is made up of comparable contributions from the trap potential and the interactions.

Throughout this thesis we consider only condensates at $T = 0$. However, the effects of finite temperature on the excitation spectrum has been an active and interesting area of research [20, 21, 22, 23]. At zero temperature, a condensate is a collection of atoms all occupying the same quantum state. The many-body wave function of such a state can be written simply as the product of N single particle wave functions. For a noninteracting system, this wave function is given by the solution of the Schrödinger equation.

When interactions are present, however, this wave function is changed. In this case, each atoms feels an additional potential due to the presence of all the other atoms. This potential is due to the local atomic density and gives rise to a nonlinear term in the Schrödinger equation. The resulting equation, called the nonlinear Schrödinger equation or Gross-Pitaevskii (GP) equation is [24],

$$i\hbar\frac{\partial\psi}{\partial\psi} = H_0\,\psi(\mathbf{r},t) + N_0U_0\,|\psi(\mathbf{r},t)|^2\,\psi(\mathbf{r},t), \tag{1.14}$$

where H_0 includes the kinetic energy and the trap potential. The second term is the nonlinearity due to interactions and the coefficient U_0 is given by $U_0 = 4\pi\hbar^2 a/m$, where m is the mass of a single condensate atom and a is the s-wave scattering length.

The potential can be written in this particularly simple form because the gas is extremely cold and dilute [15, 25]. The diluteness means that we need consider only binary scattering and since the gas is so cold, we can neglect all but the lowest order (s-wave) scattering events. The de Broglie wavelength of the atoms is enormous, compared to the range of the interactions, which allows us to model the interactions with a hard sphere potential using the method of pseudo potentials [15]. This greatly simplifies calculations for interacting gases.

The Gross-Pitaevskii equation has proven to be one of the most useful tools in BEC theory. It has been widely used, with great success, to investigate the properties and dynamics of BECs.

1.4 Experimental overview

The first observation of BEC in a weakly interacting dilute gas was achieved with ^{87}Rb atoms at JILA in 1995 [8]. This was rapidly followed by reports of BEC in ^{7}Li at Rice University [10] and in ^{23}Na at MIT [11]. Since then there has been an explosion of interest in this field of research and currently 22 institutions around the world have successfully observed BEC.

Typical experiments in Na and Rb result in condensates containing a few million atoms with number densities around 10^{14} cm^{-3}, however, these parameters vary widely. For example, ^{7}Li has attractive interactions which sets an upper limit to the number of atoms that the condensate can support [26, 27]. For current experimental parameters, the maximum number of atoms in a ^{7}Li condensate is around 1000. By contrast, condensates in spin polarised hydrogen containing 10^9

atoms have been observed [28].

All atomic condensates, so far, have been produced by a combination of laser cooling and evaporative cooling in magnetic traps. The atoms are laser cooled before being trapped and compressed in a magnet-optical trap (MOT) and then evaporatively cooled. A good review of these techniques is given by [29, 30]. In laser cooling, atoms are bombarded with photons from counter-propagating laser beams, which are red-detuned from an atomic resonance. Due to the Doppler effect, the laser that opposes each atom's motion with be shifted towards the resonance and atoms will be more likely to absorb a photon from this laser than the other one. Atoms will therefore preferentially get momentum kicks which slow them down. Optical molasses is the term given to this Doppler cooling scheme when it is extended to three dimensions with three pairs of counter-propagating beams in orthogonal directions. No matter what direction an atom moves in this 'molasses' it feels a force opposing its motion. The cooling stops when the atoms, because of the change in velocity, are no longer in resonance with the laser. This can be overcome by chirping the laser frequency or by tuning the atomic frequency with magnetic fields. Optical molasses was first demonstrated in 1985 with sodium atoms [31].

At the end of the laser cooling process, atoms are typically cooled to temperatures of a few millionths of a degree, however the phase space density is still as many as six orders of magnitude smaller than that required for BEC. Evaporative cooling allows this density limit to be surpassed and can achieve sufficiently high phase space densities for BEC. It was first developed by Hess in 1986 as a method for cooling atomic hydrogen [32, 33] and relies on removing the high-energy component of the thermal distribution of atoms from the trap. The evaporated atoms take away more than the average energy, so that when the remaining atoms rethermalise (by undergoing elastic collisions), the temperature of the vapour decreases. One can increase the density of the remaining atoms even though the total number of atoms decreases. The essential condition for evaporative cooling is a slow loss rate from the trap compared to the rethermalisation rate. Evaporative cooling typically provides six orders of magnitude increase in phase space density at a cost of a factor of 1000 reduction in the number of atoms.

Pritchard and Walraven suggested that evaporation could be performed conveniently if the rim of the trap was defined by an RF-resonance condition rather than simply by the tomography of the magnetic field [34, 35]. The idea is to use an RF transition between m_F sub-states to remove atoms from the magnetic trap

at a distance from the trap centre defined by the Zeeman shift of the transition associated with the trapping field.

The RF radiation flips the atomic spins and, as a result, the attractive trapping force turns into a repulsive force and expels the atoms from the trap. The scheme is energy-selective because the resonance frequency is proportional to the magnetic field strength, and therefore to the potential energy of the atoms.

The MIT and JILA groups were the first to combine laser cooling with evaporative cooling allowing evaporative cooling to be extended to alkali atoms. This led directly to the first experimental observations of BEC. Since then, numerous groups have implemented RF evaporative cooling of magnetically trapped atomic vapours.

Evaporation in a time-averaged orbiting potential (TOP) trap is more complicated than for a static (e.g. Ioffe-Pritchard) trap due to the rotating magnetic field. In a TOP trap, in addition to RF-induced transitions, one can also induce Majorana spin-flips using the zero magnetic field point of the rotating quadrupole trap. Near the zero point, the Lamor frequency becomes sufficiently small that the magnetic moment of the atoms can flip, ejecting the atoms from the trap. The zero point orbits the atomic sample on a path which is known as the circle of death.

For a lossless trap, in which atoms are removed only by evaporation, the cooling efficiency can be made arbitrarily large by truncating further out on the tail of the thermal distribution. In real traps, however, there are loss mechanisms. If the truncation energy is made too large, the slow increase in phase space density will be overwhelmed by the decrease due to losses. Efficient cooling therefore requires a favourable ratio of elastic collisions which enable rethermalisation, to inelastic collisions which lead to trap loss and heating. At the energies of trapped atoms, the elastic collision rate is given by $\gamma_e = nv\sigma_a$, where n and v are respectively the density and mean relative velocity of the atoms, and σ_a is the s-wave collision cross-section. As evaporation proceeds, the mean velocity decreases but the density increases. Collisional rethermalistion can take seconds due to the fact that the gas is extremely dilute.

The dominant inelastic process for alkali atoms is collisions with the background gas. When such a collision takes place, the most likely outcome is that both atoms are cleanly ejected from the trap without further collisions. This process is proportional to the background gas pressure and experimentalists go to great lengths to achieve an ultra-high vacuum environment to minimise these effects. There are two common methods used in BEC labs for achieving a large laser

cooled sample in an extreme vacuum: an atomic beam and Zeeman slower, or a double MOT and push beam setup.

In addition to background gas collisions, there is also loss from dipolar relaxation (a 2-body process) and 3-body recombination [36]. These inelastic collisions are particularly troublesome since they give rise to loss at the most dense and lowest energy part of the atomic sample, and so are more significant in a condensate because the density is much higher than in a thermal cloud. At low energies, the dipolar relaxation rate, γ_{2b} and the 3-body recombination rate, γ_{3b} are independent of collisional energy, and we can write

$$\gamma_{3b} = \lambda n^2 \qquad \text{and} \qquad \gamma_{2b} = \beta n, \tag{1.15}$$

where λ and β are the respective rate constants.

For good evaporation, one requires the elastic collision rate to be greater than these inelastic collision rates. By serendipity, this is precisely the case for ^{87}Rb and the lower hyperfine level of ^{23}Na. It is this happy coincidence that has led to a prevalence of Bose condensates in these species in laboratories around the world. With other atoms, the cold collision properties are in general not so favourable and evaporative cooling has proved to be a lot more difficult.

1.5 Overview of thesis

In this thesis, we are interested primarily in the quantum phase of condensates and its connection with entanglement. We begin in Chapter 2 with an overview of phase and discuss the difference between the phase coherence of a condensate and the phase between two condensates. We show that for condensates produced in the laboratory, only *relative* phase is a meaningful concept and show that this is due to entanglement between two condensates. We discuss how phase may be created and measured and set some important foundations for the remainder of the thesis.

Everything presented from Chapter 3 onwards represents original research that I have carried out during the course of my doctorate. In Chapter 3 we show that it is possible to define a consistent phase standard - a reference against which the phase of other condensates may be compared. This gives a precise definition to what we mean by the phase of a condensate and allows us to give phase a pseudo-absolute sense.

In Chapter 4 we investigate the phase between coupled condensates. We begin by studying the phase relationship between a condensate and a component that has been coupled out. We show that the phase relationship can be controlled by varying the parameters of the transfer process. We also consider phase locking along a chain of condensates. We show that measurements are not necessary to create phase and that it can arise naturally due to processes such as interparticle interactions and dissipation.

Next we investigate the resolution with which the relative phase between two condensates can be defined. In particular, we show that measurement induced phase results in a state with shot noise limited phase resolution. However, if two number correlated condensates are Raman coupled, Heisenberg limited phase resolution can be achieved. This is the best possible phase resolution allowed for by the Uncertainty Principle and suggests that such a state may be a valuable quantum resource.

The second half of the thesis considers the link between phase and entanglement. In particular, we consider experimentally feasible methods of creating specific entanglements and then compare their merits. In Chapter 6, we outline a technique for creating number correlated pairs of BECs. These are an important resource for achieving states with phase defined to the Heisenberg limit. The technique is based on coupling condensates with the right balance between the coupling strength and the interparticle interactions.

In Chapter 7 we consider how Schrödinger cat states may be generated in condensates by manipulating their phases. We present two schemes: one is a simple scheme based on interferometry and the other is a more complex scheme that has the advantage of being relatively robust to loss during the creation process. Cat states have long been intriguing to quantum physicists and the generation of them in atomic systems would provide a valuable tool for studying measurement and entanglement.

Both cat states and number correlated states give rise to phases that have a Heisenberg limited resolution. This means that each entangled state would be equally good (and the best possible) in an interferometer. In Chapter 8 we compare the merits of these two states in an interferometer both with and without loss present. We show that while they have the same performance in the lossless case, they behave very differently when there is loss. The cat state is completely destroyed by the loss of a single atom, whereas the number correlated state is only gently affected by loss. We conclude that the number correlated state is the max-

imally entangled one and discuss how it may be used to create a more accurate clock or frequency standard.

Finally, in Chapter 9, we discuss how the techniques we have developed may be used in an entanglement concentration scheme for BECs. This chapter is a little separate from the general flow of the thesis, but it highlights the link between phase and entanglement. It also suggests that BECs may become an important tool in quantum information. In Chapter 10 we conclude with an overview of our results and suggest some interesting possibilities for further research.

CHAPTER 2

THE QUANTUM PHASE OF A BOSE CONDENSATE

A central problem in the theory of matter wave sources is whether we can attribute a definite quantum phase to a condensed gas. Can such a phase be defined in a manner that everyone will agree on? Is it more than a convenient fiction, or an unwarranted extrapolation of the ideas of spontaneous symmetry breaking from infinite systems to the finite condensates produced in the laboratory?

These issues and many related ones have caused great discussion and confusion and make Bose condensates an interesting environment for investigating the subtle concept of phase. In this chapter, we develop this subject and discuss some of the important issues that it raises. We begin with a discussion of the phase coherence of a condensate before investigating how coherence can arise between two distinct condensates. We discuss the link between absolute and relative phase and the circumstances under which each is meaningful, and conclude with a summary of the measures that we will use to quantify phase throughout this thesis.

2.1 Phase coherence

Long range phase coherence is perhaps the key defining feature of a Bose condensate. We can understand what this is with an operational definition of a coherence measurement. Suppose we were to take atoms from two particular spatial points in an atomic cloud, and allow them to fall onto a detector in such a way that we could not determine which point a given atom had come from. The amplitudes of

atoms arriving from the two points would interfere and so the number of atoms detected would be sensitive to the difference in their local quantum phases. A condensate differs fundamentally from a cloud of cold atoms in this regard since the relative phase in a condensate is completely predictable. This means that the position of the interference fringes between any two points of a condensate can be known in advance. This is what is meant by the coherence of a condensate.

Anderson demonstrated this result by considering a box containing a stationary condensate of N free bosons [37, 38]. He showed that, if we imagine dividing this box up into m cells of equal size, the system cannot be treated as a collection of cells each containing a condensate of N/m atoms. This model fails because it does not account for the phase coherence between the cells.

Another way to show this is to consider the density correlation between any two spatial points in a condensate. If we expand the field operator at point $\mathbf{r}$, $\psi(\mathbf{r})$, in terms of the annihilation operators for the single particle states of momentum $\mathbf{k}$, $a_{\mathbf{k}}$, the correlation function can be written as,

$$\langle \psi^\dagger(\mathbf{r})\psi(\mathbf{r}')\rangle = \frac{1}{V}\langle a_0^\dagger a_0\rangle + \int \frac{\mathrm{d}^3k}{(2\pi)^3}\, \mathrm{e}^{i\mathbf{k}.(\mathbf{r}-\mathbf{r}')}\langle a_{\mathbf{k}}^\dagger a_{\mathbf{k}}\rangle, \tag{2.1}$$

where we have removed the condensate mode from the integral as in Chapter 1. For large spatial separations, $|\mathbf{r}-\mathbf{r}'| \to \infty$, we see that the contribution from the second term in (2.1) vanishes and the correlation between the two points is given by the density of particles in the condensate mode. This means that the long range coherence vanishes for noncondensed gases, but acquires a finite value, ρ_0, when a condensate is present. This result can be reformulated as the following general definition of Bose condensation,

$$\langle \psi^\dagger(\mathbf{r})\psi(\mathbf{r}')\rangle \longrightarrow \rho_0 \qquad \text{for } |\mathbf{r}-\mathbf{r}'| \longrightarrow \infty. \tag{2.2}$$

The phase coherence of a condensate has been compellingly demonstrated in experiments performed at MIT [39] and Munich [40]. In the Munich experiment, atoms were coupled out of two spatially distinct positions, $\mathbf{r}$ and $\mathbf{r}'$, of a single trapped condensate in much the same way as our operational definition described above. Falling under gravity the two beams of output-coupled atoms were allowed to overlap, and atoms were detected. The appearance of an spatial interference pattern in the number of detected atoms proved that $\mathbf{r}$ and $\mathbf{r}'$ were phase coherent. The experiment was repeated for different temperatures and showed that the

visibility of the interference pattern decreased with an increase in temperature. Above the critical temperature, $T > T_C$, the interference completely vanished showing that phase coherence is a property of Bose condensates and not simply of cold atoms.

In analogy with (2.2), Penrose and Onsager [19] proposed the following general criterion for Bose condensation, which embodies the concept of phase coherence,

$$\langle \psi^\dagger(\mathbf{r})\psi(\mathbf{r}')\rangle \longrightarrow \langle \psi(\mathbf{r})\rangle^* \langle \psi(\mathbf{r}')\rangle, \qquad \text{for } |\mathbf{r}-\mathbf{r}'| \to \infty, \tag{2.3}$$

where

$$\langle \psi(\mathbf{r})\rangle = \sqrt{\rho(\mathbf{r})}\, \mathrm{e}^{-i\theta}. \tag{2.4}$$

This formalism introduces the concept of broken symmetry whereby the ensemble average of the Bose mode is assigned a finite mean amplitude.

This formalism is both convenient and useful as evidenced by the great success of mean-field theories in investigating the properties of Bose condensates. However, its form can be misleading and we must be careful with its interpretation. In particular, we should not interpret this to mean that the condensate has an absolute phase, as we shall show in the next section.

2.2 Phase symmetry

The question of whether a condensate has an overall phase has caused a great deal of discussion. It is distinct from the question in the previous section of whether two points within a condensate have a predictable phase relationship.

For this investigation, it is common in the literature to adopt the Ginzburg-Landau approach for studying the qualitative nature of the Bose transition. This involves introducing a local order parameter, $\phi(\mathbf{r})$, which is a expectation value of $\psi(\mathbf{r})$. This means that $\phi(\mathbf{r})$ is a complex number and implicitly assumes that the condensate has an overall phase. We shall see how this arbitrary phase is eliminated.

The Landau free energy functional of this system can be written in terms of the order parameter as [15]

$$E[\phi] = \int_{-\infty}^{\infty} d\mathbf{r} \left(\frac{\hbar}{2m} |\nabla\phi|^2 - \mu|\phi|^2 + U|\phi|^4 \right), \tag{2.5}$$

where U is strength of the interactions between atoms, μ can be treated simply

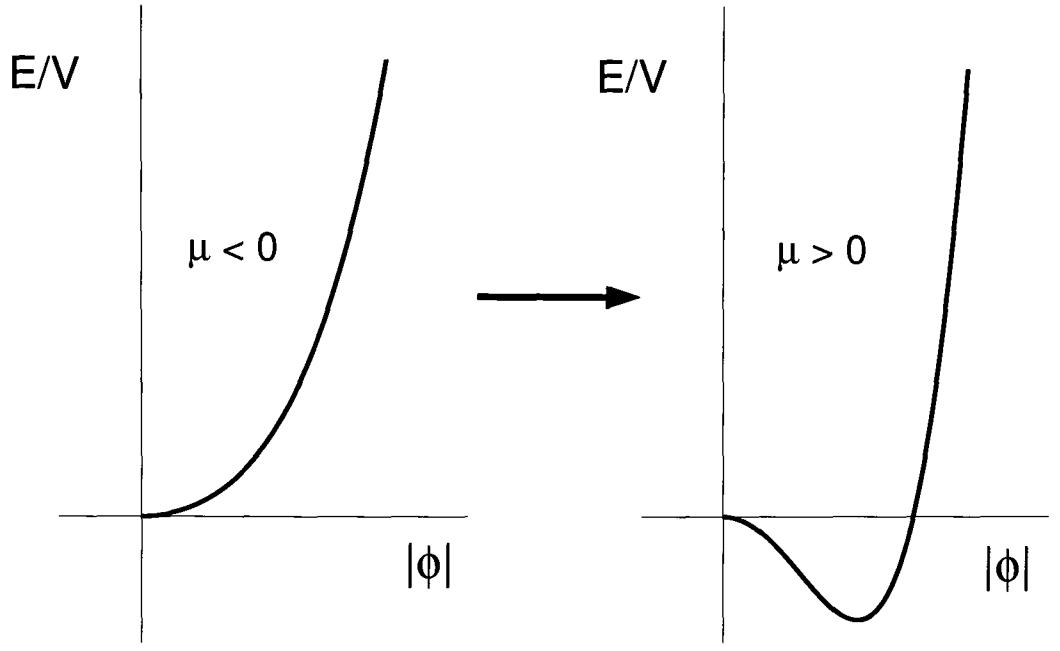

Figure 2.1: Free energy density as a function of $|\phi|$ above ($\mu < 0$) and below ($\mu > 0$) the Bose transition temperature.

as a Lagrange multiplier which sets the number of atoms in the ground state, and m is the atomic mass. This is simplified considerably for a homogeneous system since the kinetic energy term vanishes and we can write the free energy density as

$$E/V = -\mu|\phi|^2 + U|\phi|^4, \tag{2.6}$$

where V is the volume of the system. We take the interaction strength to be fixed and positive (since an homogeneous system is not stable for a negative interaction strength [15, 41]).

The energy density is plotted as a function of $|\phi|$ in Figure (2.1). There are two distinct cases. For $\mu < 0$, the energy density has a minimum at $|\phi| = 0$. This corresponds to a temperature above the transition for BEC and, as we might expect, the amplitude of $|\phi|$ vanishes since there is only a microscopic occupation of the condensate mode. Below the Bose transition temperature, $\mu > 0$, the energy is minimised for a non-zero value of $|\phi|$. This means that $|\phi|$ acquires a finite amplitude and indicates that there is a macroscopic occupation of the condensate mode.

If we now turn our attention to the phase rather than the amplitude of the

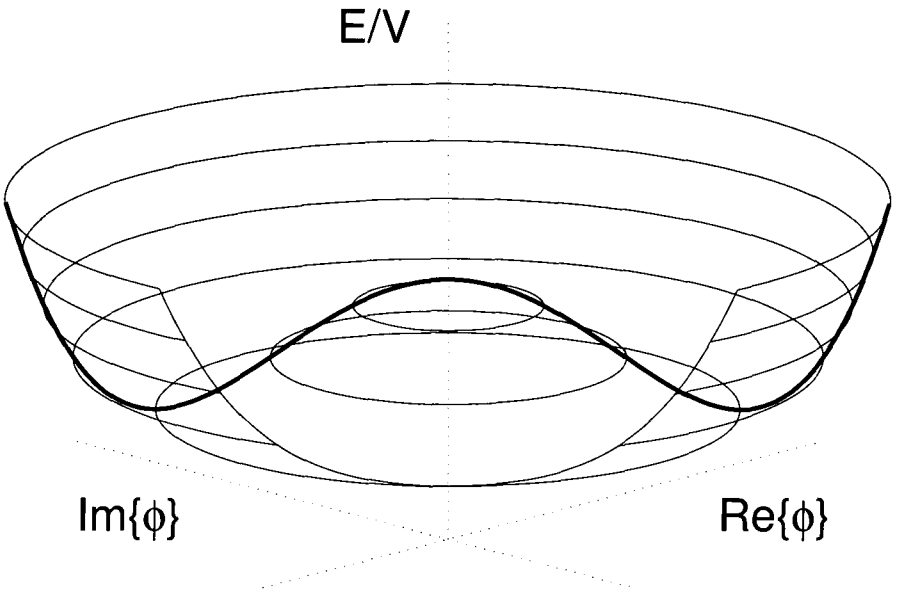

Figure 2.2: Free energy density as a function of ϕ below the Bose transition temperature. The function exhibits phase symmetry.

ground state, inspection of (2.5) reveals that the free energy does not depend on the phase of ϕ. This is a direct consequence of the fact that the total number of particles is conserved in the system. Rotating ϕ by an arbitrary angle does not affect the free energy and so the plot of free energy against ϕ is symmetric around the energy axis. In Figure (2.2), we show this plot for $\mu > 0$, i.e. when a condensate is present.

The free energy density has the form of a 'Mexican hat', where the minimum has a well defined finite amplitude but is completely degenerate in phase. There is no reason why the system should prefer one phase over another. Goldstone has shown that this phase degeneracy can be seen in the existence of a zero energy excitation of the system, which corresponds to a global rotation of the condensate phase [42].

Another way to think of the phase symmetry is in terms of the state of the condensate. Since atoms cannot be created or destroyed, particle number is conserved in a single isolated condensate. This means that such a system is in either a number state or a mixture of number states. A number state can be written in

terms of coherent states, $|\alpha\rangle$, as

$$|N\rangle \propto \int_0^{2\pi} \mathrm{e}^{-iN\theta} |\alpha\rangle \, \mathrm{d}\theta, \tag{2.7}$$

where $\alpha = |\alpha| \, \mathrm{e}^{i\theta}$. We see from this that a number state has no phase information, since it is an average over coherent states of all phases with equal weighting. It follows that a mixture of number states (and therefore an isolated condensate) must also have no phase. This is linked closely with the well-known uncertainty relationship between phase and number, $\Delta N \Delta\theta > 1$, which has the consequence that if the number of atoms in a BEC is precisely known, the phase is completely uncertain.

It is this conclusion that gives rise to the problem in using (2.3) as a definition of Bose condensation. Since the phase of an isolated condensate is undefined, the ensemble average of the Bose amplitude vanishes, $\langle\psi\rangle = 0$. This means that the right hand side of (2.3) vanishes. However, as we have seen, a condensate exhibits phase coherence and so (2.2) requires that the left hand side remains finite. Despite this problem, the usefulness of (2.3) is undeniable [43, 44, 45]. In the next section we will attempt to resolve this apparent contradiction.

2.3 Transitivity of phase

Phase coherence naturally leads to a transitive property of phase within a condensate. We can think of this by considering any three spatial points in the condensate, $\mathbf{r}$, $\mathbf{r}'$, and $\mathbf{r}''$. If we define our notation such that $\theta(i,j)$ represents the phase of i relative to j, where $i, j \in \{\mathbf{r}, \mathbf{r}', \mathbf{r}''\}$, then the transitive property of phase can be written as

$$\theta(\mathbf{r}', \mathbf{r}) = \theta(\mathbf{r}', \mathbf{r}'') - \theta(\mathbf{r}, \mathbf{r}''). \tag{2.8}$$

This allows us to interpret (2.4) in a more consistent manner. Instead of taking θ to be the 'phase' of the wave function at a certain point, we take it to be the phase at that point *relative* to another fixed point in the condensate. In other words, we take (2.4) to mean

$$\langle\psi(\mathbf{r})\rangle = \sqrt{\rho(\mathbf{r})} \, \mathrm{e}^{-i\theta(\mathbf{r},\mathbf{r}'')}, \tag{2.9}$$

where the phase is interpreted to be the phase relative to the arbitrary but fixed point $\mathbf{r}''$. This quantity is always non-zero for a condensate since phase coherence

ensures a well-defined relative phase. Let's now consider the form of (2.3) in this new context. The left hand side may be written as

$$\left\langle \psi^\dagger(\mathbf{r})\psi(\mathbf{r}')\right\rangle = \left\langle \sqrt{\rho(\mathbf{r})\rho(\mathbf{r}')}\, \mathrm{e}^{-i\theta(\mathbf{r}',\mathbf{r})}\right\rangle . \tag{2.10}$$

Making use of the transitivity property (2.8), we can write this as

$$\begin{aligned} \left\langle \psi^\dagger(\mathbf{r})\psi(\mathbf{r}')\right\rangle &= \left\langle \left(\sqrt{\rho(\mathbf{r})}\, \mathrm{e}^{i\theta(\mathbf{r},\mathbf{r}'')}\right)\left(\sqrt{\rho(\mathbf{r}')}\, \mathrm{e}^{-i\theta(\mathbf{r}',\mathbf{r}'')}\right)\right\rangle \\ &= \left\langle \psi(\mathbf{r})\right\rangle^* \left\langle \psi(\mathbf{r}')\right\rangle , \end{aligned} \tag{2.11}$$

where the last step follows since the two bracketed quantities in the first line are independent. We see that (2.3) is now consistent: both sides are finite and equal to one another, independent of the state of the condensate. It holds even for number states with completely undefined overall phase.

Such an interpretation also gives a feel for when mean field theories are valid. We can assign a finite value to $\langle\psi\rangle$ when the system is phase coherent which is equivalent to all the atoms being in the same mode. However, near T_c, many macroscopically distinguishable modes occur with non-negligible probabilities and so the mean field approximation may not be a good one near T_c. This region of validity is formalised by the Ginzburg criterion.

2.4 Absolute phase versus relative phase

An analogy is often drawn with a ferromagnet when discussing issues of symmetry breaking in Bose systems. A ferromagnet is similar to a Bose gas in that a plot of free energy against magnetisation has the same form as the Mexican hat of Figure (2.2). However, below a critical temperature known as the Curie temperature, the symmetry is broken and a ferromagnet assumes a particular direction of magnetisation.

The symmetry breaking can be explained by the fact that any stray magnetic field will 'tilt' the Mexican hat giving an energetically favourable direction for the spins. Below the Curie temperature, this effect dominates over the randomising thermal effects. Once the symmetry has been broken, the magnetisation is robust even when the field is no longer present since, for a large system, the probability of all the spins simultaneously rotating to another particular value is very small.

When this argument is extended to the thermodynamic limit, a symmetry

breaking field is no longer needed. In such a case, the symmetry is said to be spontaneously broken. This can be seen by introducing a small symmetry-breaking field (which we will later remove) with some arbitrary particular direction. If we now take the thermodynamic limit of the state, $N \to \infty$ and $V \to \infty$ such that N/V remains finite, and then take the limit that the symmetry breaking field vanishes, the system retains a net magnetisation in the direction that the symmetry-breaking field had.

A number of authors have extended this approach to show that an infinite condensate also undergoes spontaneous symmetry breaking and acquires an absolute phase [15]. The difference is that for a Bose system, this symmetry breaking field is unphysical and must be treated purely as a mathematical tool. For this reason, the analysis only works in the strictly infinite limit where the field can be formally eliminated.

For finite condensates, it is enlightening to consider a different model consisting of two coupled condensates. This has the advantage of doing away with the need for an unphysical symmetry breaking field and will also show the link between absolute and relative phase. Our model consists of a number state condensate, $|N\rangle$, coupled to a vacuum mode, $|0\rangle$. These modes respectively have the annihilation operators a and b. We consider that the coupling takes the form of quantum mechanical tunnelling between the modes or equivalently to resonant Raman coupling.

The state after evolution for time, t, is given by

$$|\psi(t)\rangle = \exp\left[-i\Gamma t\left(a^\dagger b + b^\dagger a\right)\right]\ |N\rangle_a|0\rangle_b, \tag{2.12}$$

where $\Gamma \geq 0$ is the coupling strength.

We would now like to examine the relative phase relationship between the two modes as a function of time. As a simple approach, we will take the mean value of the phase of a relative to b to be given by $\phi_{ab}(t) = \arg\{\langle\psi(t)|b^\dagger a|\psi(t)\rangle\}$. We discuss this measure of phase in more detail in Section (2.6). Substituting from (2.12) and rearranging the operators using the operator theorem [46]

$$\mathrm{e}^{\zeta B} A \mathrm{e}^{-\zeta B} = A + \zeta[B, A] + \frac{\zeta^2}{2!}[B, [B, A]] + \cdots, \tag{2.13}$$

the relative phase can be written as

$$\phi_{ab}(t) = \arg\left\{iN\sin(2\Gamma t)\right\}. \tag{2.14}$$

We see that for non-zero values of the coupling, $\Gamma t \neq 0$, the relative phase is $\phi_{ab} = \pi/2$ apart from the special cases when Γt is an integer multiple of $\pi/2$. In these cases, the phase is undefined, since the population is all in one mode or all in the other and the idea of a relative phase between the modes is meaningless.

We would now like to consider what happens in the limit of infinitely large condensates, $N \to \infty$, since this is the limit in which the symmetry is spontaneously broken in ferromagnetic systems. The relative phase in this case is,

$$\phi_{ab} = \lim_{N\to\infty} \arg\left\{iN \sin(2\Gamma t)\right\}. \tag{2.15}$$

We see now that no matter how small Γt is, the expression in the curly brackets is always non-zero and the relative phase is $\pi/2$. Writing out this zero-coupling limit fully, we have

$$\phi_{ab}(t) = \lim_{\Gamma t\to 0} \lim_{N\to\infty} \arg\left\{iN \sin(2\Gamma t)\right\} = \frac{\pi}{2}. \tag{2.16}$$

This is an expression for the phase of mode a relative to a vacuum with which it has never been coupled. In other words, the uncoupled limit corresponds to the *absolute* phase of the condensate. We conclude that, in the limit $N \to \infty$, a condensate can be considered to have an absolute phase.

If we now consider the result where N is arbitrarily large but finite, the phase of a relative to b in the uncoupled limit (i.e. the "absolute phase" of a) is given by

$$\phi_a \equiv \phi_{ab} = \lim_{\Gamma t\to 0} \arg\left\{iN \sin(2\Gamma t)\right\} = \arg\{0\}, \tag{2.17}$$

which is undefined.

This then establishes an important axiom: absolute phase is defined only for infinite condensates. For condensates produced in the laboratory, only relative phase is physically meaningful. In the remainder of this thesis, therefore, we will concern ourselves only with relative phase.

2.5 Creating phase

If an isolated condensate does not have a well-defined global phase, it follows that two condensates that have never been in contact with one another have no phase relationship. The results, then, of a recent experiment at MIT may seem perplexing. In this experiment, a condensate was split into two components with a light sheet. The two parts were then allowed to recombine and an interference

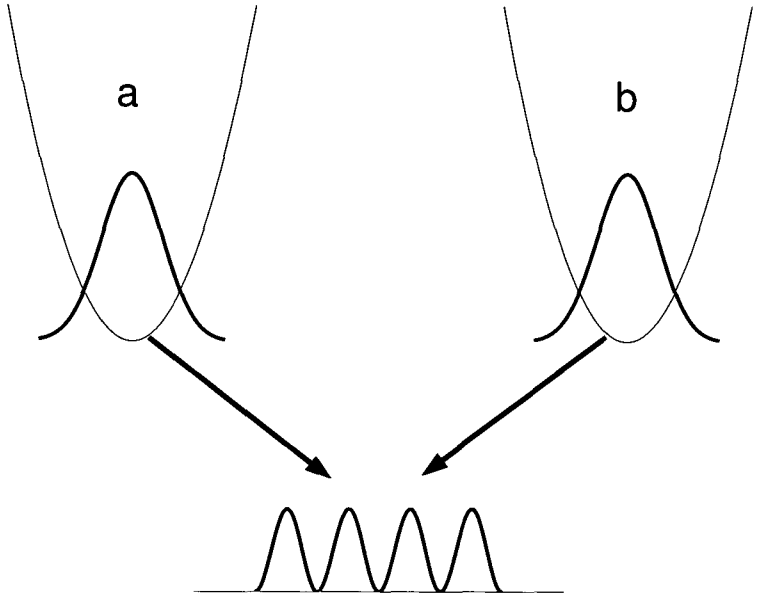

Figure 2.3: Two condensates initially in number states are allowed to fall onto an array of detectors. If atoms are detected in such a way that we cannot know which condensate an atom came from, a spatial interference pattern is seen.

pattern was observed in the region of overlap [39].

At first sight this may appear to contradict the fact that the phase of a condensate is undefined. Javanainen and Yoo [47], however, have shown how the observed interference pattern can be explained without assuming any particular phase properties of the two clouds of atoms. They have shown that if the two condensates are initially in number states (i.e. states with completely undefined phase), the act of sequentially detecting atoms builds up correlations in the remaining particles and leads to an observed interference between them. The interference pattern is formed by the back action of the measurement process itself: in effect, by looking for a relative phase, one is created.

We can understand how this comes about with the following argument. We consider two condensate modes denoted by a and b (see Figure (2.3)) which are each initially in a number state, $|N\rangle$. If we allow these to overlap and detect an atom in such a way that we cannot know which trap it originated from, the new state is

$$\frac{1}{\sqrt{2}}(a + b\mathrm{e}^{i\theta(x)}) \,)|N\rangle_a|N\rangle_b = \frac{1}{\sqrt{2}}\left(|N-1\rangle_a|N\rangle_b + \mathrm{e}^{i\theta(x)}\,|N\rangle_a|N-1\rangle_b\right), \quad (2.18)$$

where $\theta(x)$ is a phase that depends on the position, x, at which the atom was

detected. The two modes are now entangled since the total state cannot be written as the product of the states of modes a and b. Furthermore, $\langle a^\dagger b \rangle$ now has a nonvanishing value which indicates that a coherence has been established between the modes.

After a relatively small number of detections, the two remaining condensates find themselves in a relative coherent state. Castin *et al.* [48] have shown that the interference pattern observed is indistinguishable from one that would be obtained if the condensates started in coherent states. The value of the relative phase is undetermined before the actual measurement, but once it has been established it is robust. This demonstrates that the observation of an interference pattern in this experiment is not at odds with the fact that a single isolated condensate has no global phase.

Uncondensed clouds do not possess internal phase coherence and so allowing two such clouds to overlap would not result in the observation of an interference pattern. This experiment then, along with the phase coherence experiment of the Munich group, is very important since it shows unambiguously that a condensate has been produced rather than just a very cold, dense cloud of atoms.

2.6 Measures of phase

We conclude this introduction to the quantum phase of a BEC by discussing ways that phase can be quantified. We will limit ourselves to a discussion of relative phase.

We shall use two definitions in this thesis: one is an operational definition for the mean relative phase between two condensates which could be experimentally implemented. The second is a theoretical definition of the relative phase distribution.

The operational definition relies on allowing two condensates to overlap and measuring the interference pattern between them in much the same way as the MIT experiment. Of course, this process may not just measure the phase but also create one, but once this phase is established, subsequent measurements will yield the same result. For now, we consider just the case where a relative phase is initially defined. The position of the fringes give a measurement of this phase as the following treatment demonstrates.

We consider two condensates with corresponding annihilation operators $\hat{a}$ and $\hat{b}$. If these condensates are allowed to overlap and fall onto an array of detectors

the probability that an atom will be detected at position, x, is

$$\begin{aligned} P(x) &= \frac{1}{2}\left\langle \left(\hat{a}\,\mathrm{e}^{ikx} + \hat{b}\,\mathrm{e}^{-ikx}\right)^{\dagger}\left(\hat{a}\,\mathrm{e}^{ikx} + \hat{b}\,\mathrm{e}^{-ikx}\right)\right\rangle \\ &= \frac{1}{2}\left\langle \hat{a}^{\dagger}\hat{a} + \hat{b}^{\dagger}\hat{b} + \hat{a}^{\dagger}\hat{b}\,\mathrm{e}^{-2ikx} + \hat{b}^{\dagger}\hat{a}\,\mathrm{e}^{2ikx}\right\rangle, \end{aligned} \tag{2.19}$$

where the exponential factors account for the differential phase which accumulates while the atoms are being transported to the detector, and $x = 0$ is defined to be the point where this is identical for both beams.

If there is a relative phase ϕ between the modes, we can write

$$\langle \hat{a}^{\dagger}\hat{b}\rangle = |\langle \hat{a}^{\dagger}\hat{b}\rangle|\,\mathrm{e}^{i\phi}. \tag{2.20}$$

Substituting this into (2.19) we obtain

$$P(x) = \frac{1}{2}\left[\langle \hat{a}^{\dagger}\hat{a}\rangle + \langle \hat{b}^{\dagger}\hat{b}\rangle + 2|\langle \hat{a}^{\dagger}\hat{b}\rangle|\cos\left(\phi - 2kx\right)\right]. \tag{2.21}$$

We see from the final term in this expression that the detected atoms exhibit spatial interference fringes and that the position of these fringes depends on ϕ.

It is, therefore, experimentally feasible to extract the mean relative phase of two condensates by recording the position of the fringes. For this reason, we define the phase of $\hat{b}$ relative to $\hat{a}$ as

$$\phi = \arg\left\{\left\langle \hat{a}^{\dagger}\hat{b}\right\rangle\right\} = \arg\left[\mathrm{Tr}\left\{\rho\hat{a}^{\dagger}\hat{b}\right\}\right], \tag{2.22}$$

where ρ is the density matrix of the system. This definition of phase is particularly useful when discussing what is experimentally observable.

The second definition we use is more theoretical and is very useful, among other things, for calculating the phase distribution of a state. This definition relies on the Pegg-Barnett basis of states of well-defined phase [49, 50, 51],

$$|\theta_l\rangle = \frac{1}{\sqrt{s+1}}\sum_{p=0}^{s}\mathrm{e}^{ipl\epsilon}|p\rangle, \tag{2.23}$$

where $l = 0, 1, ..., s$, $\{|p\rangle : p = 0, ..., s\}$ denotes the Fock states, and $\epsilon = 2\pi/(s+1)$ is the rotation between adjacent phase states. The index s parametrises the Hilbert space and, in general, we need to take the limit $s \to \infty$. As described elsewhere [52], we should calculate the moments as a function of s and then take the limit

$s \to \infty$, rather than the other way around. This is an important distinction to make for light states, for which the Hilbert space is infinite due to photons readily being created and destroyed.

A condensate, however, has a fixed finite number of atoms and when we take the overlap of its state with (2.23), terms for which s is larger than the total number of atoms in the condensate, N, vanish. This means that we simply need our basis to extend over the total number of atoms in the state that we are examining, i.e. $s = N$.

This basis can be used to calculate the relative phase distribution of two modes. The probability that the relative phase between two modes is $\Delta\theta$ is found by calculating the overlap of the state with the joint phase state $|\theta_l\rangle|\theta_{l-\Delta\theta/\epsilon}\rangle$ and summing over all values of the absolute phase, which is parametrised by l.

2.7 Summary

We have provided an overview of the subject of the quantum phase of a Bose condensate. Our subsequent investigations in this thesis rest on the platform of this chapter and so it is worthwhile reviewing the main points here. The basic axioms of phase we have established are as follows.

- Bose condensates are characterised by phase coherence across the entire system.
- Only in the limit of infinite atoms does a condensate have an absolute phase. Therefore, for all condensates produced in the laboratory, relative phase is the only meaningful concept.
- Relative phase appears due to an entanglement of condensate modes. This entanglement can be created by the phase measurement process itself.

CHAPTER 3

A PHASE STANDARD FOR BOSE CONDENSATES

Most of us are happy with the fact that in everyday life we can think of certain relative quantities as if they were absolute. Direction is one such example. It is common to speak of compass points as if they were absolute directions, even though strictly they are defined relative to the direction of the Earth's magnetic field. Such usage, however, is perfectly acceptable so long as the reference direction is well-defined and implicitly understood.

Using the same reasoning, one might ask whether a similar standardisation can be applied to the phase of a condensate. Strictly, we know that only relative phases are defined. However, if we could define a consistent "phase standard": a reference condensate with which the phases of other condensates can be compared, we could give phase the same pseudo-absolute sense that direction has.

In this chapter, we outline how such a phase standard may be defined. The existence of a phase reference is important since it gives a clear and precise definition to what we mean by the phase of a condensate.

3.1 Introduction

A phase standard for Bose condensates has been discussed in previous work both in the context of Josephson junctions [53, 54], and atomic condensates [55]. Leggett, in particular, has considered whether it is possible to set up a consistent phase reference. He considered the case of three superconductors (or superfluids), A, B,

and C, that are placed in contact with one another via Josephson coupling [56]. In his model, A is first placed in contact with B, with C absent, and sufficient time is allowed for equilibrium to be established. The contact is then broken and B and C are placed in contact and allowed to reach equilibrium. Finally this contact is broken and A and C are put in contact. He then asked whether, by observing the Josephson currents between A and B and between B and C, it is possible to predict the current that will flow when finally A and C are connected.

Since the instantaneous Josephson current is directly related to the phase difference, this is the same as asking whether phase is transitive. In other words, does superconductor B act as a phase standard in this model? Intuitively, we might feel that the phase relationship that is established between A and B in the first step will in some way be degraded when B and C are subsequently allowed to come to equilibrium. Leggett demonstrated that, when the effects of the environment are included, this is indeed the case and concluded that a phase standard for Bose condensates cannot be defined in this sense.

He did, however, suggest that a phase standard might still be meaningful on shorter timescales. Provided that this timescale is long compared to the length of an experiment, it may still be a useful concept. After all, the Earth's magnetic field, which defines North, changes with time and it is the fact that this change is slow compared with our lifespans that it still forms a valuable and meaningful direction standard.

In this chapter, we test this proposal and include the key effect of measurements establishing the phase. We also investigate whether phase is preserved in a measurement; in other words, if we repeat the measurement do we get the same result?

3.2 Scheme

Our scheme is based on recent work [47, 48, 57, 58] which has demonstrated that, by making measurements which entangle two condensates, a relative phase can be generated between them even if they are initially in states of undefined phase. Cirac *et al.* showed that the interference patterns observed between number states are indistinguishable from those obtained if the condensates start in coherent states, i.e. states of well defined phase. From this observation, they proposed that if relative phases were generated between each of two condensates (A and C) and a third one (B), the relative phase between A and C can be predicted from the

results of the other two measurements. Such a proposal has B acting in precisely the role of a phase standard.

The entanglement between the three modes is crucial to such a scheme, and we need to keep a full record of its evolution. Previous methods which use conditional probabilities to determine the position (or time) of detection of the next atom in interference schemes [47, 57], will not work. We need to keep track of the quantum state of the system at all times and hence follow a new calculational route.

We have chosen to apply the quantum jump method (see, for example, [59]) to a system of two condensates to study the evolution of the system as atoms are detected. This enables us to keep track of the entanglement throughout a particular realisation and may be viewed as a representative history of an experiment [60]. We will see that the transitive nature of phase holds for any such realisation. Of course, in this case we will not have to think of many realisations, since the idea of a phase standard is that it is a single, unique reference.

The set-up is analogous to the theoretical work of Javanainen and Yoo [47], who analysed the case of two initially spatially separated condensates that are allowed to overlap and the positions of atoms in the interference pattern recorded. An entanglement between the two 'modes' is established due to the fact that one cannot know from which condensate the atoms have come. This entanglement leads to a relative phase seen in the build up of an interference pattern in the spatially detected atoms. We begin by studying a simple model involving the detection of just two atoms. This gives considerable insight into how the phase standard scheme works. We will discuss a more general multiparticle detection scheme later.

Our basic model consists of three condensate modes, A, B and C, each initially in a number state with no phase information. For convenience, we take each mode to have the same number of atoms, N, and the same rate of loss of atoms. If we now allow modes A and B to fall onto a detector and detect one atom in such a way that we cannot know which condensate it came from, the two modes are entangled. This detection both creates and measures a phase between A and B, ϕ_{AB}. We can write the total state after this step as

$$|\psi\rangle = \frac{1}{\sqrt{2}}\left(|N-1,N,N\rangle + \mathrm{e}^{i\phi_{AB}}\,|N,N-1,N\rangle\right). \tag{3.1}$$

We now consider detecting a single atom from the overlap of modes B and C. If the phase associated with this detection is ϕ_{BC}, we can write the total state after

this step as

$$|\psi\rangle = \frac{1}{2}(|N-1,N-1,N\rangle + e^{i\phi_{BC}}|N-1,N,N-1\rangle + e^{i\phi_{AB}}|N,N-2,N\rangle + e^{i(\phi_{AB}+\phi_{BC})}|N,N-1,N-1\rangle), \quad (3.2)$$

where, for illustrative purposes, we have taken N to be sufficiently large that we can neglect the difference between N and $N-1$ in the coefficients. The phase of mode A relative to C, which have never directly interacted, is then given by

$$\phi_{AC} = \arg\left\{\langle\psi|c^\dagger a|\psi\rangle\right\} = \phi_{AB} + \phi_{BC}. \quad (3.3)$$

This result demonstrates that the phase is transitive and has mode B acting as a phase standard.

Although the transitivity of mean phase is present even after the detection of a single atom from each pair of condensates, the phase resolution is poor. A phase standard will be of limited use unless the phases are well defined. For this reason, we would now like to consider the more general case where many particles are detected and so the statistics are improved. The permutations of this calculation rapidly become very complicated, so we perform a numerical analysis which will also enable us to model the random nature of the atomic detections.

For convenience, we consider the time analogue of the scheme outlined above, observing the time, rather than the position, at which atoms are detected. As in the spatial model, we would expect a relative phase to develop. This temporal scheme has the advantage of allowing us to consider condensates in energy eigenstates rather than momentum eigenstates. In an experiment, we expect the condensate to be in the ground state energy level of the trap.

There have been various proposals for measuring the relative phase between condensates. These are based on recording interference patterns [47], or by inducing Raman transitions which couple the condensates [61, 62, 63, 64]. The precise way in which the measurement is made does not matter as all of these schemes rely on detecting a superposition of the two fields. We have chosen to use a beam splitter to produce this superposition but a variant of the same analysis would work for any of these schemes.

We consider a 50:50 beam splitter with a condensate as the input to each of the two ports. The two condensate modes are identified with the operators a and b. If we transform to a frame rotating at the frequency of mode a, ω_a, the field

operators at the two output ports of the beam splitter are

$$C_1 = \sqrt{\frac{\kappa}{2}}\left(a + ib\,\mathrm{e}^{-i\Omega t}\right) \tag{3.4}$$

$$C_2 = \sqrt{\frac{\kappa}{2}}\left(ia + b\,\mathrm{e}^{-i\Omega t}\right), \tag{3.5}$$

where κ is the rate of detection of atoms and $\Omega = \omega_\mathrm{b} - \omega_\mathrm{a}$.

We wish to calculate the quantum state of the system conditioned on all the previous detections, $|\psi_\mathrm{c}\rangle$. The procedure for simulating this measurement process is outlined below.

(i) Firstly, we determine the probability that an atom is detected at port $j \in \{1, 2\}$ in a time interval, Δt

$$P_j(t, \Delta t) = \Delta t \langle \psi_\mathrm{c}(t)|C_j^\dagger C_j|\psi_\mathrm{c}(t)\rangle. \tag{3.6}$$

We then generate random numbers, r_j, from a flat distribution between zero and one, and compare these with P_j.

(ii) We define our protocol so that if $r_j < P_j$, a detection is made in port j during Δt and the system jumps to the renormalised form,

$$|\psi_\mathrm{c}(t)\rangle \longrightarrow \frac{C_j|\psi_\mathrm{c}(t)\rangle}{\sqrt{\langle\psi_\mathrm{c}(t)|C_j^\dagger C_j|\psi_\mathrm{c}(t)\rangle}}. \tag{3.7}$$

(iii) If $r_1 > P_1$ and $r_2 > P_2$, there is no detection in the interval, Δt, and the system evolves due to the unitary part of the Hamiltonian,

$$|\psi_\mathrm{c}(t)\rangle \longrightarrow \exp\left[-iH_\mathrm{eff}\Delta t\right]|\psi_\mathrm{c}(t)\rangle. \tag{3.8}$$

We have defined $\hbar \equiv 1$, and the effective Hamiltonian, H_eff is given by, $H_\mathrm{eff} = H_0 - i\kappa(a^\dagger a + b^\dagger b)/2$, where H_0 is the system Hamiltonian. The state needs to be renormalised after each step since H_eff is non-Hermitian.

(iv) Steps (i)–(iii) are repeated to propagate the state forward in time until the desired number of atoms has been detected.

We can summarise this procedure as a stochastic Schrödinger equation (SSE),

which the reader may find helpful. For each port, this equation contains a stochastic term which consists of the change in the state vector when a detection takes place at that port, multiplied by a random variable which determines whether or not an atom is detected at that time. There is also a deterministic term describing the evolution when an atom is not detected. More formally, we can write the SSE as

$$\begin{aligned} d|\psi_c\rangle &= \left\{ dN_1 \left(\frac{C_1}{\sqrt{Q_c^1(t)}} - 1 \right) + dN_2 \left(\frac{C_2}{\sqrt{Q_c^2(t)}} - 1 \right) \right. \\ &- \left. dt \left[iH_0 + \frac{\kappa}{2} \left(a^\dagger a + b^\dagger b - \langle a^\dagger a \rangle - \langle b^\dagger b \rangle \right) \right] \right\} |\psi_c\rangle, \end{aligned} \tag{3.9}$$

where we have defined $Q_c^j(t) \equiv \langle \psi_c(t)|C_j^\dagger C_j|\psi_c(t)\rangle$. The random variables, dN_1 and dN_2, must have the properties,

$$dN_j(t)^2 = dN_j(t) \tag{3.10}$$

$$E[dN_j(t)] = Q_c^j(t)dt = P_j(t, dt), \tag{3.11}$$

where $\mathrm{E}[dN_j(t)]$ denotes the ensemble average of $dN_j(t)$. This is because for a single trajectory at a given time, t, $dN_j(t) \in \{0, 1\}$ since either a jump takes place or it doesn't. The expectation value for each of the random variables, however, must be equal to the probability of a detection in that port at time, t.

Another way to consider (3.9) is as an 'unravelling' of the master equation [59, 65, 66, 67, 68]. We can show this by calculating the time derivative of the system's density matrix, $\rho(t) = |\psi_c(t)\rangle\langle\psi_c(t)|$, on an ensemble average.

$$\dot{\rho}(t) = \mathrm{E}\left[\frac{d}{dt} \left(|\psi_c\rangle\langle\psi_c| \right) \right]. \tag{3.12}$$

A simple calculation gives

$$\dot{\rho}(t) = -i\left[H_0, \rho(t)\right] + \mathcal{D}[a]\rho(t) + \mathcal{D}[b]\rho(t) \tag{3.13}$$

where

$$\mathcal{D}[s]\rho(t) = \kappa \left(s\rho(t)s^\dagger - \frac{1}{2}s^\dagger s\rho(t) - \frac{1}{2}\rho(t)s^\dagger s \right). \tag{3.14}$$

This is the master equation for the system, which is what we would expect for an ensemble average over all the trajectories. There is no unique unravelling of the master equation. However, Equation (3.9) is the special case for which each

trajectory can be thought of in terms of a representative experimental run [60]. This is what we want, since when comparing a condensate with a phase standard, we must consider a single trajectory not an ensemble average.

For an initial number state, the master equation can lead only to mixtures of number states and, as such, does not allow for the build-up of phase. However, this need not concern us since, as we shall see in the results below, each trajectory demonstrates the same fixed and predictable phase relationship between the modes. Our concept of a phase standard is that there is only one, and so this must obey the same phase relationship as that of a single trajectory. The phase information would be wiped out only if we were to take the ensemble average over all phase standards. The notion of a phase standard thus relies on everybody using the same reference condensate.

3.3 Results

We are now in a position to study how the phase builds up between condensates when we detect atoms at the output ports of the beam splitter. We use the calculational procedure outlined in Equations (3.6)–(3.8). The three mode set-up is shown in Figure (3.1). We take each condensate to be initially in a number state with 1000 atoms, and so the system begins with no phase information. The total system will remain in a state of known number throughout the simulation since we detect and record every atom that escapes from the traps. As we shall see, however, this does not prevent relative phases from developing between the three parts of the system.

For simplicity, we set the trap frequencies and detection rate so that $\omega_a = \omega_c = \omega_b/4 = 40\kappa$. In the rotating frame, we also set the system Hamiltonian, H_0, equal to zero. This last condition amounts to considering atoms which do not interact with one another. It is very straightforward to generalise H_0 to include interactions between atoms, which give rise to interesting effects such as collapses and revivals of the phase [69].

To begin with, we allow atoms to leak out of traps a and b and we record the times at which atoms are detected in beam splitter ports 1 and 2. We continue until about 10% of the atoms in traps a and b (i.e. about 200) have been detected. Throughout the simulation, we dynamically calculate the phase of a relative to b,

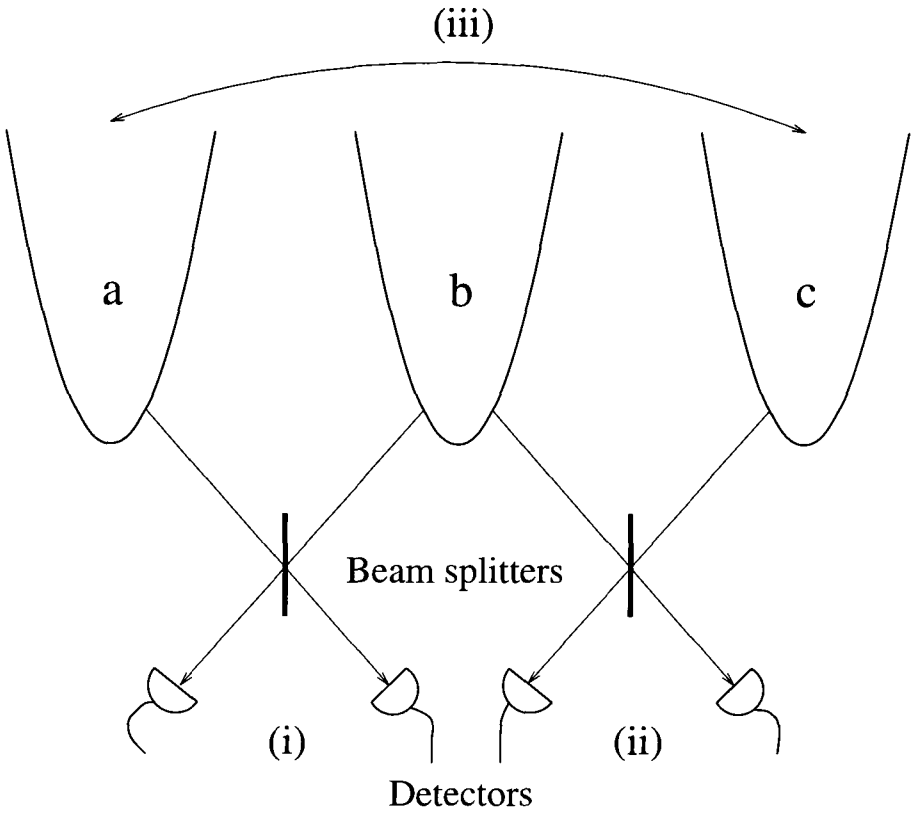

Figure 3.1: The phase standard scheme. (i) In the first stage, condensates a and b are the inputs to a beam splitter and we record atomic detection times at the two output ports. (ii) In the second stage we repeat the process but with b (now entangled with a) and c as the two inputs. (iii) Finally, we measure the relative phase between a and c and compare with the results of the phase measurements in (i) and (ii).

ϕ_{ab}. This is given by

$$\phi_{ab}(t) = \arg\left\{\langle\psi_c(t)|b^\dagger a|\psi_c(t)\rangle\right\}. \tag{3.15}$$

The measurement scheme serves the dual role of both creating and measuring the relative phase. This phase (3.15) may be found by taking the difference in the number of atoms detected at each port, $D(t)$, per time interval, Δt. For zero phase difference, we would expect equal numbers of detections at each port, and for a leading (lagging) b by $\pi/2$ we would expect more detections at port 1(2). This means that for degenerate modes, we would expect to see a sinusoidal time dependence of the difference in numbers of atoms detected at the two ports. In analogy with the position of the spatial fringes in interference experiments, we can use the 'time-position' of the temporal fringes as a measurement of the relative

phase.

On average, the difference in the number of atoms detected at each port per time interval is given by

$$D(t)/\Delta t = \left\langle \psi_c(t) \left| C_1^\dagger C_1 - C_2^\dagger C_2 \right| \psi_c(t) \right\rangle \tag{3.16}$$

$$= i\kappa \left(\langle a^\dagger b \rangle \, \mathrm{e}^{-i\Omega t} - \langle b^\dagger a \rangle \, \mathrm{e}^{i\Omega t} \right). \tag{3.17}$$

We can write

$$\langle b^\dagger a \rangle = |\langle b^\dagger a \rangle| \, \mathrm{e}^{i\phi_{ab}(t)}, \tag{3.18}$$

where $\phi_{ab}(t)$ contains the non-deterministic part of the relative phase due to the randomness of each trajectory. With this substitution, we get

$$D(t)/\Delta t = 2\kappa |\langle b^\dagger a \rangle| \sin\left(\Omega t + \phi_{ab}(t)\right). \tag{3.19}$$

So the relative phase is given by the argument of the sinusoidal plot of the difference in the number of atoms detected at each port per time interval. For our results, we subtract the known deterministic component, Ωt.

A plot of ϕ_{ab} against time is shown in Figure (3.2a). As expected, the relative phase is initially undefined. Then, as atoms are detected, it fluctuates for a while before settling down to a fixed constant value, Φ_{ab}. This value is random and varies for measurements made on identically prepared systems. At the end of this detection process, modes a and b are entangled and mode c is unaffected. The state vector for the system is given by

$$|\psi_c\rangle = \left(\sum_{i=N-l}^{N} c_i \, |2N - l - i\rangle_a |i\rangle_b \right) |N\rangle_c, \tag{3.20}$$

where N is the initial number of atoms in each trap, l is the number of atoms detected ($l < N$), and $\{c_i\}$ are the coefficients determined by the numerical simulation.

The fact that a relative phase arises does not contradict our discussion in Chapter 2 that a condensate cannot have an absolute phase. We can see this by finding the reduced density matrix for either mode. The reduced density matrix describing mode b is found by tracing over the states of mode a. This gives

$$\rho_b = \mathrm{Tr}_a\{\rho\} = \sum_{i=N-l}^{N} |c_i|^2 \, |i\rangle\langle i|, \tag{3.21}$$

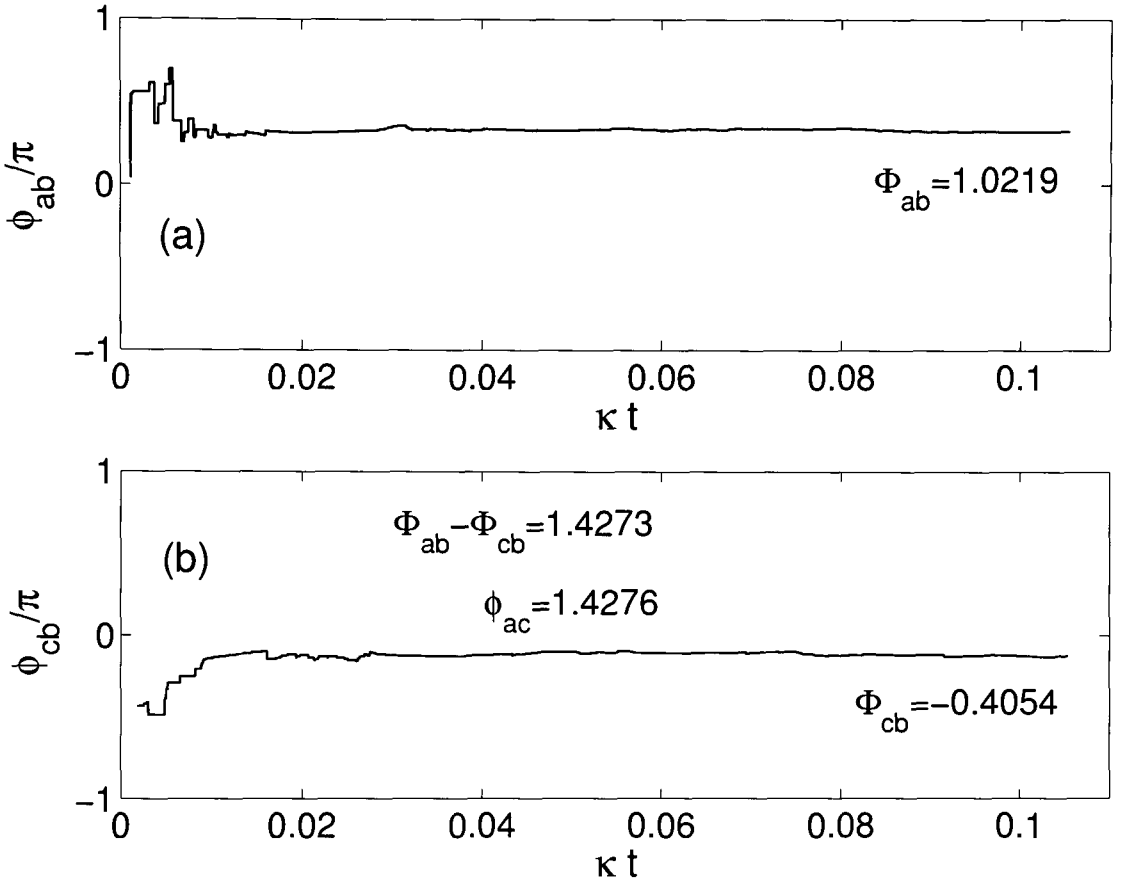

Figure 3.2: The establishment of a relative phase. The time evolution of the relative phase between modes a and b is shown in (a) and between b (now entangled with a) and c in (b). In each case, the relative phase is plotted against the dimensionless quantity κt, where κ is the rate of detection of atoms.

which is a mixture of number states and so has no phase information. We can see this by calculating the phase directly,

$$\phi_b = \arg\left[\mathrm{Tr}\left\{\rho_b b\right\}\right] = \arg\{0\}, \tag{3.22}$$

which is undefined. We conclude that, although there is a well-defined relative phase between modes a and b, each mode individually has no phase.

In the second part of the simulation, we take mode b (now entangled with a) as the input to one port of a beam splitter, and mode c as the other input. As before, we record the times that atoms are detected at the two output ports until roughly 10% of the atoms have been detected. A plot of the relative phase between modes c and b, ϕ_{cb}, is shown in Figure (3.2b). As in the first part, this eventually settles

down to a fixed constant value, Φ_{cb}, and this varies randomly for measurements made on identically prepared systems.

An important observation is that the entanglement of b and c does not affect the existing entanglement between a and b, so long as the modes are not too severely depleted in the process. This is a very desirable property for a phase standard since it means that the standard is not corrupted in the process of comparing it with another condensate.

In this simulation, we consider that there is no independent loss from the traps. Such a process, corrupts the entanglements and so degrades the phase standard. In Chapter 4, we study in more detail how dissipation degrades phase relationships. This explains why a phase standard will not work if the system is allowed to reach equilibrium with the environment as pointed out by Leggett [53]. Here we investigate the system on a different timescale: long before it reaches equilibrium. For our system, this can be long enough for useful experiments. The effect of interactions and loss are treated by Sinatra and Castin [70].

At the end of this second measurement stage, modes a and c are each entangled with b. The state vector for the system is

$$|\psi_c\rangle = \sum_{j=N-m}^{N} \sum_{i=2N-m-j}^{N} d_{i,j} \, |3N-i-j-m\rangle_a |j\rangle_b |i\rangle_c, \tag{3.23}$$

where m is the total number of atoms detected in both measurement stages ($m < N$), and $\{d_{i,j}\}$ are the coefficients determined by the numerical simulation.

Finally, in the third part, we calculate the phase of a relative to c, ϕ_{ac}. This is given by

$$\begin{aligned} \phi_{ac} &= \arg\left\{\langle\psi_c|c^\dagger a|\psi_c\rangle\right\} \\ &= \arg\left\{ \sum_{j=N-m}^{N} \sum_{i=2N-m-j}^{N-1} d_{i,j} \, d^*_{(i+1),j} \sqrt{(i+1)(3N-i-j-m)} \right\}. \end{aligned} \tag{3.24}$$

Proposals have been made for how this could be measured [61, 62, 63, 64]. Alternatively, we could simply perform another interference measurement. The difference here is that the relative phase exists *a priori* and isn't built up by the measurement. For this scheme to work successfully as a phase standard, we require that $\phi_{ac} = \Phi_{ab} - \Phi_{cb}$. From the simulation shown in Figure (3.2), we see that there is remarkable agreement. In fact, many simulations were performed and in all of them we were able to predict the relative phase between a and c with great accuracy.

Once the phases have been established between the modes, further measurements give the same results. The relative phases are now fixed and are encoded in the entanglements and further phase measurements do not corrupt these.

Of course, we could carry on and measure the relative phase between a fourth condensate and our phase standard. We know that this measurement will not destroy the entanglements with the other condensates, so we could then predict the relative phases between this condensate and the other two. The only limitation on how many times this phase reference can be used is the number of atoms it contains. Provided that the initial number of atoms is very large, many measurements can be made before the standard is depleted. As our simulations show, only a small fraction of the atoms need to be removed to make a measurement, which means our sample is not destroyed in the process. Such an arrangement demonstrates all the properties that we require in a phase standard.

The existence of a phase standard for Bose-Einstein condensates is of considerable importance. It gives us a clear and precise definition of the phase of a condensate. We can now speak sensibly of a condensate's phase in the same pseudo-absolute sense that we speak of direction, implicitly interpreting it to mean 'relative to a well-defined standard'.

The analogy between direction and phase, however, is not perfect and there are some subtle differences. In particular, direction does not require a procedure to standardise it, whereas we need to make specific measurements on condensates to standardise their phase. In the next chapter we will discuss how relative phase can naturally arise between condensates without the need for any measurements.

CHAPTER 4

ESTABLISHMENT OF PHASE BETWEEN COUPLED CONDENSATES

4.1 Introduction

In this chapter, we want to extend our analysis of phase to systems of coupled condensates. This is of special interest due to recent experimental advances in creating superpositions of condensates in two hyperfine levels [71] and chains of coupled trapped condensates [72]. In particular, we want to study how phase information is established and transferred between the condensates, both with and without the effects of dissipation.

We begin in Section 4.2, by studying how a relative phase can be established between two condensates by a Josephson-like transfer between them. This differs from the measurement-induced phase that we discussed in Chapter 3 since the evolution is unitary and therefore the phase generated is deterministic. We will discuss how the phase of the transferred component may be predicted and controlled. In Section 4.3, we investigate how phase is transported along a set of coupled condensates if we make measurements which establish a phase at one site. Finally, in Section 4.4, we extend this idea to demonstrate how dissipation and interactions can naturally give rise to phase. This has been inspired by a recent experimental demonstration of a mode-locked atom laser [72], in which the output from a lattice of coupled condensates is observed as a train of atomic pulses, providing a clear demonstration of phase locking of the condensate modes.

4.2 Phase of Josephson-transferred condensates

We begin by discussing the form of the coupling. Josephson coupling [56] of condensates can be achieved by allowing them to tunnel through a potential barrier or, equivalently, by coupling them with laser fields. It is equivalent to Raman transfer, i.e. a stimulated transfer to another internal atomic state, which can be brought about by applying two laser fields to a condensate [73]. This preserves the coherence and can be used for atomic beam splitters [74] and output couplers for atom lasers [75].

Hall *et al.* [64, 76] used Raman pulses to create an interferometer by transferring half the population in a condensate to another trapped state. They then allowed the system to evolve before recombining the two components and studying the interference pattern in their region of overlap. Among other things, they demonstrated that the relative phase between the two components is fixed and repeatable. This means that one should be able to transfer a condensate into a number of different modes, all with the same phase relationship to the original.

The question arises whether we can go one step further and predict the value of the relative phase. It may seem obvious to some that the phase of the transferred component be identical to that of the original. In fact, we shall show that it is not always so. In this section, we discuss simulations of the transfer process and investigate the reproducibility of the relative phase as well as its value. We also investigate how the phase depends on the system parameters and how to prepare condensates with a given phase relative to its mother. This is of particular interest in relation to the output pulses from atom lasers, since they rely on Josephson-like transfer as the output coupling mechanism [77].

4.2.1 Phase preparation

The first step in our scheme is to establish and measure a relative phase between the condensate and the phase standard. We follow a procedure similar to that outlined in Chapter 3.

We consider two condensate modes, identified in turn with the annihilation operators a and b. Initially a and b are taken to be in number states with N atoms, and we allow outputs from these modes to be incident on the ports of a 50:50 beam splitter (see Figure (4.1)). Detecting atoms at the two output ports entangles the modes which leads to the establishment of a relative phase between them.

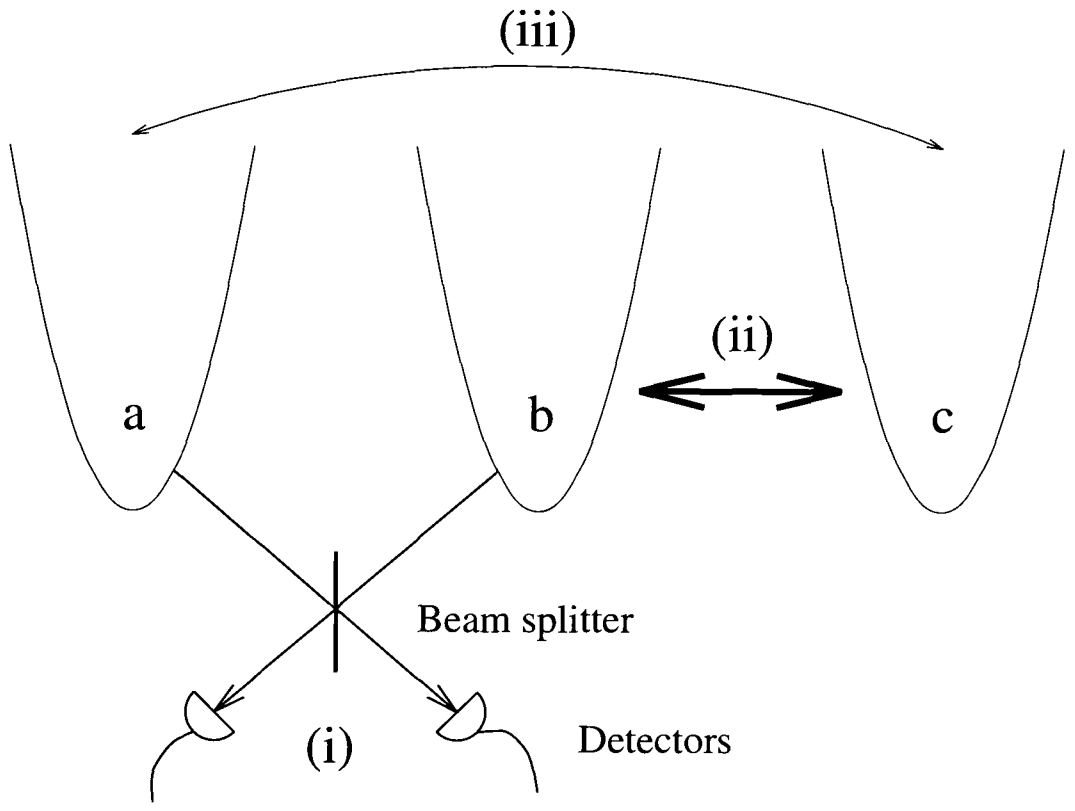

Figure 4.1: (i) In the first stage, we record the detection times at the output ports of a beam splitter which has condensates a and b as the inputs. (ii) In the second stage, part of mode b is Raman transferred to mode c which is initially empty. (iii) Finally, we measure the relative phase between a and c and also between a and b and compare with the result of the phase measurement in (i).

The state vector at the end of this process is given by Equation (3.20),

$$|\psi_c\rangle = \sum_{i=N-l}^{N} d_i \, |2N-l-i\rangle_a |i\rangle_b, \tag{4.1}$$

where l is the total number of atoms detected ($l < N$), and $\{d_i\}$ are the coefficients determined by the numerical simulation.

A plot of $\phi_{ba}(t)$ is shown in Figure (4.2a) for a system which initially has 1000 atoms in each trap and for which we detect about 10% of the atoms in the measurement process. As expected, the relative phase stabilises to an approximately fixed constant value. This value is random and varies for measurements made on identically prepared systems.

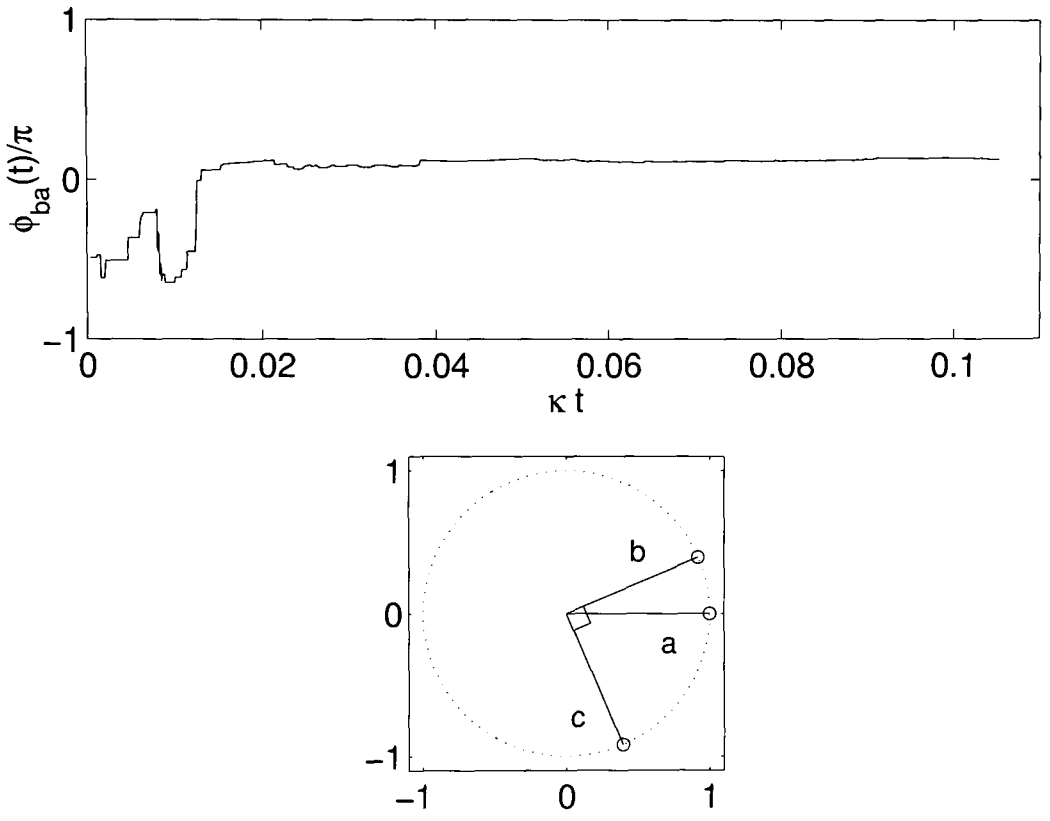

Figure 4.2: The time evolution of the relative phase between a and b for $N = 1000$ and 10% of the atoms detected. The relative phase is plotted against the dimensionless quantity κt, where κ is the rate of detection of atoms. A phasor diagram of the relative phases of the three modes after the Raman transfer for $\delta = 0$ is also shown. Mode a is used to set the zero of phase.

4.2.2 Phase transfer

In the second part of this scheme, we coherently transfer a fraction of mode b, now entangled with the phase standard, a, to a third mode c, which is initially in a vacuum state. Finally, we measure the relative phases between each of modes b and c with the phase standard a, and thereby determine the relative phase between b and c.

The Hamiltonian for the transfer may be written as

$$H = \omega_b b^\dagger b + \omega_c c^\dagger c + \Gamma \left(b c^\dagger \mathrm{e}^{-i\omega t} + b^\dagger c \, \mathrm{e}^{i\omega t} \right), \tag{4.2}$$

where ω is the driving frequency and the coupling strength, Γ, is real. For the sake of simplicity, in this section we neglect interactions between atoms. However,

these interactions, which lead to interesting effects such as collapses and revivals of the condensate phase [69, 78], can readily be included in this formalism and we will reintroduce them in Sections 4.4.2 and 4.4.3. In the interaction picture, we can write the Hamiltonian as

$$H_{\mathrm{I}} = \frac{1}{2}\Delta(b^{\dagger}b - c^{\dagger}c) + \Gamma(c^{\dagger}b + b^{\dagger}c), \tag{4.3}$$

where $\Delta = \omega_c - \omega_b - \omega$ is the detuning between the driving and transition frequencies.

We can find the Heisenberg equations of motion for b and c directly from (4.3),

$$\dot{b}(t) = \frac{i}{2}\Delta b(t) - i\Gamma c(t) \tag{4.4}$$

$$\dot{c}(t) = -\frac{i}{2}\Delta c(t) - i\Gamma b(t). \tag{4.5}$$

These can be solved by differentiating both equations and substituting. The result is,

$$b(t) = \left[\cos(\Omega t) + \frac{i\Delta}{2\Omega}\sin(\Omega t)\right] b(0) - \frac{i\Gamma}{\Omega}\sin(\Omega t)\, c(0) \tag{4.6}$$

$$c(t) = \left[\cos(\Omega t) - \frac{i\Delta}{2\Omega}\sin(\Omega t)\right] c(0) - \frac{i\Gamma}{\Omega}\sin(\Omega t)\, b(0), \tag{4.7}$$

where $\Omega^2 = (\Delta/2)^2 + \Gamma^2$.

We can now use (4.6) and (4.7) to directly calculate the moments of the system. In particular,

$$\langle c^{\dagger}(t)b(t)\rangle = \langle b^{\dagger}(0)b(0)\rangle \frac{i\Gamma}{2\Omega}\left[\sin(2\Omega t) - \frac{i\Delta}{2\Omega}(\cos(2\Omega t) - 1)\right], \tag{4.8}$$

since the moments other than $\langle b^{\dagger}b\rangle$ vanish at $t = 0$. The phase of b relative to a is then given by,

$$\phi_{bc}(t) = \arg\left\{\langle c^{\dagger}(t)b(t)\rangle\right\} \tag{4.9}$$

$$= \arg\left\{iN_b \sin(2\Omega t) + \frac{i\Delta}{2\Omega}N_b(\cos(2\Omega t) - 1)\right\}, \tag{4.10}$$

where N_b is the mean number of atoms initially in mode b.

4.2.3 Results

To begin with, we consider the case where the transition between modes b and c is driven on resonance, $\Delta = 0$. In this case, our simulations show that mode b always leads mode c by $\pi/2$. An example of this is shown in the phasor diagram of Figure (4.2b), where we have used a to fix the zero of phase, as is the role of the phase standard. As expected, the relative phase between a and b varies randomly from realisation to realisation, however, there is always a fixed phase difference of $\pi/2$ between b and c. This is consistent with the fact that resonant Raman coupling is formally equivalent to the action of a beam splitter (see Appendix C). The two outputs from a beam splitter acquire a relative phase of $\pi/2$ due to the phase shift on reflection.

We can see how this result arises by setting $\Delta = 0$ in (4.10). This gives $\Omega = \Gamma$ and

$$\phi_{bc}(t) = \arg\left\{iN_b \sin(2\Gamma t)\right\}. \tag{4.11}$$

This agrees with the result (2.14) we obtained in Section 2.4. We see that, for no interactions, all the atoms undergo independent Rabi oscillations, which is what we might expect. It is clear from (4.11) that $|\phi_{bc}|$ has the value $\pi/2$, for all times other than integer multiples of $t = \pi/(2\Gamma)$, at which times the phase is undefined. For $0 < t < \pi/(2\Gamma)$, c always lags b by $\pi/2$, which is in agreement with our simulations.

We can also explain the times for which the phase is undefined as being when all the population is in one mode. For odd multiples of $t = \pi/(2\Gamma)$, mode b is empty and mode c is in the number state $|N\rangle$, the converse is true for even multiples of $t = \pi/(2\Gamma)$. Clearly each of these situations has no phase information. The relative phase arises as soon as there is any entanglement between the modes.

We can consider (4.10) to be the function of two variables: Ωt and Δ/Ω. A plot of how ϕ_{bc} varies with Ωt and Δ/Ω is shown in Figure (4.3). In (4.3a), we set $\Omega t = \pi/4$, which is that value that corresponds to transferring half the population to c in the case of zero detuning, and we plot how ϕ_{bc} varies with Δ/Ω. In (4.3b), we fix $\Delta/\Omega = 0.5$ and investigate how ϕ_{bc} varies with Ωt. Since we are neglecting interactions, these plots are independent of the total number of atoms.

We find that the phase difference between modes b and c tends to $\pi/2$ (with mode b leading) independently in the limit of $\Delta/\Omega \to 0$ or $\Omega t \to 0$. The first limit corresponds to a detuning much smaller than the coupling strength. The second limit corresponds to the case that only a very small fraction of the population is

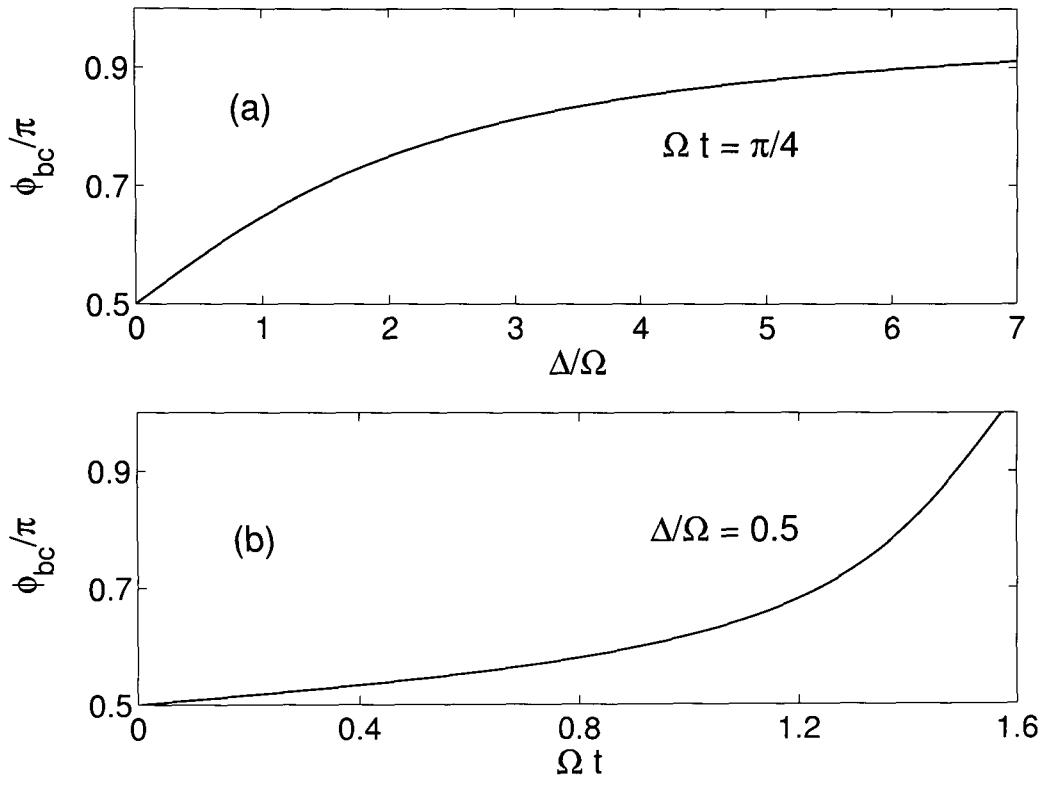

Figure 4.3: Plot of how the relative phase between b and c, ϕ_{bc} varies with (a) Δ/Ω when $\Omega t = \pi/4$, and (b) Ωt when $\Delta/\Omega = 0.5$.

transferred to mode c.

For realistic systems, the interactions play an important role and we would need to include the effect of them in our calculation before making an accurate prediction of experimental results. However, keeping this in mind, we would like to get a feel for the expected phase difference by substituting parameters from a recent experiment.

Hall *et al.* [64, 76] have carried out a transfer of population and presented results for detunings of $\Delta_1 = 2\pi \times 200\text{Hz}$ and $\Delta_2 = 2\pi \times 350\text{Hz}$. The coupling strength in their experiment was $\Gamma = 2\pi \times 625\text{Hz}$ and half the population was transferred in each step, so $\Omega t \approx \pi/4$.

Neglecting the effect of interactions, for $\Omega t = \pi/4$ and $\Delta_1/\Omega_1 = 0.32$, our calculation predicts a relative phase between b and c of $\phi_{bc}/\pi = 0.55$. For $\Omega t = \pi/4$ and $\Delta_2/\Omega_2 = 0.54$, we predict a relative phase of $\phi_{bc}/\pi = 0.58$. Experimentally, the detuning can be varied readily, allowing control over the phase of the transferred component. With a careful choice of the parameters Ωt and Δ/Ω, we should be

able to transfer condensate components with the phase we want.

4.3 Measurement-induced phase-locking

We would now like to investigate how phase information is communicated along a chain of coupled condensates. This is of particular interest due to the recent experimental demonstration of a mode-locked atom laser [72]. In this experiment, condensates were trapped in the antinodes of an optical standing wave, and each site in this chain was coupled with its neighbours by quantum mechanical tunnelling. The output from the lattice was observed as a train of "mode-locked" atomic pulses, demonstrating that each site has identical relative phases.

We investigate condensates on spatially separated sites, coupled to their nearest neighbours. By inducing a phase at one of the end sites, we can see whether phase information is transported along the chain. In particular, we wish to see whether each mode acquires a fixed and predictable phase relationship with the end mode.

Recently, a study of a coupled two-mode system has been carried out using a semiclassical (mean field) approach [79] which predicts, among other things, phase-locking of the condensate modes. Here, we perform a quantum calculation which also deals with the issue of how the phase symmetry is broken, rather than assuming *a priori* that each condensate can be assigned a phase.

4.3.1 Simulation of phase-locking

The system we consider consists of two condensates, b and c, which are Josephson-coupled. We make measurements which entangle one site with a phase reference condensate as discussed in Chapter 3. Our arrangement is very similar to the one shown in Figure (4.1). In the present case, however, all the modes are in number states with the same number of atoms, and we measure the interference pattern between a and b in the presence of Josephson coupling between b and c. In the previous section, we established a relative phase between a and b and, only after that was done, did we couple modes b and c.

Our simulation in Section 4.2 can easily be modified for this system by including a Josephson coupling term in the system Hamiltonian. The coupling takes the same form as (4.3) with $\delta = 0$. With this inclusion, the system Hamiltonian in the

interaction picture becomes

$$H_0 = \omega_a a^\dagger a + \omega_b b^\dagger b + \omega_c c^\dagger c + \Gamma\left(b^\dagger c + c^\dagger b\right), \tag{4.12}$$

We need to perform a three mode calculation rather than two two-mode calculations as in Section 4.2. This slows down the calculation considerably and for this reason we consider only small atom numbers. For the simulations shown here, we consider 50 atoms in each trap. Halfway through each of the simulations, we turn the detections off and observe how the relative phase evolves under the influence of the Josephson coupling alone.

4.3.2 Results

Results are shown in Figures (4.4) and (4.5). For our simulations, we consider modes b and c to be degenerate with $\omega_b = \omega_c = 5\Gamma$. We take the frequency difference between a and b to be 40 times larger than the atomic detection rate, $\omega_b - \omega_a = 40\kappa$, and we detect about 30 atoms in each realisation.

In (4.4a) and (4.5a) the relative phases between each of the condensates in the chain and the phase standard, ϕ_{ba} and ϕ_{ca}, are plotted as a function of time. In each case, we see that the relative phases jump around for a while before settling down to a regular periodic pattern demonstrating a linear relationship between relative phase and time. This dependence is established while the detections are being made and continues after they are turned off. The discontinuities in Figures (4.4a) and (4.5a) are simply due to the fact that we have plotted the relative phases modulo 2π.

The striking difference between these two results is that in (4.4a) the phases of b and c lock to the same value relative to the phase standard whereas in (4.5a) they are completely out of step. This is illustrated more clearly in Figures (4.4b) and (4.5b), where we have plotted the relative phase between modes b and c as a function of time, $\phi_{bc}(t) = \phi_{ba}(t) - \phi_{ca}(t)$. We see that in (4.4b), ϕ_{bc} oscillates for a while before settling to the constant value $\phi_{bc} = 0$, and in (4.5b) $|\phi_{bc}|$ settles to π, i.e. the modes are exactly out of phase. All our simulations randomly give one of these two results: the phases of the two modes in the chain always either lock or antilock.

We can understand these results if we consider the eigenstates of the system. For a two mode system with linear coupling and no interactions between atoms, the eigenstates are simply the symmetric and antisymmetric superpositions of the

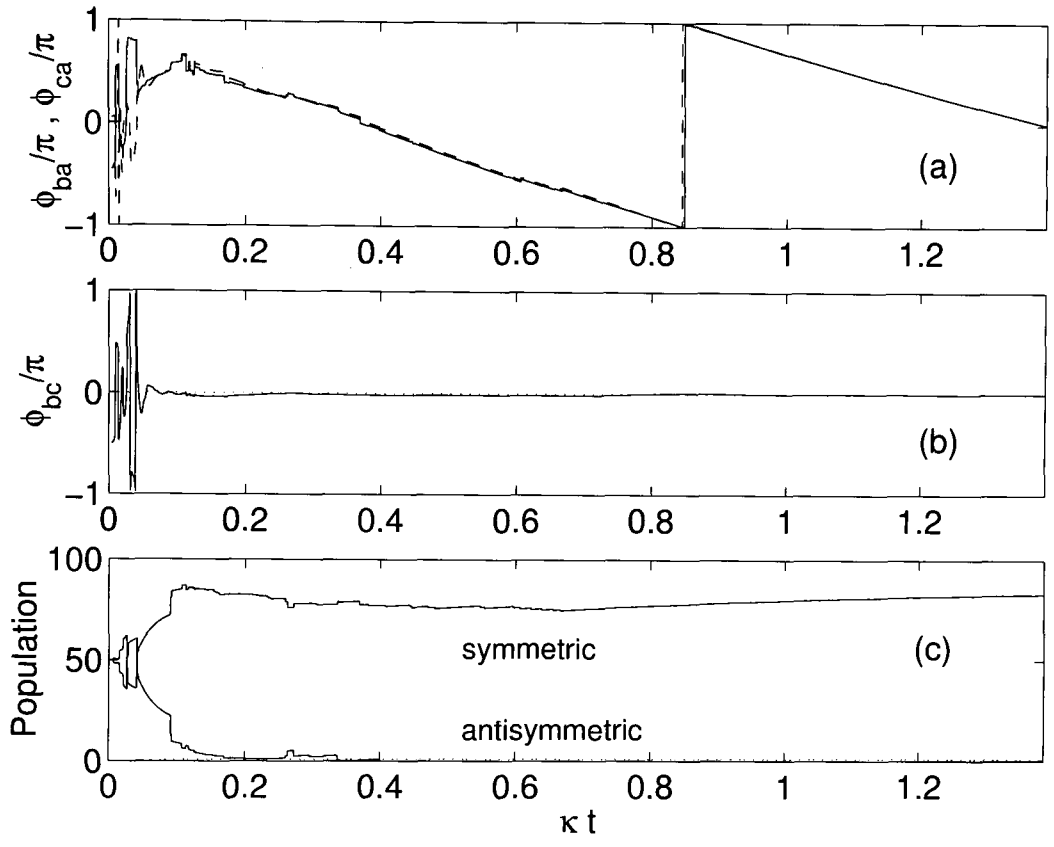

Figure 4.4: Demonstration of phase locking. (a) Plot of the phases of modes b and c relative to the phase standard, ϕ_{ba} (full curve) and ϕ_{ca} (broken curve), as a function of time. (b) Plot of $\phi_{bc} = \phi_{ba} - \phi_{ca}$ against time. (c) Time variation of the populations in the symmetric and antisymmetric superpositions of the trap modes.

trap modes. If we write the trap wave functions for modes b and c respectively as ψ_b and ψ_c, then the eigenfunctions are $\psi_{\rm sym} = \psi_b + \psi_c$ and $\psi_{\rm asym} = \psi_b - \psi_c$. We can write this as

$$\psi = \psi_b + \mathrm{e}^{i\phi}\psi_c, \tag{4.13}$$

where $\phi = 0$ for the symmetric mode, $\psi_{\rm sym}$, and $\phi = \pi$ for the antisymmetric mode, $\psi_{\rm asym}$. The eigenstates correspond to the phases of the two traps either being in phase or antiphase. An analogy can be drawn with two coupled pendulums. The normal modes for this system are the ones where the pendulums swing perfectly in step or half a cycle out of phase.

The tendency for the system to occupy one of the eigenstates is shown in Figures (4.4c) and (4.5c). In these, we have plotted the populations of the symmetric and antisymmetric eigenstates as a function of time. In (4.4c), we see that the

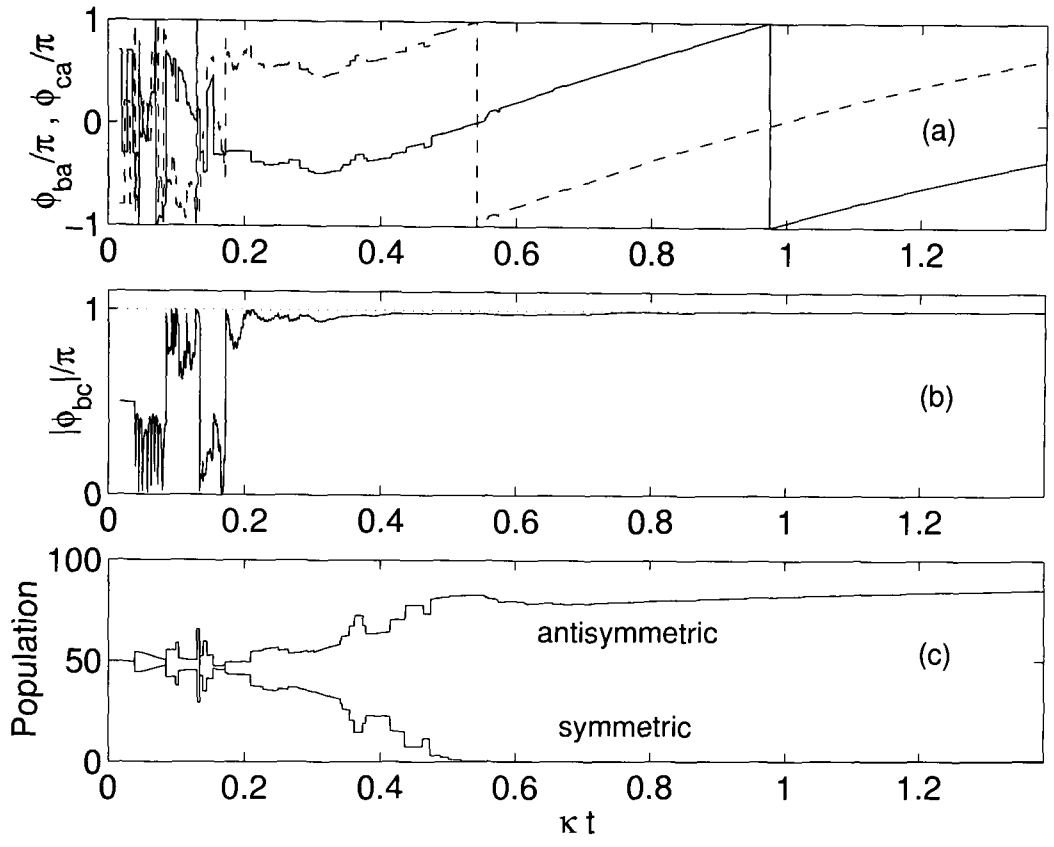

Figure 4.5: Demonstration of phase anti-locking. (a) Plot of the phases of modes b and c relative to the phase standard, ϕ_{ba} (full curve) and ϕ_{ca} (broken curve), as a function of time. (b) Plot of $|\phi_{bc}| = |\phi_{ba} - \phi_{ca}|$ against time. (c) Time variation of the populations in the symmetric and antisymmetric superpositions of the trap modes.

population of the antisymmetric mode vanishes and all the atoms occupy the symmetric mode. This is consistent with the fact that the relative phase between modes b and c tends to zero. The converse is true in (4.5c): all the atoms occupy the antisymmetric mode and the relative phase between b and c tends to π.

It is not surprising that a phase relationship develops between the modes. The coupling between b and c, when we measure the interference pattern between a and b, means that we cannot know from which of the three modes a detected atom has come. This leads to entanglement between all three condensates.

4.3.3 Comparison with a semiclassical model

A useful way to understand these results is to perform a semiclassical analysis of the system. Such an approach is only approximate and requires that we make

certain assumptions, such as each condensate initially having a well defined phase. Nonetheless, it is a powerful technique for understanding the dynamics of the system and has allowed previous authors to predict interesting features such as π-oscillations and macroscopic quantum self trapping [80].

The Hamiltonian for the system is given by

$$H = \omega_b b^\dagger b + \omega_c c^\dagger c + \Gamma \left(b^\dagger c + c^\dagger b \right), \tag{4.14}$$

where $\omega_b = \omega_c$. We can make a semiclassical approximation by making the replacements

$$b(t) = \sqrt{N_b(t)}\, \mathrm{e}^{i\theta_b(t)} \tag{4.15}$$

$$c(t) = \sqrt{N_c(t)}\, \mathrm{e}^{i\theta_c(t)}. \tag{4.16}$$

where $N_{b,c}$ corresponds to the number of atoms in mode b, c and $\theta_{b,c}$ corresponds to the phase of b, c.

Next we define the new quantities of fractional population imbalance,

$$z(t) \equiv \frac{\langle b^\dagger b \rangle - \langle c^\dagger c \rangle}{\langle b^\dagger b \rangle + \langle c^\dagger c \rangle} = \frac{N_b(t) - N_c(t)}{N}, \tag{4.17}$$

where $N = N_b + N_c$ is the constant total number of atoms, and relative phase

$$\phi(t) \equiv \arg \left\{ \langle c^\dagger b \rangle \right\} = \theta_b(t) - \theta_c(t). \tag{4.18}$$

In Appendix B, we derive semiclassical equations of motion in terms of these new quantities [80]. These can be written as

$$\dot{z}(t) = -2\Gamma \sqrt{1 - z^2(t)} \sin(\phi(t)) \tag{4.19}$$

$$\dot{\phi}(t) = 2\Gamma \left(\frac{z(t)}{\sqrt{1 - z^2(t)}} \right) \cos(\phi(t)). \tag{4.20}$$

The stationary solutions are, $\phi = 2n\pi$, $z = 0$, and $\phi = 2(n+1)\pi$, $z = 0$, where n is an integer. We see that the two stationary solutions are when the populations in each trap are equal and the phases (modulo(2π)) are either in step or half a cycle out of step. That is, the stationary solutions are the symmetric and antisymmetric eigenstates of the system. This is in agreement with the results of our simulations.

We can perhaps see this more clearly by taking the time derivative of (4.20)

$$\ddot{\phi}(t) = -2\Gamma^2 \left(\frac{1 + z^2(t)}{1 - z^2(t)} \right) \sin(2\phi(t)). \tag{4.21}$$

If we now linearise (4.21) in z we obtain

$$\ddot{\phi} = -2\Gamma^2 \sin(2\phi(t)) + \mathcal{O}(z^2). \tag{4.22}$$

This is justified since, for non-interacting atoms, our simulations show that if the traps initially have equal populations, the populations remain very nearly equal for all time, i.e. $|z(t)| \ll 1$. Following the argument of Raghavan *et al.* [80], this suggests a mechanical analogy in which a particle, of mass unity, with spatial coordinate ϕ moves in the potential, V, given by $\ddot{\phi} = -\partial V/\partial\phi$. This gives

$$V(\phi) = -\Gamma^2 \cos(2\phi) + \mathcal{O}(z^2), \tag{4.23}$$

which has local minima at $\phi = 0$ as well as $\phi = \pm\pi$, and confirms the results of our simulations that the phases either lock or antilock.

Our simulations show that for non-zero interactions between atoms, the relative phase between the traps depends on the sign of the interaction. For attractive interactions, the system tends towards the symmetric mode with zero phase difference between the traps (a typical trajectory looks like Figure (4.4)). Conversely, for repulsive interactions, the system tends to the antisymmetric mode with π phase difference (a typical trajectory looks like Figure (4.4)). We can see why this is by introducing an interaction term to the Hamiltonian, $H_{\mathrm{I}} = U\left(b^{\dagger 2}b^2 + c^{\dagger 2}c^2\right)$, where U is the interaction strength. With this additional term, the equivalent potential (4.23) becomes,

$$V(\phi) = 4\Gamma UN\cos(\phi) - \Gamma^2\cos(2\phi) + \mathcal{O}(z^2). \tag{4.24}$$

For repulsive interactions ($U > 0$), the dip at $\phi = \pi$ is enhanced and the dip at $\phi = 0$ is reduced. The converse is true for attractive interactions. This is what we might expect if we again consider two coupled pendulums. If the two bobs have repulsive interactions we might intuitively feel that they would be happiest oscillating in antiphase so as to maximise their mean separation and conversely for attractive interactions.

4.4 Natural phase locking

In the previous section, we discussed phase locking along a chain of condensates when a phase was established between the end sites by measurement. In the experiment of Anderson and Kasevich [72], however, no such measurement was made. We would like to understand the mechanism by which the phases could lock in this case.

Such an investigation also has a deeper significance: so far, we have required a measurement procedure to create a relative phase. We pointed out in Chapter 3 that this was a subtle difference between a phase standard and other standards. In this section, we show that such a measurement is not necessary, but that phase can arise due to natural processes. We begin by considering the effect of dissipation at one of the sites. In the following sections, we will consider interactions and then the combined effect of interactions and loss.

4.4.1 Dissipation

We begin by calculating the relative phase for a two mode system with no loss and with each mode initially in the same number state. The phase between modes a and b is given by

$$\phi_{ba}(t) = \arg\left\{\langle N|\langle N|\, U_{ab}^{\dagger}(t)\; a^{\dagger}b\; U_{ab}(t)\,|N\rangle|N\rangle\right\}, \tag{4.25}$$

where

$$U_{ab}(t) = \exp\left[-i\Gamma t\left(a^{\dagger}b + b^{\dagger}a\right)\right], \tag{4.26}$$

if the modes are degenerate. This can be simplified, using (2.13), to give,

$$\begin{aligned}\phi_{ba}(t) &= \arg\left\{\langle N|\langle N|\left[i(b^{\dagger}b - a^{\dagger}a)\sin(2\Gamma t) + (a^{\dagger}b - b^{\dagger}a)\cos(2\Gamma t) + a^{\dagger}b + b^{\dagger}a\right]|N\rangle|N\rangle\right\} \\ &= \arg\{0\}, \end{aligned} \tag{4.27}$$

which is undefined for all time, i.e. the system has no phase information. In fact, a more general definition of phase [50] shows that phase information does exist for this system, but cycles with time. At odd multiples of $\pi/4\Gamma$, the relative phase between the modes is zero, and at even multiples of $\pi/4\Gamma$, the relative phase is undefined. We are only interested in the case where the phase stabilises with time. However, when dissipation is introduced at one site (or both sites), the number symmetry of the system is broken and, as we shall see below, a stable relative

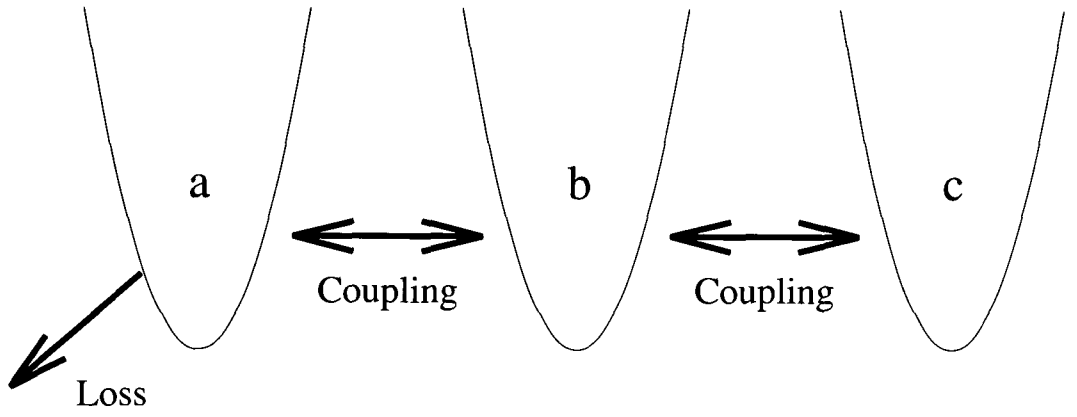

Figure 4.6: Chain of coupled condensates. Each pair of adjacent condensates is coupled by quantum mechanical tunnelling and there is dissipation from mode a

phase can develop between the modes.

For our simulations, we consider a chain of three condensates, all initially in number states with the same number of atoms. Each mode is coupled to its neighbours by quantum mechanical tunnelling (see Figure (4.6)).

We use a quantum jump method (as outlined above) to simulate the loss process from mode a. A phase will not be established if the modes are degenerate. For simplicity, we take the mode frequencies to be in the ratio $\omega_a : \omega_b : \omega_c = 1 : 2 : 3$. We take the ratio of the mode couplings to the trap frequencies as, $\Gamma/\omega_a = 0.1$ and the ratio of the detection rate to the trap frequencies as, $\kappa/\omega_a = 0.01$. This means that the loss rate is much smaller than the coupling frequency which is, in turn, much smaller than the trap frequencies. We take $N = 50$, i.e. each trap is initially in a number state with 50 atoms. Typically about 30 atoms are lost from mode a for each trajectory. To begin with, we ignore interactions between atoms.

The result of a simulation for a single trajectory is shown in Figure (4.7). In (4.7a) we have plotted the relative phase between modes a and b. As expected, the phase is initially undefined, which corresponds to the time before an atom is lost from the trap. However, once an atom has been lost, a phase develops between the modes. We see in (4.7a) that this is initially unstable and fluctuates for a while before settling down to a steady linear relationship with time. The discontinuities are again an artifact of plotting the phase modulo 2π.

The linear relationship in the plot is due to the fact that there is a frequency difference between modes a and b. We would expect there to be a deterministic

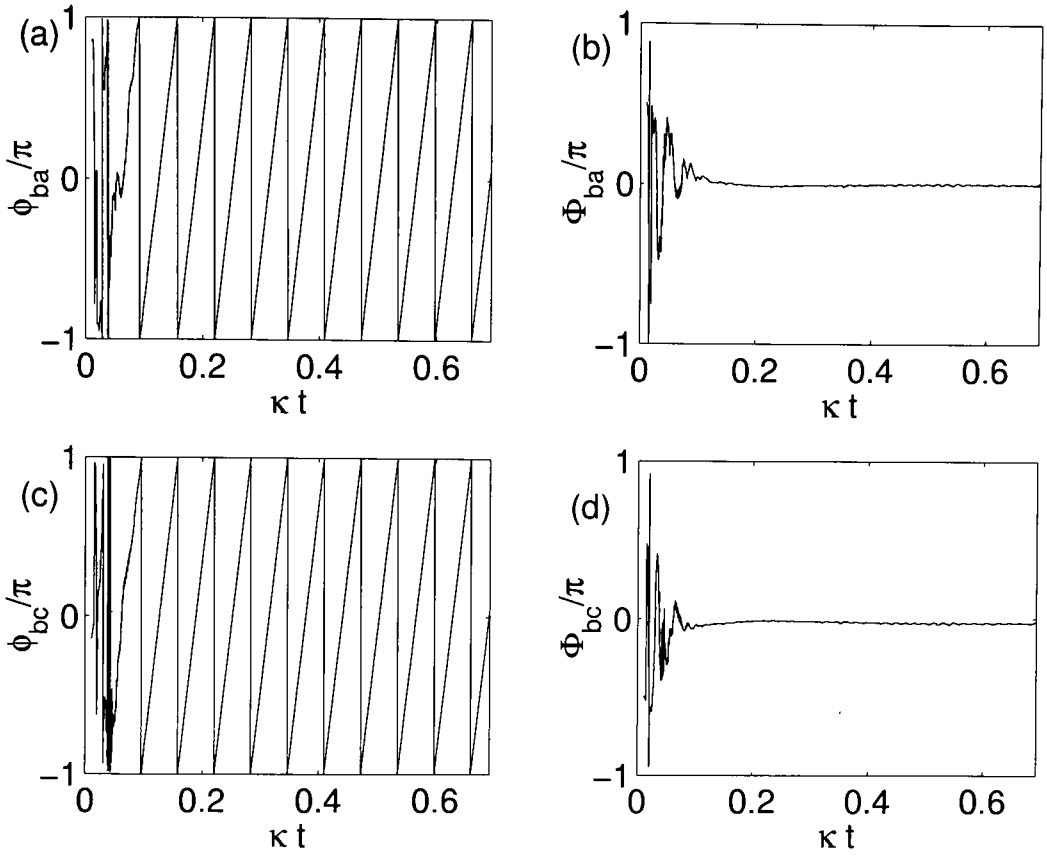

Figure 4.7: Phase locking due to dissipation. In each figure we have plotted phase against the dimensionless quantity κt: (a) ϕ_{ba}, (b) ϕ_{ba} with the deterministic part removed, (c)ϕ_{bc}, (d) ϕ_{bc} with the deterministic part removed. There are initially 50 atoms in each mode.

component of the relative phase dependent on $\omega_b - \omega_a$, which allows us to write the time dependence of the relative phase as

$$\phi_{ba} = (\omega_b - \omega_a)\, t + \Phi_{ba}, \tag{4.28}$$

where Φ_{ba} accounts for the stochastic non-deterministic part and can be thought of as the ϕ_{ba}-axis intercept if we were to fit a line to the linear part of the plot. In Figure (4.7b), we have plotted the time dependence of Φ_{ab}. This fluctuates for a while before settling to zero. The corresponding results for modes b and c are shown in (4.7c) and (4.7d) and we see that we get very similar results.

In this case, we do not detect atoms as they are lost from the condensate and so do not know the times at which they escape. This means that, unlike previous cases which deal with direct detection [81], we need to average over all trajectories. This

is equivalent to using a density matrix description which formalises our uncertainty of the escape times.

The relative phase between the condensate modes is given, in terms of the density matrix, as

$$\phi_{ba}(t) = \arg\left[\mathrm{Tr}\left\{\rho(t)a^\dagger b\right\}\right]. \tag{4.29}$$

It is straightforward to show that the time dependence of the phase of our system is given by simply averaging over the relative phases of individual trajectories.

We might expect that each trajectory will settle to a well defined phase, but that this phase will vary randomly from run to run. This would mean that on the ensemble average the phase information would be wiped out, which was the interpretation of the results in the papers for which a relative phase was established by measuring the interference pattern between two condensates [47]. In our case, however, a remarkable thing happens. In Figures (4.7a) and (4.7c), the results of each trajectory are random and different for the initial fluctuating time, but then they always overlap in the linear region. This is seen more clearly in (4.7b) and (4.7d) when the deterministic part of the phase has been removed. We see that, although random to begin with, every trajectory rapidly settles to zero phase difference between the modes.

Since all the trajectories settle to the same value, we have an example of a system for which the phase persists even in the ensemble average. This is a remarkable result: our uncertainty in the times of the loss of the atoms does not wipe out the phase.

The establishment of phase can be explained in a similar way to that of Javanainen *et al.* [47]. Although all the atoms are removed from a, the modes are all coupled, so we do not know which mode the atom has come from. This uncertainty leads to entanglement and the establishment of a relative phase.

4.4.2 Interactions

Up until now, we have ignored an effect that will be present in any realistic system: nonlinearities in the Hamiltonian due to the interactions between atoms. In this section, we neglect dissipation and consider the effects of interactions alone.

This is easily simulated within the existing framework by setting the rate of loss to zero and introducing nonlinear terms to the system Hamiltonian. The full

three mode Hamiltonian including interactions and coupling becomes,

$$H_0 = \omega_a a^\dagger a + \omega_b b^\dagger b + \omega_c c^\dagger c + \Gamma\left(a^\dagger b + b^\dagger a + b^\dagger c + c^\dagger b\right) + U\left(a^{\dagger 2}a^2 + b^{\dagger 2}b^2 + c^{\dagger 2}c^2\right) \tag{4.30}$$

where, U is the interaction strength. For simplicity, we have assumed that the coupling strength is the same between both pairs of modes and that the same is true of the interaction within each mode. We will take the modes to be degenerate $\omega_a = \omega_b = \omega_c \equiv \omega$. The evolution for this system is deterministic and so we can evolve a state in time by direct integration.

The validity of the Hamiltonian (4.30) is discussed in detail elsewhere [82, 83] and essentially rests on the assumption that the many-body interactions produce only small modifications of the ground state properties of the individual potentials. In the weakly interacting limit we can ignore the cross interaction terms. Our results do not rely on this assumption, but it is a convenient one to make as it simplifies our calculations.

We use the experimental parameters of the experiment of Anderson and Kasevich [72]. In this case, the kinetic energy per particle is $E = k_{\mathrm{B}} \times 157\mathrm{nK}$, the interaction energy per particle is $U/N \equiv \tilde{U} = k_{\mathrm{B}} \times 4\mathrm{nK}$, and the wavelength of the optical standing wave that forms the lattice is $\lambda = 850\mathrm{nm}$. From these, we can determine the ratio of the interaction energy per particle to the kinetic energy per particle, $\tilde{U}/E \approx 0.03$. If we make the same assumption as Anderson and Kasevich, that the well depth, ϵ, is approximately equal to the kinetic energy per particle, E, we can estimate the coupling rate per oscillation

$$\frac{\Gamma}{\omega} \approx \exp\left(\frac{-\lambda E^2}{8\hbar^2 g}\right) \approx 0.01, \tag{4.31}$$

where g is the acceleration due to gravity. This exponential sensitivity to the acceleration due to gravity suggests that this scheme may have a useful application as a sensitive detector of g. We now have realistic experimental parameters for our simulations, we take $U/N\omega = 0.03$ and $\Gamma/\omega = 0.01$. As was shown in Equation (4.27), we need to start with a different number of atoms in each of the modes.

The result of a simulation, for modes a, b, and c initially having 50, 49, and 48 atoms respectively, is shown in Figure (4.8). We see that the relative phase between each pair of modes rapidly damps to zero. For the parameters we use here, it takes about 30 trap oscillations to stabilise to zero relative phase. Other simulations demonstrate that the rate of damping increases with the interaction energy. For

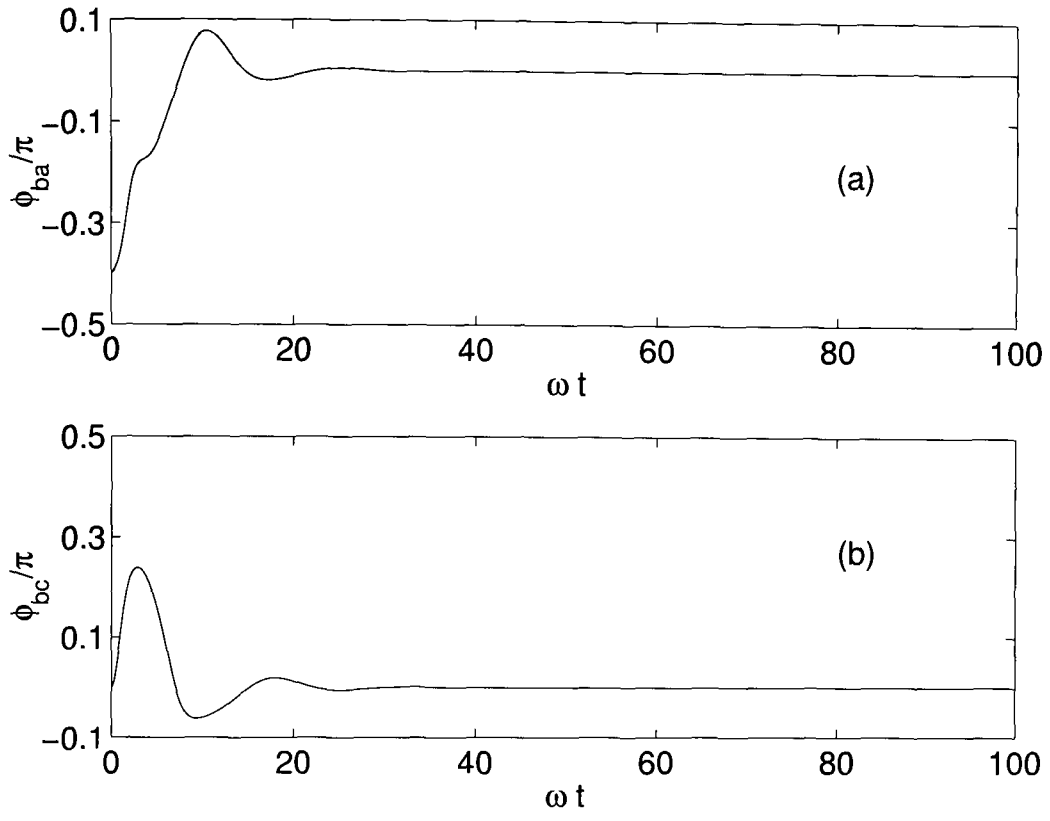

Figure 4.8: Phase locking due to atomic interactions. In each case, the phase is plotted against ωt (i.e. number of trap oscillations).

repulsive interactions, the modes lock in phase and for attractive interactions, the modes anti-lock. This is consistent with the results for measurement-induced phase establishment.

Our results show that interactions (as well as dissipation) when combined with Josephson coupling between condensates, establish a phase. This can be explained by the modes becoming entangled due to the coupling. Interactions have the advantage of establishing a phase for degenerate modes. Unlike the case of dissipation, however, there must be a number asymmetry between the modes in the initial state. Ideally, we would like a scheme that supports both, so that a phase "naturally arises" for the most symmetric initial case.

4.4.3 Dissipation and interactions

In a full realistic model, there will be interactions between atoms as well as dissipation from the condensate modes. In this section, we wish to see whether,

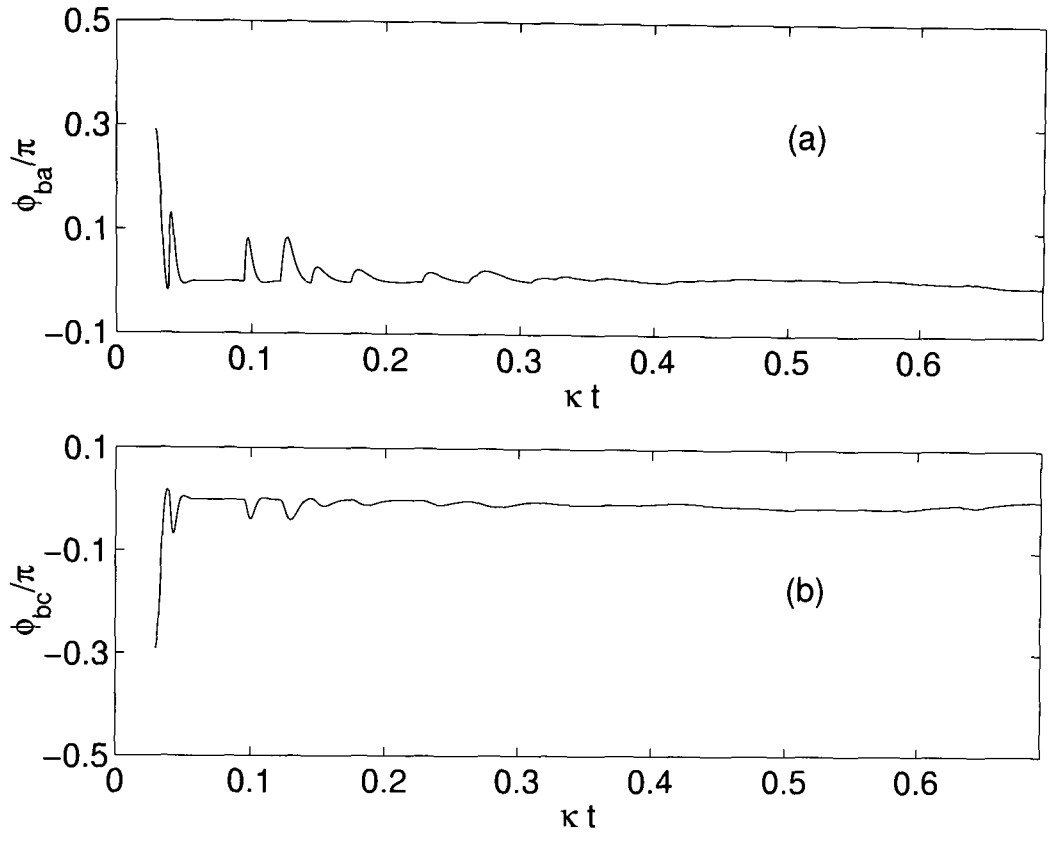

Figure 4.9: Phase locking due to interactions and dissipation. There are initially 50 atoms in each mode and the system parameters closely match experiments (see text). The phase is plotted against the unitless quantity κt.

by including both effects, phase locking arise for all cases: notably for the most rigorously symmetric case of degenerate modes in equal number states.

Our simulation process is the same as in Section 4.4.1, but with the nonlinear terms included in the Hamiltonian, as in (4.30). We take the experimental parameters as outlined in Section 4.4.2, with the one additional parameter of dissipation rate. It was noted in [72] that this rate was much smaller than the coupling rate. So, for our simulations, we take $\kappa/\omega = 0.001$.

When we include dissipation as well as interactions, we can start with degenerate modes each in the same number state. The result for one trajectory, with 50 atoms initially in each mode, is shown in Figure (4.9). For repulsive interactions, the modes lock in phase for each trajectory. This means that the phases lock on the ensemble average and we do not have to make a measurement for this process to occur. For attractive interactions, the phases of adjacent modes antilock. Again, this is consistent with our previous results.

We see that the phase locking is not as rapid or as clean as for the case of interactions alone. For the parameters used here, it takes about 300 trap oscillations for the phases to lock as compared with about 30 for no dissipation. This can be explained by the fact that the dissipation corrupts the entanglements between the modes and so degrades the phase relationship between them.

Since we have shown that phases lock (or antilock) for the most symmetric system, we know that this is true for all initial states. We have shown that Josephson coupled condensate modes with repulsive interactions and dissipation will always lock in phase, *independent of the initial state.* This is a powerful result and explains the experimental observations of the mode-locked atom laser [72].

4.5 Conclusions

We have seen that a transfer of population between two modes leads to a relative phase between them due to entanglement. This phase is $\pi/2$ for resonant coupling which is consistent with its correspondence with a beam splitter. For non-zero detunings, the relative phase can take different values. A study of this transfer process shows how we could predict and control the phase of the output pulses from an atom laser and the position of interference fringes in interferometry schemes involving condensates.

By extending these ideas, we have studied the effect on a chain of coupled condensates of making measurements which establish a phase at one of the lattice sites. Our simulations show that the system always relaxes into one of the eigenstates of the system and which eigenstate this is depends on the sign of the interatomic interactions. These results should be able to be extended to a long chain of condensates.

Finally, we have considered mechanisms by which a phase naturally arises for the case of degenerate modes initially in equal number states. We have found that phase locking occurs for all systems where dissipation and interactions are present.

Our findings in this last section are three-fold. Firstly, by considering a model that closely matches the mode-locked atom laser of Anderson and Kasevich, we have demonstrated a mechanism by which the phases of the condensate modes lock and that this is completely independent of the initial state of the system. Secondly, we have demonstrated a system where the phase persists even on the ensemble average. Thirdly, we have provided an example of a system for which we would expect relative phases to occur naturally due to dissipation and interactions.

This is in agreement with observation of such systems and is a significant advance on previous proposals which have required a measurement on a pair of condensates to *create* a relative phase between them.

CHAPTER 5

PHASE RESOLUTION

We have discussed two different ways that a relative phase may be established between Bose-Einstein condensates. One way is to measure an interference pattern between them in their region of overlap [47, 48, 84]. Another is to allow them to exchange atoms by coupling them. These two methods are distinct, but both rely on creating an entanglement. Up until now, we have considered only the mean value of the relative phase. In this chapter we investigate the resolution of the phase produced by these two methods. We want to see whether these methods can be distinguished by the nature of the phase of the final state.

The fact that the interference pattern measured between two condensates, initially in number states, cannot be distinguished from the interference pattern that would be measured if the two condensates were initially in coherent states [55] suggests that the phase developed by such a measurement is 'classical' in nature. We would like to investigate this further and to see if it is also true for condensates which have been entangled by coupling. In particular, we would like to see whether coupling can lead to better phase resolution than can be obtained by measurement.

5.1 Measurement resolution

Let us begin by considering the case of measurement. We consider two condensates, a and b, both initially in number states with n atoms, $|\psi_0\rangle = |n\rangle|n\rangle$. We allow atoms from the two traps to fall onto a detector and record the times at which atoms are detected.

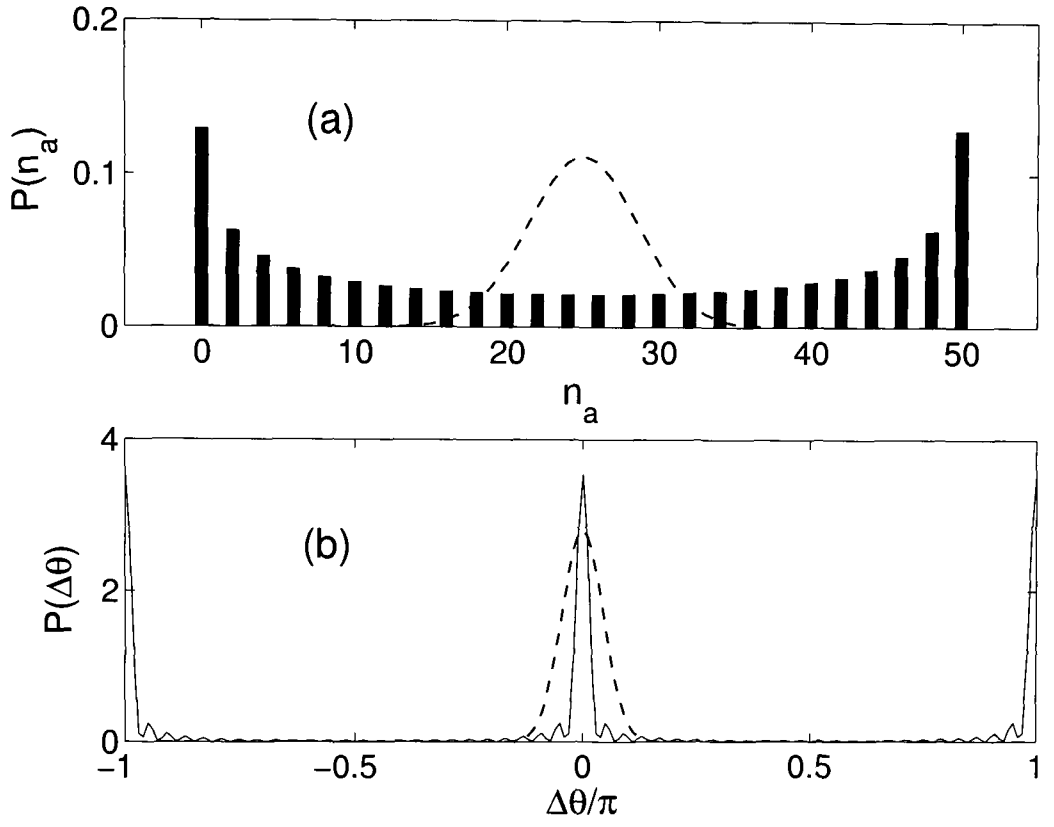

Figure 5.1: (a) The number probability distribution for mode a for a measurement-induced entanglement (dashed line) and for entanglement due to coupling (bar graph) for a state with 50 atoms. (b) The relative phase distribution for the same two states (dashed line for measurement and solid line for coupling).

In the Heisenberg picture, when an atom is detected at time, t, the state, $|\psi_0\rangle$, is acted on by

$$C = \frac{1}{\sqrt{2}}\left(a\,\mathrm{e}^{-i\omega_a t} + b\,\mathrm{e}^{-i(\omega_b t-\phi)}\right), \tag{5.1}$$

where ω_a and ω_b are the frequencies of traps a and b. The additional phase factor, $\phi = 2\pi\delta/\lambda_{dB}$, depends on the path length difference, δ of the two traps from the detector, and the de Broglie wavelength of the atoms, λ_{dB}. For equal path lengths, ϕ would vanish. Each detection contributes a different value of ϕ depending on where the atom is detected. This leads to a random mean relative phase. The phase resolution, however, does not depend on where the atoms are detected so, without loss of generality, we set $\phi = 0$.

If the modes are degenerate, $\omega_a = \omega_b$, and we transform (5.1) to a frame rotating at the same frequency, this can be written as $C = (a + b)/\sqrt{2}$. For simplicity, we

consider that a total of n atoms are detected (i.e. half of them). The final state, $|\psi\rangle$, is then given by

$$\begin{aligned} |\psi\rangle &\propto \left[\frac{1}{\sqrt{2}}(a+b)\right]^n |n\rangle|n\rangle \\ &\propto \sum_{m=0}^{n} \left(\frac{n!}{m!\,(n-m)!}\right)^{3/2} |n-m\rangle|m\rangle. \end{aligned} \tag{5.2}$$

As we would expect, this is an entangled state and so there is a phase relationship between the modes. The probability distribution for there being n_a atoms in mode a is shown as the dashed line in Figure (5.1a) for $n = 50$. The number distribution has acquired a finite width due to the entanglement.

We would now like to examine the nature of the phase distribution of this state. To do this, we make use of the Pegg-Barnett basis of states of well-defined phase [49, 50, 51] that we introduced in Chapter 2. A straightforward calculation of this distribution yields,

$$P(\Delta\theta) \propto \left| \sum_{m=0}^{n} \left(\frac{n!}{m!\,(n-m)!}\right)^{3/2} \mathrm{e}^{im\Delta\theta} \right|^2 . \tag{5.3}$$

This phase distribution is shown as the dashed line in Figure (5.1b) for $n = 50$.

This function can readily be calculated, allowing us to extract the dependence of the phase resolution on the total number of atoms, $N = n$, in the final state. We determine the full width at half maximum (FWHM), σ_θ, of the phase distribution (5.3) for a range of values of N and then plot $\log_{10}(\sigma_\theta)$ against $\log_{10}(1/N)$. The result, shown in Figure (5.2a), is a straight line with slope 0.50. This means that the phase resolution of the state varies with N as $\sigma_\theta \propto 1/\sqrt{N}$. This is the so-called 'standard limit' and supports the discussion of Cirac *et al.* [55] as it is the same resolution that would be obtained if the two condensates were initially in coherent states.

5.2 Coupling resolution

5.2.1 Coupling to a vacuum state

With this as our benchmark, we would now like to see whether better phase resolution can be achieved when the condensates are entangled by coupling. We begin by considering the case of coupling a number state, $|n\rangle$, to a vacuum state, $|0\rangle$. We

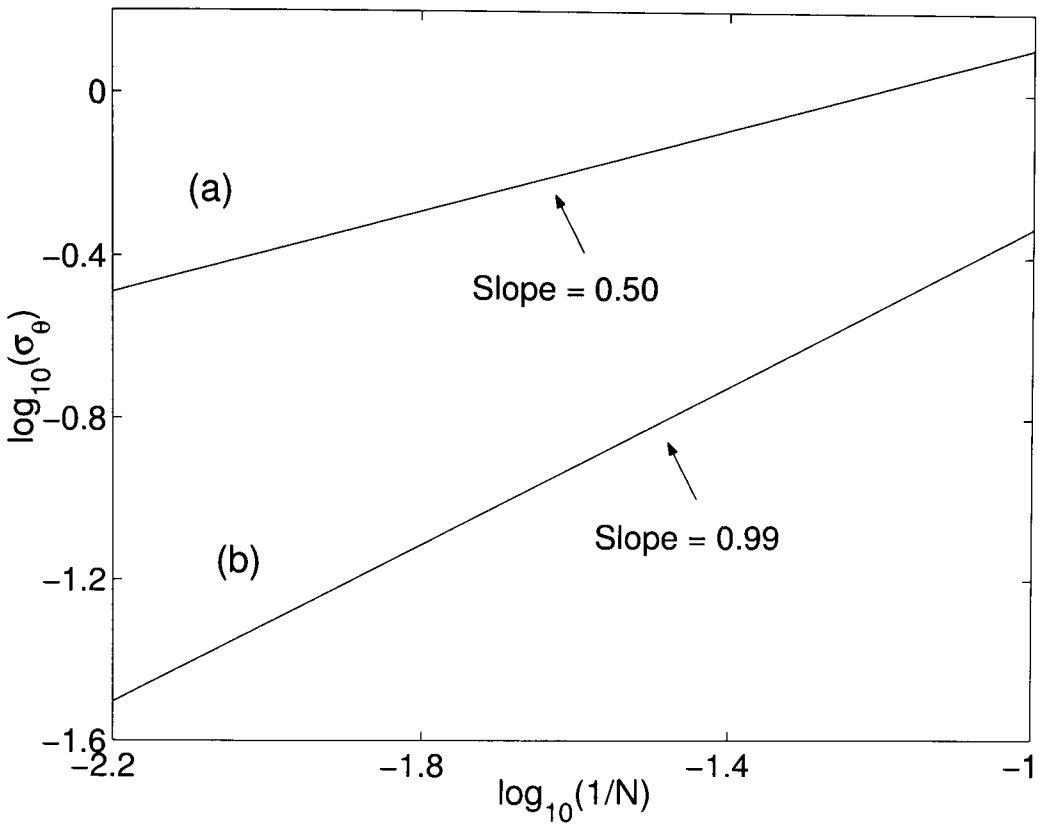

Figure 5.2: Variation of the phase resolution, σ_θ, with total atom number, N, for (a) measurement-induced entanglement, and (b) entanglement due to coupling of number correlated pairs.

consider that the coupling takes the form of resonant Raman coupling as discussed in the previous chapter.

Bouyer and Kasevich have shown that the operation of passing two photon modes, a and b, through a 50:50 beam splitter is formally equivalent to coupling condensate states with resonant Raman pulses for time $t = \pi/4\Gamma$, where Γ is the coupling strength [85] (see Appendix C). The unitary operator for this procedure is,

$$U = \exp\left[i\frac{\pi}{4}\left(ab^\dagger + a^\dagger b\right)\right]. \tag{5.4}$$

In Appendix A, we derive the output of passing the state $|\psi\rangle = |n\rangle|0\rangle$ through a 50:50 beam splitter. The result is

$$|\psi\rangle = \frac{1}{\sqrt{2^n}}\sum_{m=0}^{n}\left(\begin{array}{c} n \\ m \end{array}\right)^{1/2} \mathrm{e}^{-im\pi/2}|m\rangle|n-m\rangle. \tag{5.5}$$

The two modes are entangled by the coupling and, as discussed in Chapter 4, a relative phase of $\pi/2$ is naturally introduced between the modes.

We would now like to examine the relative phase distribution. Instead of calculating the probability distribution directly, we can obtain an analytical estimate of the phase resolution by calculating the fidelity, F, of (5.5) with the state shifted by a relative phase $\Delta\theta$, $|\psi_{\Delta\theta}\rangle$. We take the phase resolution to be the value of $\Delta\theta$ for which $F = 1/2$. From (5.5), the fidelity is given by

$$\begin{aligned} F(\Delta\theta) = |\langle\psi_{\Delta\theta}|\psi\rangle|^2 &= \left|\frac{1}{2^n}\sum_{m=0}^{n}\binom{n}{m}\mathrm{e}^{-im\Delta\theta}\right|^2 \\ &= \cos^{2n}(\Delta\theta/2), \end{aligned} \tag{5.6}$$

where the last step follows from recognising that the sum is in the form of a binomial expansion.

We now set $F = 1/2$ and solve for $\Delta\theta$. We use the result that, for $n \gg 1$, $(0.5)^{1/2n} \approx 1 - \ln(2)/2n$. This allows us to write

$$1 - \frac{\ln(2)}{2n} \approx \cos\left(\frac{\Delta\theta}{2}\right) \approx 1 - \frac{1}{2}\left(\frac{\Delta\theta}{2}\right)^2. \tag{5.7}$$

Solving for $\Delta\theta$ we obtain

$$\Delta\theta \approx 2\sqrt{\frac{\ln(2)}{n}}, \tag{5.8}$$

and we recover the same n-dependence of the phase resolution as for the measurement entangled state described in Section 5.1, $\Delta\theta \sim 1/\sqrt{n}$.

5.2.2 Number correlated condensates

In both the methods for entangling condensates described in this chapter so far we have seen that the relative phase resolution is governed by the standard quantum limit. We would now like to see whether it is possible to surpass this limit. As our guide, we turn to a closely related study of optical interferometry.

It has been shown that by using correlated number states as the inputs, the phase resolution of a Mach-Zehnder interferometer can reach the Heisenberg limit, $\sigma_\theta \propto 1/N$ [86, 87, 88, 89]. We take an analogous approach to discuss how a Heisenberg limited relative phase between condensates may be able to be achieved.

In the optical case, if two identical number states are fed into the input ports of a 50:50 beam splitter, the relative phase between the two output modes is Heisenberg

limited. The beam splitter can be considered to rotate the state in phase space in such a way that the phase fluctuations are transferred to the amplitude quadrature and vice versa [87]. A state with minimal amplitude fluctuations before the beam splitter will have minimal phase fluctuations afterwards.

This suggests that for condensates we can follow a scheme similar to that for correlated optical interferometry, by using Raman coupling as the equivalent of the beam splitter. To make an accurate comparison with the measurement case, we start with the state, $|\psi_0\rangle = |n\rangle|n\rangle$. We then turn on two laser fields which resonantly Raman couple the condensates for time $t = \pi/4\Gamma$. The entangled state after this step is,

$$\begin{aligned} |\psi\rangle &= \exp\left[i\frac{\pi}{4}\left(ab^\dagger + a^\dagger b\right)\right]|n\rangle|n\rangle \\ &= \frac{1}{2^n}\sum_{m=0}^{n}\sqrt{\frac{(2(n-m))!}{(n-m)!^2}}\sqrt{\frac{(2m)!}{m!^2}}\,|2(n-m)\rangle|2m\rangle. \end{aligned} \tag{5.9}$$

The full derivation of this result is shown in Appendix A.

The probability distribution of the number of atoms, n_a in mode a of (5.9) is shown as a bar graph in Figure (5.1a) for $2n = 50$. There are two notable features. Firstly, the probability vanishes for odd numbers of atoms in each mode. Secondly, and more importantly, the uncertainty in the number of atoms in each mode is much greater than for measurement-induced coupling. In fact, the width of the number distribution in this case is as large as the total number of atoms in the system. This is encouraging since, by the uncertainty principle, an increase in the width of the number distribution may be compensated by a commensurate decrease in the width of the phase distribution.

We would now like to study this phase distribution for this state and compare it with the result for measurement-induced entanglement. Making use of (5.9) and following the same technique as before, the relative phase distribution is

$$P(\Delta\theta) = \frac{1}{2^{2n}(2n+1)}\left|\sum_{m=0}^{n}\sqrt{\frac{(2(n-m))!}{(n-m)!^2}}\sqrt{\frac{(2m)!}{m!^2}}\,\mathrm{e}^{2im\Delta\theta}\right|^2. \tag{5.10}$$

The same result has been derived for photons passing through a beam splitter [86].

The phase distribution for a state of this form with a total number of 50 atoms is shown as the solid line in Figure (5.1b). We see that there is indeed a narrowing of the phase distribution relative to the comparable measurement-induced state.

An additional way in which the two distributions differ is that for the coupled state the relative phase is only known modulo(π). There are additional peaks in the phase distribution at relative phases $\Delta\theta = \pm\pi$. This is a feature which turns out to be very useful when it comes to exploring the possibility of creating Schrödinger cat states in Bose condensates. We shall revisit it in Chapter 7 when we consider how such states may be made. This is also consistent with our findings in Chapter 4 that the relative phase always settles to $\Delta\phi = 0$ or $\Delta\phi = \pi$.

As for the measurement case, we find the N-dependence of σ_θ by calculating this distribution for different values of $N = 2n$. A plot of $\log_{10}(\sigma_\theta)$ against $\log_{10}(1/N)$ is shown in Figure (5.2b). As was the case for the results shown in Figure (5.2a), this is a straight line which indicates that σ_θ has the same functional form as for the measurement case, $\Delta\theta \propto 1/N^r$. However, we immediately notice two differences from the result in (5.2a). Firstly we see that the phase resolution is much better than for the measurement case: for 160 atoms, the resolution is roughly an order of magnitude better. Secondly, the slope of (5.2b) is greater than (5.2a), which indicates that σ_θ has a stronger N-dependence. A fit through the points gives a value very close to $r = 1$, which means that $\sigma_\theta \propto 1/N$, i.e. the phase is Heisenberg limited. This is an important result as it shows that we can achieve the fundamental limit of phase resolution (as governed by the uncertainty principle) by coupling condensates.

To achieve the Heisenberg limit, it is important that the initial number states are correlated in order to minimise amplitude fluctuations. This may be able to be achieved by amplitude squeezing the initial joint state [90, 91] or by creating correlated atom pairs by a process such as four-wave mixing [92, 93]. In the next chapter, we present a straightforward scheme for how such relative number squeezing may be able to be achieved.

Our starting state, $|\psi_0\rangle = |n\rangle|n\rangle$, is highly squeezed and non-classical. We see from the results in the first part of this chapter that, by measuring the phase of this state, we degrade the quality of the phase information that it can contain to the standard limit. In general, however, our initial state will not be squeezed but will qualitatively be like Equation (5.2), i.e. it will be an entangled state which allows the total number of atoms to be fixed but the number in each condensate to be uncertain. In this latter case, the measurement process doesn't degrade the quality of the phase as it has already been brought down from the squeezed Heisenberg limit. Classical states of the form of Equation (5.2) are attractors of phase measurements and so further measurements will not disrupt them. This

tells us that if we start with a non-classical squeezed state, we should perform the operations we want with this state (e.g. as the input to an interferometer) and extract information from it only at the end. As soon as measurements are made on the state, the useful phase information that it can contain is degraded until it reaches the classical level.

In summary, we have demonstrated that the nature of the relative phase between condensates depends on the method of entangling them. The entanglement that arises when we measure an interference pattern between condensates, leads to a phase resolution given by the classical standard limit, $\sigma_\theta \propto 1/\sqrt{N}$. This is the same resolution that is achieved when a condensate is coupled to a vacuum mode. However, when number correlated condensates are entangled by coupling, the nature of the phase is very different and the phase resolution can reach the fundamental Heisenberg limit, $\sigma_\theta \propto 1/N$. These Heisenberg limited states may have important consequences for applications such as interferometry and frequency standards where phase resolution is of utmost importance. They may also provide a valuable tool for investigating the nature of entanglement. We will discuss further uses for them in the following chapters.

CHAPTER 6

RELATIVE NUMBER SQUEEZING IN CONDENSATES

6.1 Introduction

In the previous chapter we saw that number correlated condensates are a powerful quantum resource. They can be used to generate states with Heisenberg-limited relative phase [85, 94] which may be of great importance in interferometry schemes [86, 91]. In this chapter we describe how number correlated pairs of condensates may be created. The method we outline does not depend strongly on knowing the number of atoms in the initial condensate and works even in the presence of large losses. It may therefore prove to be a practical technique for generating this resource.

We begin with a quantum calculation for small numbers and show that, using only light pulses, it is possible to generate states that are strongly squeezed in their relative number. This enables us to validate a semiclassical model and derive some analytical results. We then use the semiclassical model to predict the scaling for large numbers. Finally, we consider the effects of dissipation and show that this method is relatively robust to the loss of atoms.

6.2 Quantum analysis

The model we use is similar to one proposed by Cirac *et al.* for creating superposition states of Bose condensates [95]. We consider two condensate modes

represented by the annihilation operators a and b. Mode a is initially in a number state, $|N\rangle$ and b is initially in the vacuum state, $|0\rangle$. We then couple these two modes with resonant Raman pulses to create a pair of condensates with a relative phase defined to the standard quantum limit. If this step is very fast compared with the timescale of the nonlinear evolution, we can ignore the effects of interactions. After a quarter Raman cycle, the state is given by

$$|\psi\rangle = \mathrm{e}^{i\pi\left(a^\dagger b + b^\dagger a\right)/4}\,|N\rangle_a|0\rangle_b = \frac{1}{\sqrt{2^N}}\sum_{k=0}^{N}\left(\begin{array}{c} N \\ k \end{array}\right)^{1/2} \mathrm{e}^{-i\pi k/2}\,|k\rangle_a|N-k\rangle_b. \qquad (6.1)$$

This is a superposition of states with different relative numbers of atoms in the two modes. The relative phase, $\Delta\theta$, of this state scales with number in the same way as the broken symmetry state that can be produced by measurement, $\Delta\theta \sim 1/\sqrt{N}$, as discussed in Chapter 5. The number correlation between the modes in (6.1) is weak and we would like to squeeze the relative number distribution.

To do this, we first apply an intense far detuned light pulse to one or both modes to shift the phase of a relative to b by $-\pi/2$ [96]. This pulse shifts the zero point of the energies and, provided that the pulse interacts with each mode with a different coupling strength, will result in a fast phase evolution which changes the relative phase between the modes. Another scheme for achieving this phase shift is outlined by Gordon and Savage [96] and involves shifting the phase of the light fields that provide the Josephson coupling in creating state (6.1). The state after this step is

$$|\psi\rangle = \frac{1}{\sqrt{2^N}}\sum_{k=0}^{N}\left(\begin{array}{c} N \\ k \end{array}\right)^{1/2} \mathrm{e}^{-i\pi k}\,|k\rangle_a|N-k\rangle_b, \qquad (6.2)$$

which we take to be the initial state of our squeezing procedure.

Next we couple the two condensate modes with resonant Raman pulses, which is equivalent to Josephson coupling the modes, and we allow them to evolve under the influence of the nonlinear interactions. The Hamiltonian for this evolution is taken to be

$$H = U\left(a^{\dagger 2}a^2 + b^{\dagger 2}b^2\right) + \Gamma\left(a^\dagger b + b^\dagger a\right), \qquad (6.3)$$

where Γ is the coupling strength and U is the interatomic interaction strength which, for simplicity, we take to be the same for each mode. For convenience, we have taken the cross interactions to vanish [83]. This is not a necessary assumption for this scheme to work. We also take the trap frequencies to be the same for the two modes and have removed them by transforming to a rotating frame. The

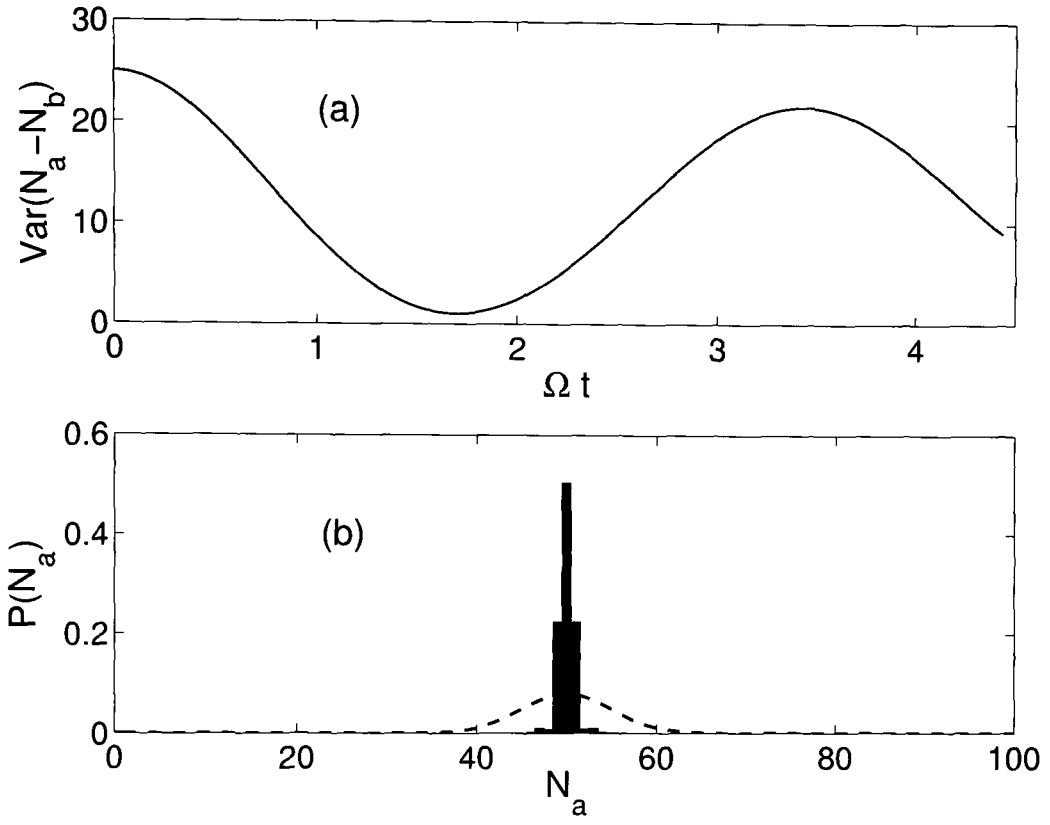

Figure 6.1: (a) Time variation of the variance of $(N_a - N_b)$ as a function of Ωt, where $\Omega = 2\sqrt{\Gamma UN + \Gamma^2}$ (b) Number distribution of mode a at the optimum squeezing time (bar graph) compared with the initial number distribution (broken curve).

parameter U depends on the intrinsic atomic interactions and the shapes of the traps. This can be tuned in principle [97], but for a given experiment is fixed. The coupling rate, Γ, can be controlled by the experimentalist by varying the strength of the coupling laser.

In Figure (6.1), we have plotted how the relative number distribution of (6.2) evolves for the parameters $N = 100$, $U = 0.5$, and $\Gamma = 1$ where, for convenience, U and Γ are unitless quantities scaled by Γ. In Figure (6.1a), we have plotted the variance of $N_a - N_b$ as a function of Ωt, where $\Omega = 2\sqrt{\Gamma UN + \Gamma^2}$. This is a measure of the width of the relative number distribution and we see that it undergoes oscillations. To begin with, the distribution gets narrower with time which is precisely the result we want. For the parameters used here, the maximum squeezing occurs at $\Omega t = 1.67$ and it is encouraging how strong the squeezing is. For the present parameters, a reduction in the variance by a factor of 25 is observed.

The number distribution of mode a at the optimum squeezing time is shown in Figure (6.1b). This is identical to the number distribution of mode b since the total number of atoms in the system is fixed. The original number distribution is also shown as a dashed line for comparison and we see that the modes are strongly number squeezed around the mean value of $N/2$. In other words the two modes are strongly number correlated. Of course, it would be possible to have number squeezing with different a mean number of atoms in each mode. However, the symmetry of the system ensures that the modes are number correlated.

6.3 Semiclassical model

In order to understand these results, we perform a semiclassical analysis of the system [80, 82]. Our results do not depend on this analysis, but we believe it gives considerable further insight into them. The Hamiltonian for the system is given by (6.3) and we can make a semiclassical approximation by making the replacements

$$a(t) = \sqrt{N_a(t)}\, e^{i\theta_a(t)} \tag{6.4}$$

$$b(t) = \sqrt{N_b(t)}\, e^{i\theta_b(t)}. \tag{6.5}$$

where $N_{a,b}$ corresponds to the number of atoms in mode a, b and $\theta_{a,b}$ corresponds to the phase of a, b. This is a reasonable approach to take since, if we look at the form of (6.2), we see that each mode has the form of a coherent state. We can replace the operators with complex numbers containing the mean amplitude and mean phase of each mode.

Next we define the new quantities of fractional population imbalance,

$$z(t) \equiv \frac{\langle b^\dagger b\rangle - \langle a^\dagger a\rangle}{\langle b^\dagger b\rangle + \langle a^\dagger a\rangle} = \frac{N_b(t) - N_a(t)}{N}, \tag{6.6}$$

where $N = N_a + N_b$ is the constant total number of atoms, and relative phase shifted by π,

$$\begin{aligned}\phi(t) &\equiv \arg\left\{\langle a^\dagger b\rangle\right\} - \pi \\ &= \theta_b(t) - \theta_a(t) - \pi.\end{aligned} \tag{6.7}$$

We introduce this shift since we shall see that it is convenient if the initial value of (6.7) is zero when we come to linearise the system. This transformation in no way

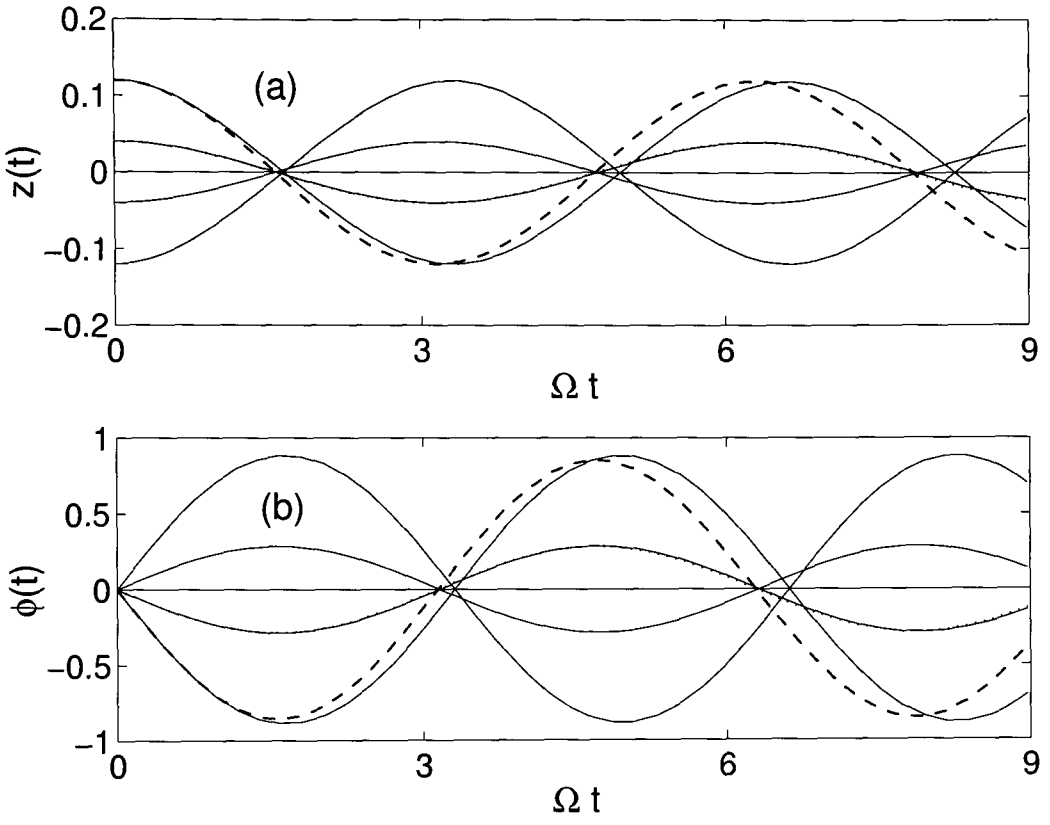

Figure 6.2: Solutions of the semiclassical equations for different initial conditions as a function of Ωt. The $z(t)$ solutions are shown as the full curves in (a) and the corresponding $\phi(t)$ solutions are shown as the full curves in (b). The dashed and dotted curves are corresponding $z(t)$ and $\phi(t)$ solutions of the linearised equations for two different initial conditions.

changes our results. In Appendix B, we derive semiclassical equations of motion for this system [80] in terms of these new quantities. These can be written as

$$\dot{z}(t) = 2\Gamma\sqrt{1-z^2(t)}\,\sin(\phi(t)) \tag{6.8}$$

$$\dot{\phi}(t) = -2UNz(t) - \frac{2\Gamma z(t)}{\sqrt{1-z^2(t)}}\cos(\phi(t)). \tag{6.9}$$

In Figure (6.2), the solid lines show numerical solutions of (6.8) and (6.9) for different initial conditions. We set the parameters to be the same as for the quantum calculation, $U = 0.5$, $\Gamma = 1$, and $N = 100$. Each trajectory corresponds to $z(0) \in \{-0.12, -0.04, 0, 0.04, 0.12\}$ and, since the initial state has a relative phase of π between the modes (see Equation (6.2)), we take $\phi(0) = 0$ for each trajectory.

The quantum state can be thought of loosely as a superposition of these classical realisations. Here we interpret each trajectory to represent part of the initial state and, in particular, a few adjacent terms in (6.2), i.e terms with similar numbers of atoms in mode a. The way that the state is split up into trajectories is arbitrary and does not affect our results. The parameters z and ϕ now respectively represent the mean number difference between modes and the mean phase for each of these parts. The evolution of the whole state can be seen by observing the evolution of each of its parts or trajectories.

We notice that z and ϕ both undergo oscillatory motion, which is what we observed in the full calculation. Importantly, at certain times, z vanishes independent of the initial value of z. We see in Figure (6.2a) that the first focus is sharp and that subsequent focus points become more and more blurred. This means that if we started with an initial state that was a relatively broad superposition of different values of z, and allowed this to evolve under the Hamiltonian (6.3), after some time, the state would be strongly squeezed about $z = 0$. The predictions of the semiclassical model agree well with the full calculation.

Firstly, we would like to understand the times at which the squeezing is optimised. To do this, we assume that $|z(t)| \ll 1$ and $\sin(\phi(t)) \approx \phi(t)$. The second assumption is accurate to within a few percent for $\phi(t) < 0.5$. We will justify these assumptions later.

Linearising (6.8) and (6.9) allows us to write

$$\dot{z}(t) \approx 2\Gamma\phi(t) \tag{6.10}$$

$$\dot{\phi}(t) \approx -2(UN + \Gamma)z(t) \tag{6.11}$$

These equations are very straightforward to solve and give the result

$$z(t) \approx z(0)\cos(\Omega t) \tag{6.12}$$

$$\phi(t) \approx -\frac{\Omega}{2\Gamma} z(0)\sin(\Omega t), \tag{6.13}$$

where $\Omega = 2\sqrt{\Gamma UN + \Gamma^2}$. We see that the conditions $|z(t)| \ll 1$ and $|\phi(t)| < 0.5$ hold for $|z(0)| \ll 1$ and $(\Omega/\Gamma)\, z(0) < 1$.

If we assume that our initial relative number distribution is Gaussian (as is the case for the full calculation) then $|z(0)| <\sim 1/\left(2\sqrt{N}\right)$, and $(\Omega/\Gamma)\, z(0) <\sim \sqrt{U/\Gamma}$. This means that the system is well described by the linear equations (6.10) and (6.11) for $N \gg 1$ and $U/\Gamma < 1$. These conditions are satisfied by the parameters

we use here.

In Figure (6.2), we have plotted the solutions of (a) $z(t)$ and (b) $\phi(t)$ for $(z(0), \phi(0)) = (0.12, 0)$, dashed line, and $(z(0), \phi(0)) = (0.04, 0)$, dotted line. For the dotted solution, $\max(z(t)) = 0.04$ and $\max(\phi(t)) = 0.28$ and our two conditions are satisfied. We see that this approximate solution is very close to the solution of the full equations and it is hard to distinguish the two trajectories in Figure (6.2). For the dashed line, $\max(z(t)) = 0.12$ and $\max(\phi(t)) = 0.86$, the two conditions are not satisfied and we see that this approximate solution is not very good for long times. It does, however, still predict the first squeezing time quite well. We can conclude that the linearised equations should provide a good description of the full model. This allows us to write down an analytical approximation for the optimal squeezing time

$$t_{sq} = \frac{\pi}{2\Omega} = \frac{\pi}{4\sqrt{\Gamma(UN + \Gamma)}}. \tag{6.14}$$

This is in agreement with the result shown in Figure (6.2) and agrees with the quantum prediction of $\Omega t = 1.67$ to within a few percent.

6.4 Effect of loss

In any realistic physical system, there will be some degree of loss due, for example, to collisions. In this section we consider how loss affects our ability to create states with squeezed relative number by including some random loss from modes a and b in the quantum model.

We consider a system with the same parameters as before, $N = 100$ and $U/\Gamma = 0.5$, and consider the rate of damping to be the same from each mode. In Figure (6.3a) we show the number distribution for mode a at the optimum squeezing time and compare it to the initial distribution. For this particular trajectory, 9 atoms were lost from a and 8 from b. We see that the mean number of atoms in a is reduced to around 41 as we might expect, but interestingly the distribution is still strongly squeezed.

In fact, the variance of this number distribution is as small as for the lossless case. The variance of the two modes must be identical since the total number of atoms is equal to some particular value. This means that even for large losses (in this case 17%) the relative number distribution will be strongly squeezed by this method. In realistic cases we would expect the loss to be much less than this.

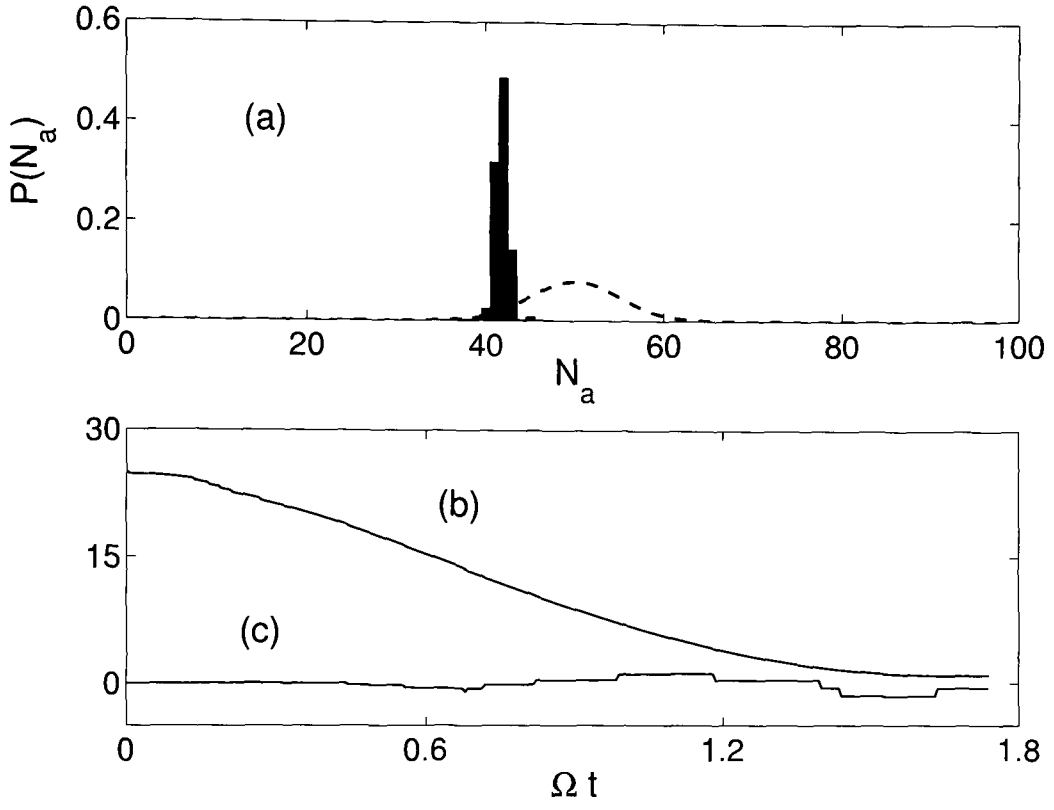

Figure 6.3: (a) Number distribution of mode a at the optimum squeezing time (bar graph) compared with the number distribution of the initial state (dashed curve). (b) Variance of $(N_a - N_b)$ as a function of Ωt. (c) Mean value of $(N_a - N_b)$ as a function of Ωt. For this simulation, 9 atoms were lost from a and 8 from b.

The variance of the number distribution of mode a as a function of Ωt is shown in Figure (6.3b). It exhibits the same behaviour as the lossless case and an almost identical optimum squeezing time. In Figure (6.3c) we show the time variation of the difference of the mean number of atoms in modes a and b. Owing to the loss, this is not necessarily zero and this effect introduces some additional uncertainty into the number correlation between the two modes.

An estimate of the width of the distribution of the difference in mean number is given by $\sqrt{N_{\rm loss}}$, where $N_{\rm loss}$ is the total number of atoms lost. We can write

$$N_{\rm loss} \approx \gamma N t \approx \gamma \sqrt{\frac{N}{\Gamma U}}, \tag{6.15}$$

where γ is the rate of loss per atom per unit time and we have put in the optimum squeezing time. This means that our uncertainty in the difference of the mean

numbers scales as $\sqrt{\gamma}N^{1/4}$. So, for large N or small γ, this is much smaller than the uncertainty in the number difference of the original Gaussian state, which scales as $\sqrt{N}$. This method for creating number correlated condensates therefore works even in the presence of large losses. We have shown that dissipation has little effect on the variance of the squeezed number state and that the relative mean number uncertainty that is introduced is much smaller than the number uncertainty of the original state.

It is not physically clear why this method should be so robust to loss. This seems like an important issue which requires further investigation. We can, however, gain some insight by referring to Figure (6.2a). If we imagine a solution following one of the trajectories in Figure (6.2a), the loss of a few atoms will simply move us to a different trajectory. Since all trajectories focus at the same time, our initial reaction is that it doesn't matter if atoms are lost, there is still optimum relative number squeezing at $t = \pi/2\Omega$. The reason that the number correlation is not as good as the lossless case is that when atoms are lost, although the z solution is moved to another trajectory, the ϕ solution is unchanged. From (6.11) we see that the phase of this new trajectory differs from what it should be for perfect focusing by an amount proportional to the amount z is changed by the loss. From (6.6), we see that the change in z scales as $1/N$ so, for large N, the disruption to the phase of the trajectory is small even for significant losses. This is why this method is relatively robust to loss.

An operational way of thinking of this is to ask how well it is possible to predict the result of a measurement of the number of atoms in the second condensate given the result of an accurate measurement of the number of atoms in the first one. As we have mentioned, there are two effects which reduce the predictability of the number in the second condensate. One is the width of the number distributions in each mode. For the parameters used here, the width of the optimally squeezed state in each mode is given approximately by $\sqrt{N}/10$. The second effect is due to the distribution of the difference in mean numbers of atoms in the two modes, which arises from the loss. As we have seen, this is given approximately by $\gamma\sqrt{N/(\Gamma U)}$. Combining these contributions, the variance of the distribution of possible values of the number of atoms in the second condensate given an accurate measurement of the first is

$$\sigma^2 = \sqrt{N}\left(\frac{1}{5} + \frac{\gamma}{\sqrt{\Gamma U}}\right). \tag{6.16}$$

We see that for large N, there is a dramatic improvement over the result without

squeezing, $\sigma^2 = N$, even for large losses.

So far things look good for the experimental feasibility of this scheme. However, one practical difficulty that arises is that the optimum squeezing time depends on the number of atoms in the system. This suggests that to implement optimum squeezing, we would need to know how many atoms were in the system to begin with. It is very unlikely that we would have this information. Fortunately, the squeezing is relatively insensitive to evolution time. We can see this in Figure (6.1). For example, even if we underestimated N by a factor of 2 and so allowed the system to evolve for $t = t_{\text{opt}}/\sqrt{2}$, where t_{opt} is the optimum squeezing time, the final relative number distribution would still be strongly squeezed. For the parameters used here, the final variance would be about 4.5, which is about 5.5 times smaller than the original state.

For improved correlation, we can imagine a two (or more) step process. In this we could estimate the number of atoms, allow the system to evolve for the estimated optimum squeezing time and then perform a destructive measurement of the number of atoms in one condensate. This would give us an accurate estimate of the number of atoms in the other condensate without destroying it. We could then use this condensate as the starting point for a second relative number squeezing process. This time, however, our improved knowledge of the total number of atoms in the system would allow us to predict the optimum squeezing time more accurately and so create better number correlated condensates.

CHAPTER 7

SCHRÖDINGER CAT STATES IN BOSE CONDENSATES

7.1 Introduction

The theory of quantum mechanics, which successfully describes the physical world on a microscopic level, allows systems to exist in a coherent superposition of different states. When this is scaled up to macroscopic systems, however, an apparent contradiction arises. Our experience is that if a system has several macroscopically distinguishable states available, it will always be in one of them. This anomaly was pointed out in the well-known Schrödinger cat paradox [98]: a thought experiment in which a cat is prepared in a superposition of being alive and dead. Such a state defies our sense of reality.

Despite this, under special conditions which carefully avoid decoherence [99], so-called Schrödinger cat states can be produced in the laboratory. They have been demonstrated in a number of systems including the spatial coordinates of a single atom [100], the internal state of four ions [101], and the current in a superconductor [102].

A Bose condensate consists of a macroscopic number of particles in a single quantum state and so seems to be an ideal system to create similar macroscopic superpositions. There have been some proposals for how approximate cat states may be produced [95, 96, 103], however no such states have been observed yet.

In this chapter, we make use of the understanding of phase and entanglement developed in this thesis to demonstrate a practical way of creating "ideal" cat

states in Bose condensates and suggest how they may be observed. The scheme we present is straightforward and all the steps could be performed with current technology. We want to create states that are a coherent superposition of all the atoms of the system being in one condensate mode (alive) and all the atoms being in the other condensate mode (dead). We can write this as

$$|\psi\rangle = \frac{1}{\sqrt{2}}\left(|N,0\rangle + \mathrm{e}^{i\eta}|0,N\rangle\right). \tag{7.1}$$

States of this form are of great theoretical interest since they may allow us to probe the boundary between quantum and classical physics and perform controlled studies of quantum measurement. They may also have important applications in interferometry [104], frequency standards [105], and quantum information [106, 107].

Our technique is based on the fact that the output from a interferometer can be controlled by varying the relative path length of the two arms. In particular, it depends on the fact that, by introducing a phase shift to one arm, we can arrange for all the atoms (or photons) to emerge from one output port or, conversely, for them all to emerge from the other. We begin by discussing this result.

7.2 Interferometer scheme

In Figure (7.1), we show an interferometer scheme. We consider the input at a to be a number state, $|N\rangle$, and the input at b to be a vacuum, $|0\rangle$. We will find it convenient to use the usual angular momentum commutation relations,

$$J_x = \frac{1}{2}\left(\hat{b}^\dagger\hat{a} + \hat{a}^\dagger\hat{b}\right) \tag{7.2}$$

$$J_y = \frac{i}{2}\left(\hat{b}^\dagger\hat{a} - \hat{a}^\dagger\hat{b}\right) \tag{7.3}$$

$$J_z = \frac{1}{2}\left(\hat{a}^\dagger\hat{a} - \hat{b}^\dagger\hat{b}\right), \tag{7.4}$$

where $\hat{a}$ and $\hat{b}$ are the annihilation operators of modes a and b respectively. These satisfy the commutation relations

$$[J_x, J_y] = iJ_z \qquad [J_y, J_z] = iJ_x \qquad [J_z, J_x] = iJ_y. \tag{7.5}$$

The first step of the scheme involves passing the initial state through a 50:50

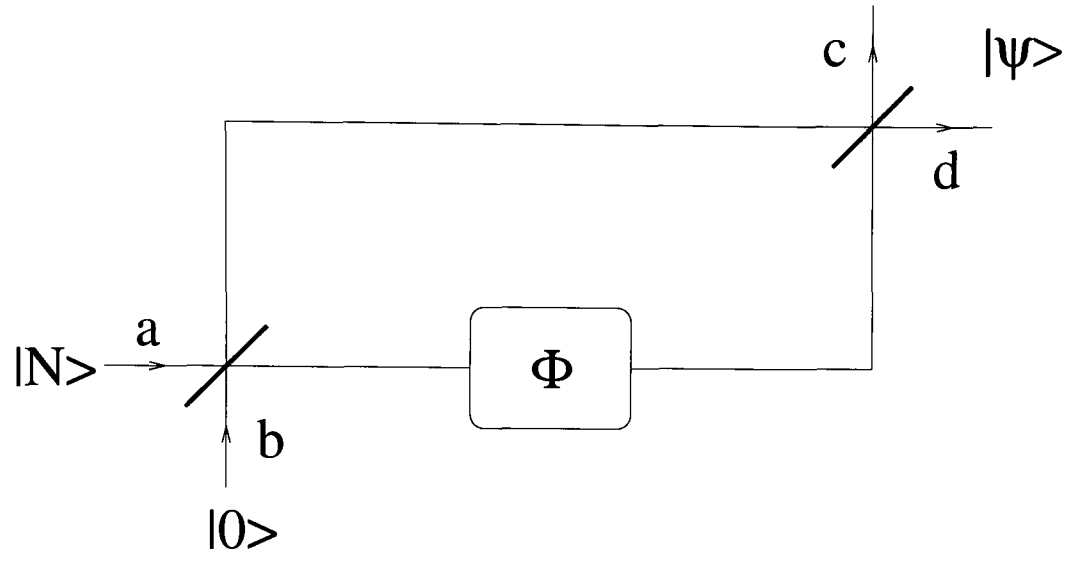

Figure 7.1: Interferometry scheme.

beam splitter. The analogue of this for atoms is to Raman couple the two modes resonantly for a time $t = \pi/4\Gamma$, where Γ is the coupling strength. These two operations are formally identical (see Appendix C) and we will refer to them interchangeably. The operator for this step is $\exp(i\pi J_x/2)$.

As we saw in Section 4.2, this introduces a relative phase of $\pi/2$ between the arms of the interferometer. We can think of this as the phase shift on the component which experiences a reflection at the beam splitter. We wish to keep track of the relative phase throughout, and so we define the phase of the lower arm relative to the upper arm as $\Delta\theta$. After this step $\Delta\theta = -\pi/2$.

Next we introduce a phase shift, ϕ, to mode a. The operator for this step is $\exp(i\phi\hat{a}^\dagger\hat{a})$. However, since we are considering a case where the total number of atoms in the two arms is fixed, we can write this (apart from an irrelevant global phase factor) as $\exp\left[i\phi(\hat{a}^\dagger\hat{a} - \hat{b}^\dagger\hat{b})/2\right] = \exp(iJ_z\phi)$. The relative phase is now, $\Delta\theta = \phi - \pi/2$.

The final step of the interferometer is to recombine the two components with an identical operation to the first step. We can now draw all these steps together and write the full operation of the interferometer as

$$\begin{aligned} e^{i\pi J_x/2}\, e^{i\phi J_z}\, e^{i\pi J_x/2}\, |N\rangle_a|0\rangle_b &= e^{i\phi J_y}\, e^{i\pi J_x}\, |N\rangle_a|0\rangle_b \\ &= -e^{i\phi J_y}\, |0\rangle_a|N\rangle_b. \end{aligned} \tag{7.6}$$

This last step follows since $\exp(i\pi J_x)$ corresponds to a half-cycle Raman pulse which coherently transfers all the population from one mode to the other.

If no phase shift is introduced, $\phi = 0$, (i.e. the relative phase of the two arms entering the second beam splitter is $\Delta\theta = -\pi/2$), the output state from the interferometer is

$$|\psi\rangle = -|0\rangle_c|N\rangle_d, \tag{7.7}$$

and if $\phi = \pi$, (i.e. $\Delta\theta = \pi/2$) the output state is

$$|\psi\rangle = -\mathrm{e}^{i\pi J_y}\,|0\rangle_a|N\rangle_b = -\mathrm{e}^{-i\pi J_z/2}\,\mathrm{e}^{i\pi J_x}\,\mathrm{e}^{i\pi J_z/2}\,|0\rangle_a|N\rangle_b. \tag{7.8}$$

The last step can be checked using the operator theorem [52]

$$\mathrm{e}^{\xi B}\mathrm{e}^{A}\mathrm{e}^{-\xi B} = \exp\left(A + \xi[B,A] + \frac{1}{2!}\xi^2[B,[B,A]] + \ldots\right). \tag{7.9}$$

Operating on the state, (7.8) becomes

$$|\psi\rangle = -|N\rangle_c|0\rangle_d. \tag{7.10}$$

Comparing (7.7) and (7.10) we see that, by varying the relative path length of the two arms, we can arrange for all the atoms to emerge from port c or for them all to emerge from port d.

In order to create our desired Schrödinger cat state (7.1), we wish to form a superposition of these two outcomes. This suggests a possible way to proceed. If we were able to create a state entering the second beam splitter that is a superposition of the two relative phases $\Delta\theta = -\pi/2$ and $\Delta\theta = \pi/2$, the output should be a superposition of the two outcomes (7.7) and (7.10), i.e. it should have precisely the form of (7.1).

Yurke and Stoler have studied such phase superpositions [108]. In particular, they have shown that an optical coherent state passing through an amplitude dispersive medium can evolve into a superposition of two coherent states π out of phase with one another. We would like to form an analogous state for Bose condensates. Conveniently, in condensates the dispersion arises naturally and is due to the nonlinear interactions between atoms. A coherent state of a condensate will undergo collapses and revivals of the phase due to this nonlinearity [69] and midway between these revival times, the state will be a superposition state of precisely the form we want.

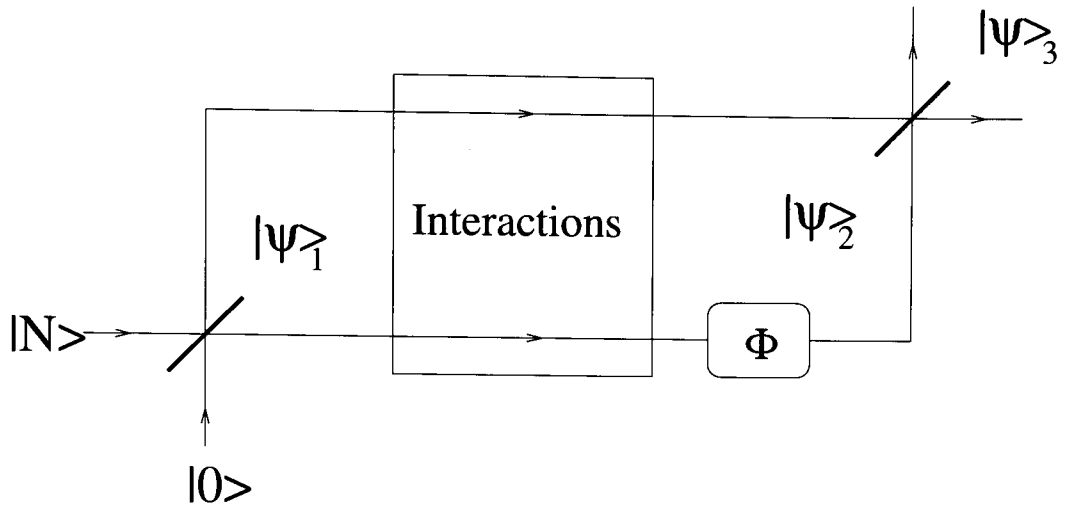

Figure 7.2: Scheme for creating Schrödinger cat states.

We now draw all these ideas together into a practical proposal for creating Schrödinger cat states of the form of (7.1). Our motivation throughout is for all the steps of this scheme to be relatively straightforward to perform in the laboratory.

7.3 Schrödinger cat scheme

The proposal is depicted schematically in Figure (7.2). Our initial state is a Bose condensate in a number state, $|N\rangle$. However, we do not need to know the number of atoms in the state. We stress the fact that this is a readily available resource in the laboratory.

The first step is to couple the condensate to a vacuum mode with resonant Raman pulses. As discussed above, if the modes are coupled for a time $t = \pi/4\Gamma$, where Γ is the coupling strength, this is mathematically equivalent to the operation of a 50:50 beam splitter, and so we depict it as one in Figure (7.2). Importantly, Hall *et al.* have already demonstrated this step in the laboratory [64, 76]. In fact, they have experimentally demonstrated a complete condensate interferometer scheme which is very similar to our proposal. This is very encouraging for the practical feasibility of our scheme.

We consider that this step is very fast compared to the timescale of the evolution due to the nonlinear interaction. This is given by the condition, $\Gamma \gg UN$, where U is the strength of the nonlinear interaction. This means that we can ignore

interactions during the coupling and the state after this step is [96]

$$|\psi\rangle_1 = \mathrm{e}^{i\pi J_x/2}\,|N\rangle|0\rangle = \frac{1}{\sqrt{2^N}}\sum_{k=0}^{N}\left(\begin{array}{c} N \\ k \end{array}\right)^{1/2} \mathrm{e}^{-i\pi k/2}\,|k\rangle|N-k\rangle. \tag{7.11}$$

We now wish to create a superposition of the relative phases $\Delta\theta = \pm\pi/2$ for this state. Here the proposed scheme differs from the interferometer depicted in Figure (7.1). Following the work of Yurke and Stoler discussed above, we can achieve this by allowing the state to evolve naturally under the influence of its interatomic interactions for time $t = \pi/4U$, where U is the interaction strength. To begin with, we consider that U has the same value for each arm of the interferometer and that there are no interactions between the two arms. It turns out that this gives a superposition of two phase states as required. However, this superposition is either of $\Delta\theta = 0, \pi$ or $\Delta\theta = -\pi/2, \pi/2$ depending on whether the total number of atoms in the two arms is even or odd. This means that we would need to know whether the number is even or odd so that we could introduce an appropriate phase shift to create the state with $\Delta\theta = \pm\pi/2$. It's not clear how this could be done experimentally. We need to find a method that creates the correct superposition independent of the total number of atoms.

We can achieve this by considering different interaction strengths in the two arms. In particular, we consider the case where the interaction strength in mode b is an integer multiple of the strength in a, U. The state after an evolution time of $t = \pi/2U$ is

$$|\psi\rangle_2 = \exp\left[i\frac{\pi}{2}\left(\hat{a}^{\dagger 2}\hat{a}^2 + m\,\hat{b}^{\dagger 2}\hat{b}^2\right)\right]\,|\psi\rangle_1, \tag{7.12}$$

where m is an integer. If m is even, $m \in \{..., -2, 0, 2...\}$, and we apply a light pulse to advance the phase of one arm by $\pi/2$, the state can be written as

$$|\psi\rangle_2 = \frac{1}{\sqrt{2^N}}\sum_{k=0}^{N}\left(\begin{array}{c} N \\ k \end{array}\right)^{1/2} \mathrm{e}^{i\pi\left[(m+1)k^2+(m-1)k\right]/2}\,|k\rangle|N-k\rangle, \tag{7.13}$$

We see that the relative phase is no longer N-dependent. For convenience, we set $m = 0$ in the remainder of this chapter, though identical results hold for any even value of m.

Cornish *et al.* have shown how magnetic fields may be used to tune the interaction strength over several orders of magnitude [97]. This would allow the interaction strength of the two arms to be adjusted to the required values and may

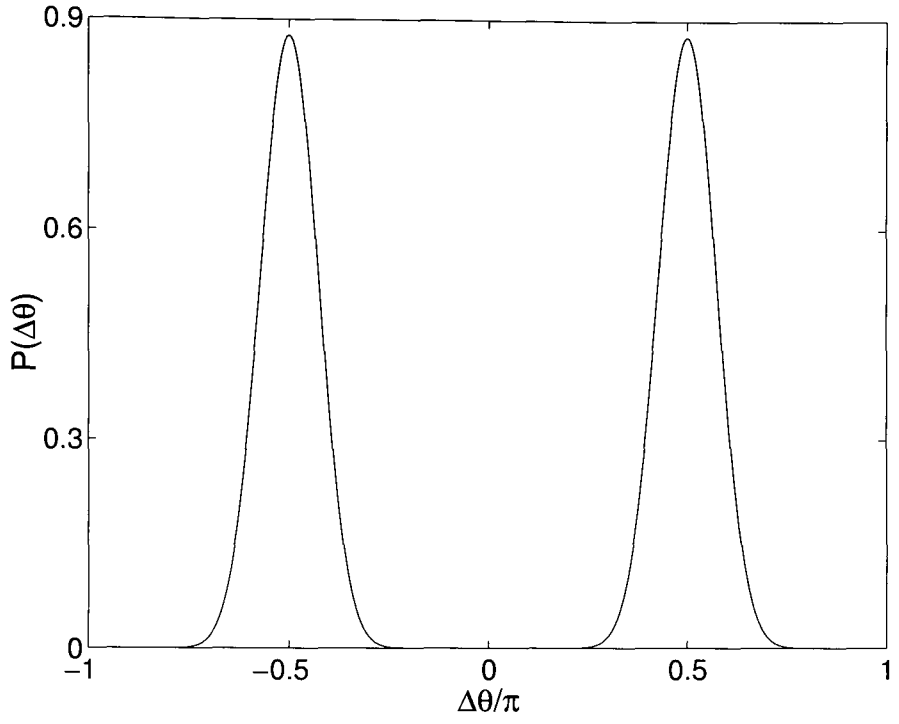

Figure 7.3: Relative phase distribution.

be important in a practical implementation of this step.

Let us now take a moment to examine the phase distribution of (7.13) and to check that it is a superposition of two relative phase values. The relative phase distribution, $P(\Delta\theta)$, of the state $|\psi\rangle_2$ is given by

$$P(\Delta\theta) = \left|\langle\theta_{l-\Delta\theta/\epsilon}, \theta_l|\psi\rangle_2\right|^2, \tag{7.14}$$

where $|\theta_l\rangle$ are the states of well defined phase [49, 50, 51] , which take the form,

$$|\theta_l\rangle = \frac{1}{\sqrt{N+1}} \sum_{p=0}^{N} \mathrm{e}^{ipl\epsilon}|p\rangle, \tag{7.15}$$

where $\{|p\rangle : p = 0, ..., N\}$ denotes the Fock states, and $\epsilon = 2\pi/(N+1)$ is the rotation between adjacent phase states.

The phase distribution of this state is shown in Figure (7.3) for $N = 20$. We see that it is a superposition of the two relative phases $\Delta\theta = -\pi/2, \pi/2$ as required. This form of the state holds for all values of N which is a very satisfying feature since no knowledge of N is required.

Finally, we complete the interferometry scheme by recombining the two components. This is done with Raman pulses identical to those used in the first step. Once again, this is performed much faster than the nonlinear evolution. The final state is then

$$|\psi\rangle_3 = \mathrm{e}^{i\pi J_x/2}\,|\psi\rangle_2. \tag{7.16}$$

After some algebra, this can be written as

$$|\psi\rangle_3 = \sum_{r=0}^{N} C_r\,|r\rangle|N-r\rangle, \tag{7.17}$$

where

$$C_r = \sqrt{r!(N-r)!}\sum_{s=0}^{N}\sum_{t=t_1}^{t_2}\binom{N}{s}\binom{s}{t}\binom{N-s}{r-t}\mathrm{e}^{i\pi(s^2+r-2t)}, \tag{7.18}$$

and $t_1 = \max(0, r+s-n)$ and $t_2 = \min(r, s)$. The derivation of this result is shown in Appendix D. A plot of these coefficients for $N = 20$ is shown in Figure (7.4). We see that the coefficients all vanish apart from C_0 and C_{20}. The final state is then

$$|\psi\rangle_3 = \frac{1}{\sqrt{2}}\left(|20\rangle|0\rangle + \mathrm{e}^{i\eta}|0\rangle|20\rangle\right), \tag{7.19}$$

where η is an unimportant phase. This is precisely the form we want. In fact, this process will work for any value of N, giving (7.1).

7.4 Frequency standard

Huelga *et al.* [105] investigated how cat states could be used to improve frequency standards. In their scheme they considered creating a cat state using a theoretical control-not (CNOT) gate. They then allowed this state to evolve freely for some time before disentangling the cat with another CNOT gate.

They showed that the final population of the two modes oscillates with a frequency enhanced by a factor of N for cat states and pointed out that this should allow for greatly enhanced resolution of the difference in frequencies of the two modes over the free evolution time. In this section, we show how this scheme may be implemented.

Our scheme for creating cats described above is equivalent to the quantum gate

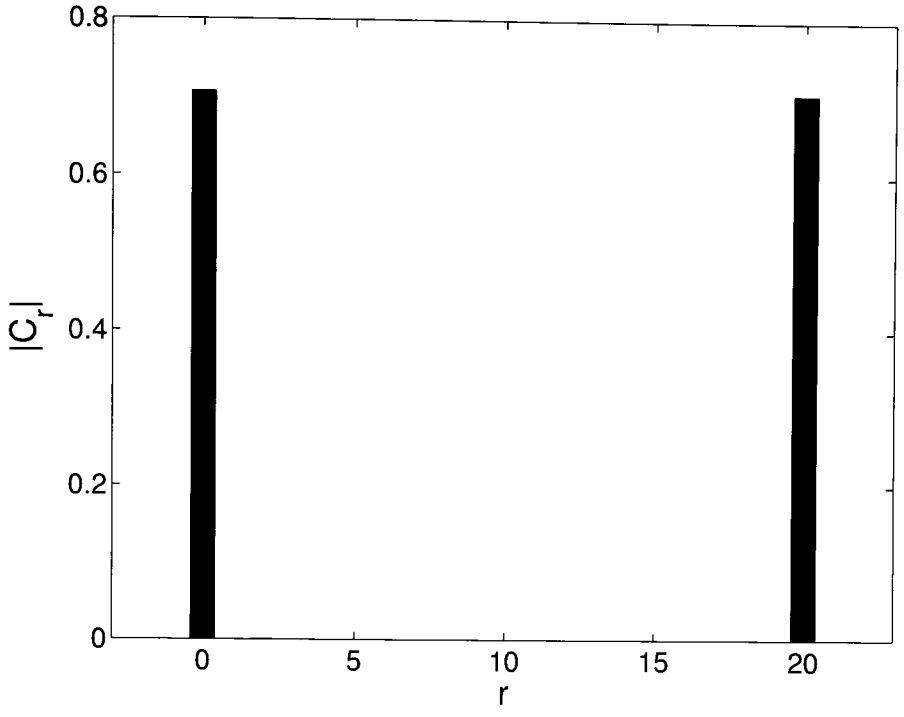

Figure 7.4: Plot of the coefficients $|C_r|$ given by (7.18) for $N = 20$.

process for generating cats. It makes the transformation

$$|N,0\rangle \longrightarrow \frac{1}{\sqrt{2}}\left(i|N,0\rangle + |0,N\rangle\right) \tag{7.20}$$

$$|0,N\rangle \longrightarrow \frac{1}{\sqrt{2}}\left(i|0,N\rangle + |N,0\rangle\right). \tag{7.21}$$

If we create a cat by this method (let's say of the form (7.20)) and then allow the state to evolve for time, t, where the two modes experience different frequencies, the state is

$$|\psi\rangle = \frac{1}{\sqrt{2}}\left(ie^{-iN\omega t}\,|N,0\rangle + |0,N\rangle\right) \tag{7.22}$$

where ω is the difference in mode frequencies. Since our method (apart from any loss) is deterministic, we can disentangle the modes simply by passing the state back through the interferometer. The sign of the nonlinear interaction needs to be reversed and this may be achieved by adjusting the magnetic fields [97].

The state back at the start of the interferometer is now given by transforming (7.22) by the inverse of (7.20) and (7.21). This gives, apart from an irrelevant

global phase factor,

$$|\psi\rangle = \cos\left(\frac{N\omega t}{2}\right)|N,0\rangle + \sin\left(\frac{N\omega t}{2}\right)|0,N\rangle. \tag{7.23}$$

This is still a superposition of two macroscopically distinct states, but the amplitudes of the two possible outcomes differ and depend on the frequency difference of the modes during the free evolution. Importantly, this frequency is enhanced by a factor N, which is potentially very large.

If we were to measure which mode the atoms are in (they should all be in one or all in the other), the probability they are in mode 1 is

$$P_1 = \frac{1}{2}(1 + \cos(N\omega t)). \tag{7.24}$$

We see that the frequency of oscillations is enhanced by a factor of N. Measuring this for different values of t allows one to determine ω much more accurately than for coherent states. This could therefore be used as a very precise way of comparing frequencies. The N-fold enhancement of the population oscillations may also prove to be a clear signature of the presence of a cat state. This means that it may also be able to confirm that the method we have outlined does indeed produce cat states, and not just mixtures of the two outcomes.

This system allows us to measure phase differences with a resolution that scales with N as $1/N$. This is reminiscent of Chapter 5, where we showed that Heisenberg limited phase resolution could be achieved with number correlated condensates. We will compare and contrast the relative merits of cat states and number correlated states in the next chapter.

7.5 Effects of loss

The main enemy of cat states is decoherence [99] and is the reason we don't see macroscopic superpositions in everyday life. Any decoherence will destroy the final cat state. However, here we would like to consider the effect of loss during the preparation of the cat.

It is straightforward to investigate the effect of the loss of an atom during the interferometry scheme. Let's say each mode has the same rate of loss and an atom is lost from mode a at time ft, where $0 \leq f \leq 1$ is the fraction of the total nonlinear interaction time, t, at which the loss occurred. The state at the end of

the interaction time is then given by

$$|\psi\rangle_2 = \frac{1}{\sqrt{2^N}} \sum_{k=0}^{\tilde{N}} \left(\begin{array}{c} \tilde{N} \\ k \end{array} \right)^{1/2} \mathrm{e}^{i\pi[k(k-1)]/2} \, \mathrm{e}^{i\pi f k} \, |k\rangle |\tilde{N} - k\rangle, \tag{7.25}$$

where $\tilde{N} = N - 1$. We notice that, apart from the obvious fact that there is one atom fewer in this system, the only difference is the second exponential factor. This factor simply shifts the relative phases of the modes by the stochastic amount $f\pi$. The system is still in a superposition of two relative phases differing by π. However, both these relative phases are shifted by the same random amount between 0 and π.

If we consider the case $f = 0$, there is no shift of the relative phases and similarly for $f = 1$. This means that if there is any loss between the beam splitters either before or after the nonlinear interaction, it will have no effect on the cat state. It is only loss during the nonlinear interaction that introduces randomness.

The random phase shift is readily generalised to multiple losses. If n atoms are lost at respective fractions of the total interaction time, $f_1, f_2, \ldots, f_n$, the relative phase shift is $\pi(f_1 + f_2 + \ldots + f_n)$. Since the relative phase is a superposition of two values differing by π, this phase shift can be recast in the form $\pi\tilde{f}$, where $0 \leq \tilde{f} \leq 1$. In other words, the effect of many losses is the same as the effect of one.

The problem with a shift of the relative phase is that it degrades the quality of the cat state. As we have seen, a perfect cat state is only obtained when the state just before the second beam splitter is a superposition of $\Delta\theta = \pm\pi/2$. For $\Delta\theta = 0, \pi$ the number distribution of the output is singly-peaked and so not cat-like at all. For all values of the relative phase between these two extreme cases, the output has varying degrees of 'cattiness'. However, for $\Delta\theta = \eta, \pi + \eta$, two macroscopically distinct peaks in the number distribution are clear for $\eta \approx 0.1\pi - 0.5\pi$. This means that about 80% of trials will produce a cat-like state regardless of how much loss there is during the preparation.

To produce ideal cat states consistently, however, no loss can be supported. This places a restriction on the maximum size of cat states that can be produced by this method. In the next section, we present a method to produce cat states even when relatively large losses are present.

7.6 Overcoming loss

We have seen that loss doesn't destroy the superposition of relative phases, but only introduces random shifts. It is the fact that the phase evolves nonlinearly with atom number that these random shifts arise. If we could find a way of creating relative phase superpositions without requiring the nonlinear evolution, atom loss should not destroy our method.

We have already seen how relative phase superpositions of precisely the form we want may be generated without a nonlinearity. In Chapter 5 we saw that, by Raman coupling two number-correlated condensate modes for a quarter cycle, the relative phase distribution consists of a superposition of peaks at $\Delta\theta = 0, \pm\pi$ (see Figure (5.1b)). Furthermore, in Chapter 6 we have demonstrated how good approximations to number-correlated condensates may be generated.

We take the squeezed state shown in Figure (6.1b) as our starting point and then resonantly Raman couple the modes for a quarter cycle. The relative phase distribution of the state after this step is shown as the dotted curve in Figure (7.5a). As expected, this consists of a superposition of peaks at $\Delta\theta = 0, \pm\pi$.

In order to create a cat state we require a state of the form (7.13), i.e. the number distribution should be Gaussian and the relative phase peaks should be centred at $\Delta\theta = \pm\pi$. The current state has a number distribution similar to the bar graph shown in Figure (5.1a). We can transform this to the required Gaussian simply by allowing loss from both modes. After the loss of a few times $\sqrt{N}$ atoms, the number distribution has the required form. The peaks in the relative phase distribution also broaden as a natural consequence of this loss. The solid curve in Figure (7.5a) shows the relative phase distribution of the state after $3\sqrt{N} = 30$ atoms have been lost. In this case 16 were lost from mode a and 14 from mode b.

Unlike the method outlined in the previous section, loss doesn't introduce a random shift in the position of these peaks, it simply broadens them. The reason there is no phase shift is that, in this case, there is no nonlinearity present during the evolution. This is probably unrealistic, there will always be some interatomic interactions. We now consider how small these need to be for this scheme to work.

If we consider that there is some small nonlinearity of strength δU, the evolution operator of the state is

$$\exp\left[i\,\delta U\,t\left(\hat{a}^{\dagger 2}\hat{a}^2\right)\right]. \tag{7.26}$$

As we have seen above, the time of evolution, t, is the time required for $\sim \sqrt{N}$

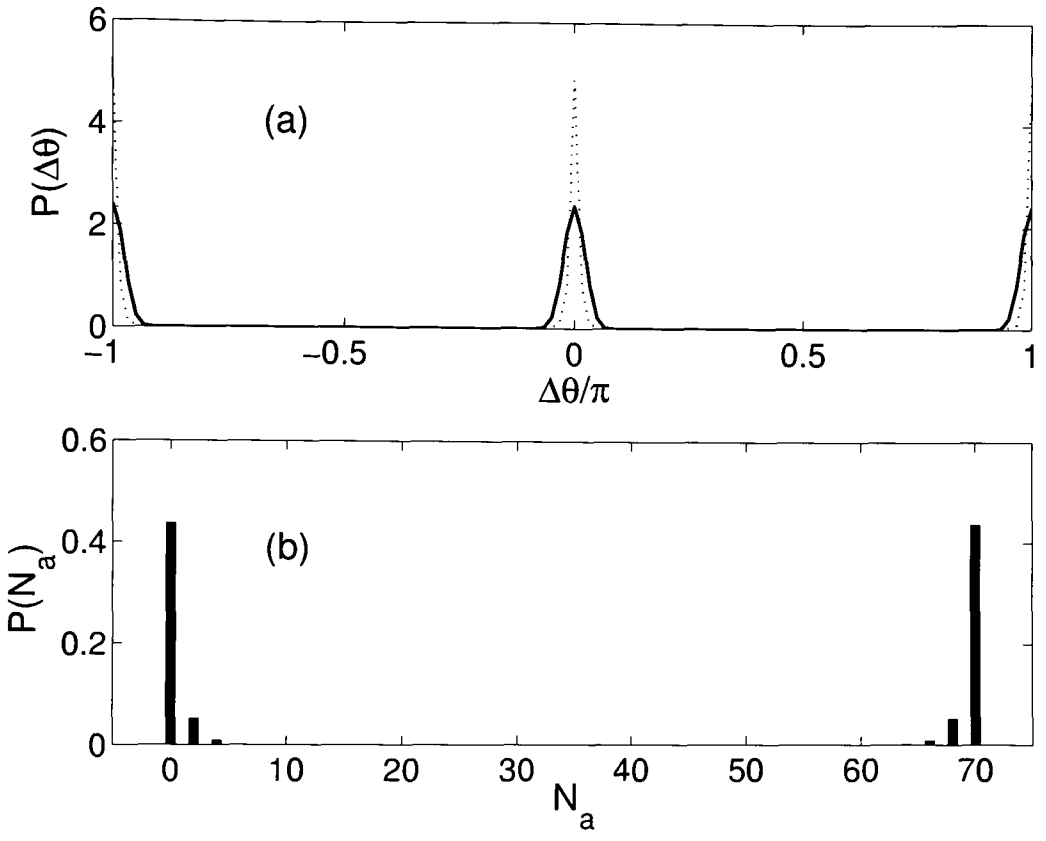

Figure 7.5: (a) Relative phase distribution for the number squeezed state shown in Figure (6.1b) (dotted curve) and the phase distribution after the loss of 30 atoms (solid curve). (b) The final number distribution of mode a after phase shifting and Raman coupling. Despite significant loss, this is still a good approximation to a cat state.

atoms to be lost from the system. For large N, this is given by

$$t = \frac{1}{\gamma\sqrt{N}}, \tag{7.27}$$

where γ is the loss rate. If we now consider the loss of a single atom at a random fraction $0 \leq f \leq 1$ of this evolution time, the phase shift introduced is $\Delta\phi = 2\delta U f/\gamma\sqrt{N}$. However, we need to consider the phase shift introduced by the loss of $\sqrt{N}$ atoms. This has an upper bound of $|\Delta\phi| = 2\delta U/\gamma$, though in practice for large N it will be much less than this since all the phases will not add constructively. If we consider the distribution of phase shifts due to the loss of $\sqrt{N}$ atoms, it will be centred on $\Delta\phi = 0$ and have a width of $N^{1/4}$. So, we can reasonably take

$$|\Delta\phi| \approx \frac{4\delta U}{\gamma N^{1/4}}. \tag{7.28}$$

This gives us a condition on the result that the relative phase peaks are not significantly shifted by the loss. This will be the case for all N if $\delta U/\gamma \ll 1$. This should be able to be arranged experimentally and it is pleasing to note that this condition becomes less stringent for large N, e.g. for $N > 10000$, δU and γ can be comparable in size.

The final step in generating the relative phase distribution that we want is to apply a far detuned light pulse to one mode to shift the phase by $\pi/2$. The phase distribution is now very similar to the one shown in Figure (7.3).

The cat state can now be produced, as in Section 7.3, by Raman coupling the modes for a quarter Raman cycle. The number distribution of mode a after this step is shown in Figure (7.5b). We see that this is a very good approximation to an ideal cat state even though there were large losses present. This demonstrates a method of generating cat states which is not destroyed by the presence of loss, but actually *requires* loss to work.

The natural question to ask next is whether the amount of loss needs to be carefully controlled. In Figure (7.6a), we show the final number distribution of mode a for the case where $5\sqrt{N} = 50$ atoms were lost. Again we see that this is a good approximation to an ideal cat state. We conclude that this method is not sensitive to the amount of loss so long as it is greater than about $2\sqrt{N}$ and the rate of loss from each mode is the same.

For completeness, we ask how well the initial state needs to be squeezed for successful generation of cat states. This question comes in two parts: firstly, how is the cat state affected if the initial state is not optimally squeezed, and secondly, what happens to the cat state if loss is present during the preparation of the number-correlated pair. In Figure (7.6b) we show the final number distribution of mode a for loss of 30 atoms (i.e. the same as in Figure (7.5)), but where the initial state is not optimally squeezed. In this case the initial state was allowed to be squeezed for time $t = t_{\text{opt}}/\sqrt{2}$, where t_{opt} is the optimum squeezing time. This corresponds to underestimating the number of atoms in the original condensate by a factor of two. We see that, although degraded relative to Figure (7.5b), the final state is still a good approximation to an ideal cat state.

In Figure (7.6c), we show the final number distribution of mode a for loss of 30 atoms (i.e. the same as in Figure (7.5b)), but where there is some loss during the preparation of the initial number squeezed pair. For the case shown here, 8% of the atoms were lost during the squeezing. We see that the final state is still a good approximation to an ideal cat state even though there is loss in all stages

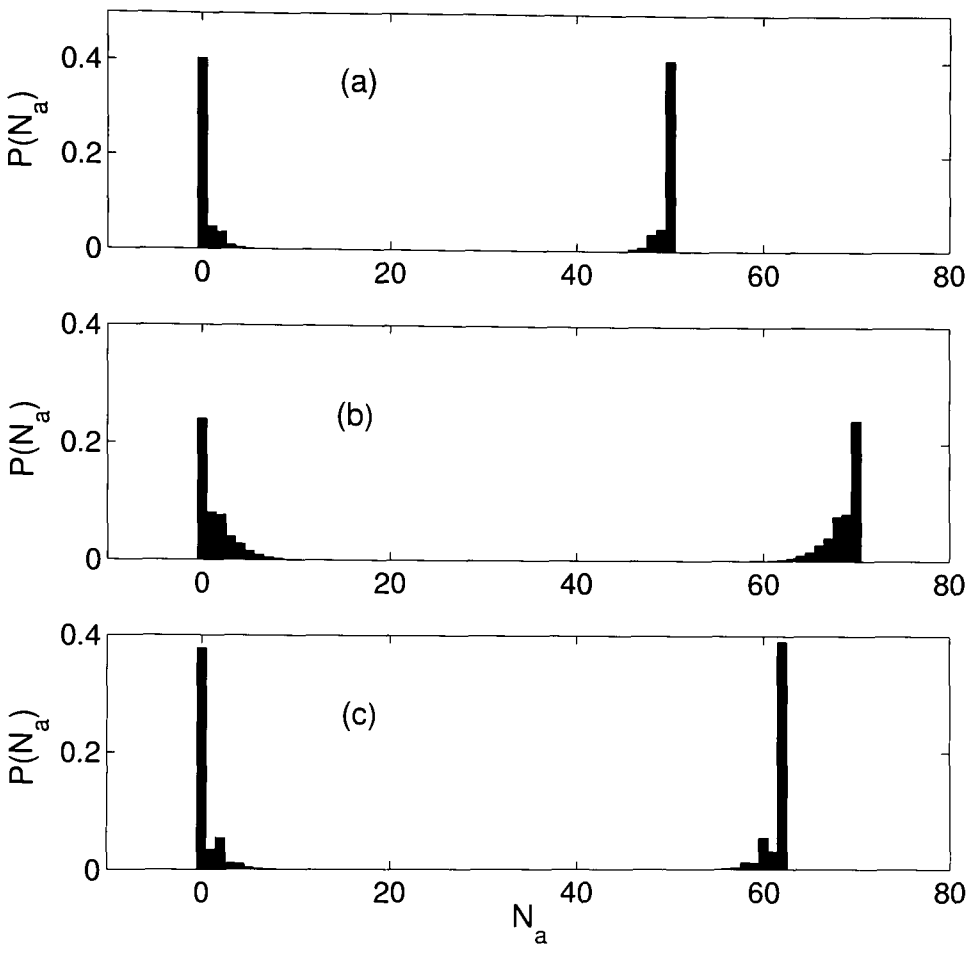

Figure 7.6: The final number distributions for mode a after the cat state generation scheme for (a) loss of 50 atoms after squeezing; (b) squeezing the initial state for only $1/\sqrt{2}$ of the optimum time and then loss of 30 atoms; (c) loss of 8% of the atoms during the squeezing time, then loss of a further 30 atoms afterwards.

of its preparation. This method is only weakly sensitive to loss and is a great improvement over the first scheme we outlined which may be destroyed by the loss of a single atom. Furthermore, the fact that it is relatively insensitive to our knowledge of the number of atoms in the original system may make it a strong candidate for the experimental generation of cat states in BECs.

7.7 Conclusion

In summary, we have demonstrated two methods by which Schrödinger cat states may be generated. The first amounts to condensate interferometry where each

component evolves due to different interaction strengths. The initial state is a readily available resource and all the steps should be able to be performed experimentally. The size of the cat states that can be created by this technique, however, are limited by loss.

We have also demonstrated a second technique which not only tolerates loss, but requires it. This involves creating a number correlated pair of condensates, allowing losses in both modes, phase shifting one component, and then recombining. Such a method should allow for the creation of much larger cat states and could prove to be a useful method for producing cat states in the laboratory.

Schrödinger cat states are not only of great theoretical interest, but may be valuable experimental tools in probing the boundary between classical and quantum physics. They may also have many useful applications such as improved accuracy in interferometry schemes and frequency standards.

Chapter 8

Cat states versus number correlated states

In Chapters 6 and 7, we showed how two different types of entangled states may be created, each with a relative phase defined to the Heisenberg limit. In this chapter, we would like to compare the relative merits of the these two states. In particular, we would like to investigate their usefulness in terms of a specific task which depends on their relative phase resolution.

Experimentally we can test their merit by posing the question: given a certain number of atoms, what entangled state should we form to give the best possible phase resolution in an interferometry scheme? At first sight, this may not appear to be a useful way to proceed since we know that both these states give the same phase resolution when there is no loss. Loss, however, is an important and intrinsic part of any system and, as we shall see, the two states behave very differently in its presence.

Another way to compare the two states is in terms of their entanglement: which state is 'more entangled' or contains more information? In quantum information literature, cat states are often referred to as maximally entangled states (e.g. in [101, 109]) in the sense that as soon as the state of one atom is measured, the states of all the others are projected into a state known with certainty. However, entangled states with flat distributions over all outcomes (such as the state generated after passing a number correlated pair through a beam splitter) are also called maximally entangled. The definition in this latter case relies on finding the state which maximises the entropy of entanglement [110, 111].

States of either sort are characterised by having Heisenberg limited relative phase, which highlights the link between relative phase and entanglement. However, we would like to know which of these two states contains more information. In Chapter 7 we saw that we could form cat states from number correlated states in the presence of dissipation. Since dissipation corresponds to a loss of information, this suggests that a number correlated state is more information-rich than a cat state.

Defining the relative merits of the two states in terms of their sensitivity in an interferometer is a useful way to resolve this issue. After all, their eventual usefulness must be gauged in terms of what we can do with them experimentally. It turns out that number correlated states are far more robust to loss than cat states, which cannot support the loss of even a single atom. This suggests that they would be far more useful in interferometry (or clock) schemes where loss is a limiting process on their accuracy.

In this chapter, we will begin by considering how the phase resolution of cat states and number correlated states is affected by loss. We will use a Gaussian entangled state as a benchmark since this exhibits standard quantum limited phase.

8.1 Cat state

We now calculate the relative phase resolution of a cat state in the presence of dissipation. This state is

$$|\psi\rangle = \frac{1}{\sqrt{2}}\left(|N,0\rangle + |0,N\rangle\right). \tag{8.1}$$

In Chapter 2, we showed that we could find the phase distribution of this state by calculating

$$P(\Delta\theta) = |\langle\theta_s, \theta_{s-\Delta\theta/\epsilon}|\psi\rangle|^2. \tag{8.2}$$

When considering loss, however, we must think in terms of the density matrix, $\rho = |\psi\rangle\langle\psi|$, (rather than the state) of the system [112]. It is straightforward to write (8.2) in terms of density matrices,

$$P(\Delta\theta) = \mathrm{Tr}\left[\rho_{\Delta\theta}\rho_{\kappa}\right], \tag{8.3}$$

where ρ_κ is the density matrix for the system with a rate of dissipation, κ, which we take to be the same for both modes, and

$$\begin{aligned}\rho_{\Delta\theta} &= |\theta_s, \theta_{s-\Delta\theta/\epsilon}\rangle\langle\theta_s, \theta_{s-\Delta\theta/\epsilon}| \\ &= \sum_{p,q=0}^{\infty}\sum_{p',q'=0}^{\infty} \exp\left[i(p-p')s\epsilon + i(q-q')(s\epsilon - \Delta\theta)\right] |p,q\rangle\langle p',q'|. \quad (8.4)\end{aligned}$$

We defined $|\theta_s\rangle$ and ϵ in Equation (2.23).

We would now like to calculate the density matrix, ρ_κ, for the cat state with loss. Barnett and Radmore [52] show that the density matrix can be written as

$$\rho(t) = \exp\left(2\kappa t\hat{L}\right)\exp\left\{\left[1-\exp(-2\kappa t)\right]\hat{J}\right\}\ \rho(0), \quad (8.5)$$

where the superoperators $\hat{J}$ and $\hat{L}$ are defined in terms of their action on the density matrix as

$$\hat{J}\rho(t) = a\rho(t)a^\dagger + b\rho(t)b^\dagger \quad (8.6)$$

$$\hat{L}\rho(t) = -\frac{1}{2}\left[(a^\dagger a + b^\dagger b)\rho(t) + \rho(t)(a^\dagger a + b^\dagger b)\right]. \quad (8.7)$$

Using (8.1), (8.4), and (8.5), we can write

$$\begin{aligned}P(\Delta\theta, t) &= \mathrm{Tr}\left[\rho_{\Delta\theta}(t)\rho(t)\right] \\ &\propto 2\sum_{l=0}^{N}\binom{N}{l}(1-\mathrm{e}^{-2\kappa t})^l(\mathrm{e}^{-2\kappa t})^{N-l} + 2\mathrm{e}^{-2N\kappa t}\cos(N\Delta\theta) \\ &= 2\left(1+\mathrm{e}^{-2N\kappa t}\cos(N\Delta\theta)\right), \quad (8.8)\end{aligned}$$

where the last line follows from identifying the sum as a binomial expansion.

We now define the phase resolution of this state to be the value of $\Delta\theta$ for which

$$\frac{\mathrm{Tr}\{\rho_{\Delta\theta}\rho\}}{\mathrm{Tr}\{\rho_0\rho\}} = \frac{1}{2}. \quad (8.9)$$

A simple calculation yields

$$\cos\left(N\Delta\theta\right) = \frac{1}{2}\left(1-\mathrm{e}^{2N\kappa t}\right). \quad (8.10)$$

In the limit of no loss, $\kappa = 0$, the solution is $\Delta\theta = \pi/(2N)$. As discussed in Chapter 7, we see that the phase resolution of this state scales as $\Delta\theta \sim 1/N$. If,

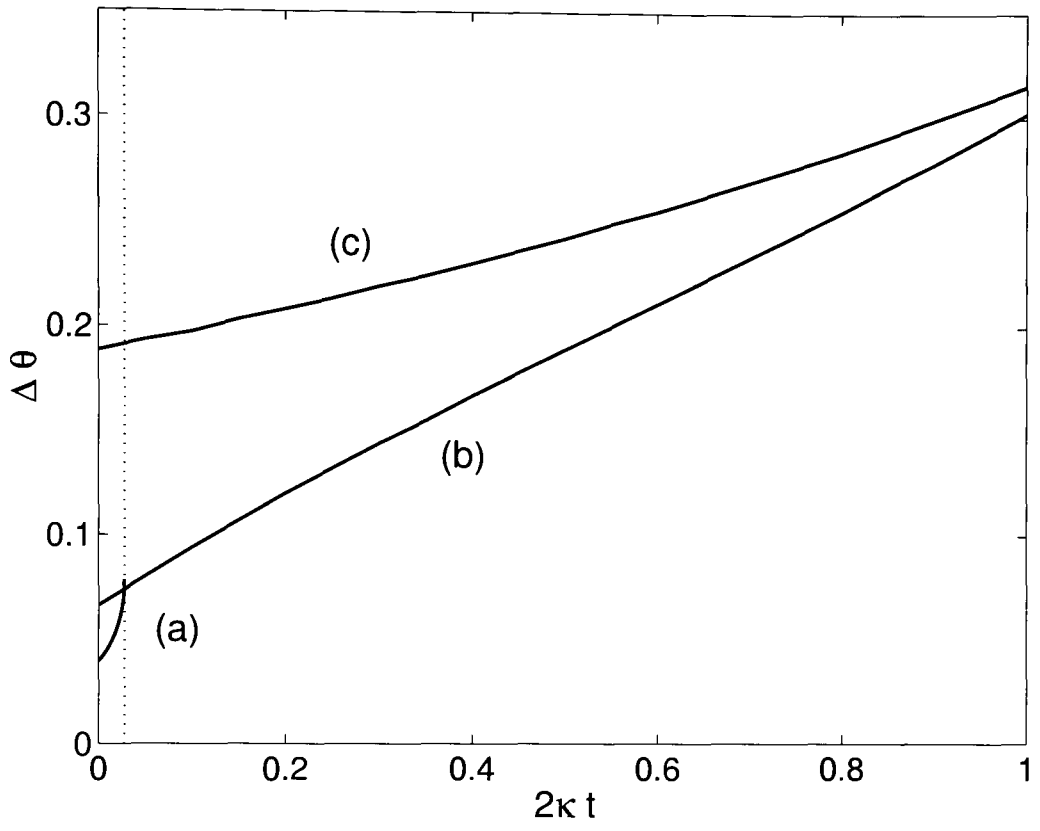

Figure 8.1: Variation of the relative phase resolution with $2\kappa t$ for (a) a cat state (b) a number correlated state, and (c) a Gaussian entangled state. In each case the total number of atoms in the system is $N = 40$. The dotted line indicates the point at which the cat state no longer contains any phase information.

however, the loss is non-vanishing, we see that (8.10) has no solution for $N\kappa t > \ln(3)/2 \approx 0.5$. This means that the phase information is completely wiped out if more than half-an-atom is lost from each mode. This is what we would expect since a macroscopic superposition state is completely destroyed by the loss of a single atom. We can infer from this that the cat state has a lifetime of $t \approx 1/(2N\kappa)$.

In Figure (8.1a) we have plotted how the solution, $\Delta\theta$, of (8.10) varies with $2\kappa t$ for $N = 40$. We see that the resolution rapidly worsens as κt is increased and, as predicted, the relative phase is undefined for $2\kappa t > \ln(3)/40$.

We conclude that, although cat states have excellent phase resolution properties, they are extremely fragile. Huelga *et al.* showed that when it comes to usefulness for a frequency standard these two effects exactly cancel and that a cat state does not give better phase resolution than a standard quantum limited state.

8.2 Number correlated state

We now turn our attention to number correlated pairs. Intuitively, we might feel that these states contain more information than cat states since we have shown that we can form a cat state from a number correlated pair when there is loss present and we know that loss corresponds to a reduction of coherence or information. We now investigate this more formally.

We show in Appendix A that Raman coupling a number correlated state for a quarter cycle gives

$$|\psi\rangle = \frac{1}{2^n} \sum_{m=0}^{n} \sqrt{\frac{(2n-2m)!}{(n-m)!^2}} \sqrt{\frac{(2m)!}{m!^2}} |2m\rangle|2(n-m)\rangle, \tag{8.11}$$

where the total number of atoms is $N = 2n$. This distribution is plotted in Figure (5.1a) and we see that, apart from near the ends, it is very flat. We can formalise this by using the Stirling approximation [113],

$$\alpha! \approx \sqrt{2\pi\alpha} \left(\frac{\alpha}{e}\right)^{\alpha}, \tag{8.12}$$

for large positive values of α. This approximation breaks down near the edges of the distribution, but the region over which it is not valid scales as $1/n$, so for large values of n, we can neglect the regions where it is not valid. Substituting (8.12) into (8.11) allows us to write the probability distribution of mode a as $P(2m) \propto 1/\sqrt{m(n-m)}$, which is flat away from the edges. This means that a good approximation to this state is

$$|\psi\rangle = \frac{1}{\sqrt{n}} \sum_{m=0}^{n} |2m\rangle|2(n-m)\rangle, \tag{8.13}$$

which we shall use for convenience. As before, the density matrix is given by $\rho = |\psi\rangle\langle\psi|$. Using this along with (8.4) and (8.5) we can write the relative phase distribution as

$$\mathrm{Tr}\{\rho_{\Delta\theta}\rho\} \propto \sum_{l,r} \left(e^{2\kappa t} - 1\right)^{l+r} \left| \sum_{m=0}^{n} \begin{pmatrix} 2m \\ l \end{pmatrix}^{1/2} \begin{pmatrix} 2(n-m) \\ r \end{pmatrix}^{1/2} e^{-2im\Delta\theta} \right|^2. \tag{8.14}$$

If we consider the lossless limit, we can set $\kappa = 0$ and $l = r = 0$. The phase

resolution is then given by solving

$$\frac{\mathrm{Tr}\{\rho_{\Delta\theta}\rho\}}{\mathrm{Tr}\{\rho_0\rho\}} = \frac{1}{n^2}\left|\sum_{m=0}^{n} \mathrm{e}^{-2im\Delta\theta}\right|^2 = \frac{1}{2}. \tag{8.15}$$

Recognising that the sum is a geometric series, we can write this as

$$\left|\frac{\sin(n\Delta\theta)}{n\sin(\Delta\theta)}\right|^2 = \frac{1}{2}, \tag{8.16}$$

which, for large n, can be solved to give the phase resolution as $\Delta\theta \approx 1.4/n = 2.8/N$. We see that, as discussed previously, this has the same number scaling as the cat state. However, the phase resolution is a factor of about 1.8 worse than for a cat state, $\Delta\theta = \pi/2N$. In the lossless limit, therefore, cat states are the best states for interferometry.

A completely lossless situation is not realistic and we would like to compare the two states in the presence of dissipation. In Figure (8.1b) we plot $\Delta\theta$ for different values of $2\kappa t$ for $N = 40$. $\Delta\theta$ is given by the solution of (8.9) and $\mathrm{Tr}\{\rho_{\Delta\theta}\rho\}$ is given by (8.14). We can compare this with Figure (8.1a) which shows the corresponding relationship for a cat state.

We notice firstly that, for no loss, the number correlated state has $\Delta\theta \approx 0.07$ in agreement with our prediction. In the lossless case, the phase resolution of this state scales with N in the same way as for the cat state. Their behaviour differs markedly, however, when loss is present.

The loss of a single atom destroys all the phase information in a cat state. However, in Figure (8.1b), we see that for the number correlated state this is not the case. The loss of a single atom only slightly degrades the phase resolution. As the loss is increased, the phase resolution is smoothly degraded but, even for large losses, a well defined relative phase still exists between the modes.

8.3 Gaussian state

Finally, we would like to compare these two states with a Gaussian state, i.e. one that is formed by coupling a number state $|N\rangle$ with a vacuum mode $|0\rangle$ for a quarter Raman cycle. We showed in Chapter 5 that this state has the form

$$|\psi\rangle = \frac{1}{2^{N/2}}\sum_{m=0}^{N}\left(\begin{array}{c} N \\ m \end{array}\right)^{1/2} \mathrm{e}^{-im\pi/2}\,|m\rangle|N-m\rangle, \tag{8.17}$$

and that its phase resolution is given by the standard quantum limit $\Delta\theta \sim 1/\sqrt{N}$ when there is no loss.

Following a similar calculation to that described in Sections 8.1 and 8.2, the relative phase distribution of this state is

$$\mathrm{Tr}\{\rho_{\Delta\theta}\rho\} \propto \sum_{l,r} \left(\mathrm{e}^{2\kappa t}-1\right)^{l+r} \left| \sum_{m=0}^{N} \binom{N}{m}^{1/2} \binom{m}{l}^{1/2} \binom{N-m}{r}^{1/2} \mathrm{e}^{-im\Delta\theta} \right|^2 . \tag{8.18}$$

In Figure (8.1c) we plot how the phase resolution, $\Delta\theta$, of this state varies with $2\kappa t$ for $N = 40$. As expected, for no loss the phase resolution is worse than for the cat state and the number correlated state. As more and more loss is introduced to the system, the width of the relative phase distribution increases. Over the range we have plotted, we see that the phase resolution of the number correlated state is always better than the Gaussian state.

8.4 Conclusion

We are now in a position to answer the question that we posed at the beginning of this chapter: given N atoms, what entanglement should we create in order to achieve the best possible phase resolution in an interferometry scheme?

The answer comes in two parts if we consider the cases where loss is present or not. In the lossless case, we have seen that both the cat and number correlated states have phase resolutions that scale as $1/N$. By contrast, the phase resolution of the Gaussian state scales as $1/\sqrt{N}$. This means that, even for modest numbers of atoms, the phase resolution of cat states and number correlated states is significantly better than for Gaussian states. For a completely lossless system, however, cat states give a phase resolution that is better than for number correlated states by about a factor of 1.8.

The situation changes, however, when loss is present. In Figure (8.1) we see that the Gaussian and number correlated states are affected relatively 'gently' by loss. This is not the case for cat states for which the loss of a single atom wipes out all the phase information. This was pointed out by Huelga *et al.* who demonstrated that a cat state gives N-enhanced phase sensitivity but, due to its fragile nature, can only be evolved for a much shorter time [105]. They showed that these two effects exactly cancel giving no improvement over the Gaussian entanglement case. Here however, we show that, by using number correlated states,

we can also get the N-enhanced phase sensitivity but with much reduced loss sensitivity. In this case the loss of atoms does not destroy the phase information of the entangled state but only slightly degrades it. This means that, unlike cat states, number correlated states are not subject to strict limits on how long they can be evolved. We see in Figure (8.1) that even for large losses, the phase resolution of the number correlated state is better than that for the Gaussian state. This is an important result as it suggests that using number-correlated pairs may allow for much improved frequency standards.

Our conclusion is that the best entangled state we can create for use in interferometry is a number correlated state. In Chapter 6 we described a scheme for how such states may be able to be generated which may allow their phase properties to be experimentally verified. We also conclude that number correlated states are more strongly entangled or more information-rich than cat states. This is consistent with our findings in Chapter 7 that a cat state can be generated from a number correlated state when loss is present.

Chapter 9

Entanglement concentration in Bose condensates

In the previous chapter, we highlighted the link between entanglement and phase. In this chapter, we develop this correspondence further by showing how we can apply our knowledge of phase to a scheme for concentrating the entanglement between Bose-Einstein condensates.

9.1 Introduction

Entanglement shared between distant parties is an important resource in various communication protocols [114, 115, 116]. Since entanglement cannot be created by local operations on separate systems, entangled pairs of systems need to be created at a source and then distributed to distant parties. It is therefore important to be able to distribute entanglement faithfully.

One scheme which aids in this distribution is entanglement concentration. This converts a large number of less entangled pairs into a smaller number of more entangled pairs using only local operations [117]. The concentrated pairs can then be used to perform the communication protocol faithfully. One such protocol, quantum teleportation [116], exploits priorly shared entanglement to transfer an unknown (or even partially unknown [118]) quantum state to a distant location. Teleporting one particle of an entangled pair results in the exchange of entangled partners across a distance, a process known as 'entanglement swapping' [116, 119]. Two of the particles which become entangled have not directly interacted at any

stage, and therefore the swapping can be used as a means of entanglement distribution. Both teleportation and entanglement swapping have been experimentally demonstrated [120, 121, 122, 123], in the domain of microscopic systems. Demonstrations of such schemes with macroscopic objects would be of fundamental interest.

As we have seen in this thesis, an increasingly controllable macroscopic quantum system is a Bose-Einstein condensed state of a trapped dilute gas [25, 124]. Bose condensates have already been used to demonstrate quantum features, like superposition, in the macroscopic domain [39]. More recently, there have also been suggestions for creating specific types of entangled atomic beams, and multiparticle entangled states from Bose condensates [125, 126, 127] and in Chapters 6 and 7 we showed how two specific entangled states can be created. However, no scheme for entanglement swapping or concentration has been yet demonstrated with BECs.

In this chapter, we propose a method for achieving entanglement swapping, using techniques which are experimentally feasible. This opens up the possibility of entanglement-aided communications using Bose condensates. We also show that a theoretical proposal for entanglement concentration by entanglement swapping, [128] is feasible, using exactly the same measurements.

9.2 Entanglement swapping scheme

We begin by presenting a general entanglement swapping protocol for Bose condensates. We consider four condensates labelled by the modes a, b, c, and d (see Figure (9.1)). Modes a and b are entangled and contain a total of n atoms between them

$$|\psi_{ab}\rangle_1 = \sum_{p=0}^{n} c_p \, |n-p\rangle_a |p\rangle_b \tag{9.1}$$

where $\sum_{p=0}^{n} |c_p|^2 = 1$. Later we will choose the form of this entanglement to be that given by a simple measurement of an interference pattern. The second two modes, c and d, are also entangled with a total number of n atoms

$$|\psi_{cd}\rangle_1 = \sum_{q=0}^{n} d_q \, |q\rangle_c |n-q\rangle_d \tag{9.2}$$

with $\sum_{q=0}^{n} |d_q|^2 = 1$. We will discuss specific ways of entangling these condensates later. The total state of the system after this first part of the scheme is, $|\psi\rangle_1 = |\psi_{ab}\rangle_1 \otimes |\psi_{cd}\rangle_1$, and contains a total of $2n$ atoms.

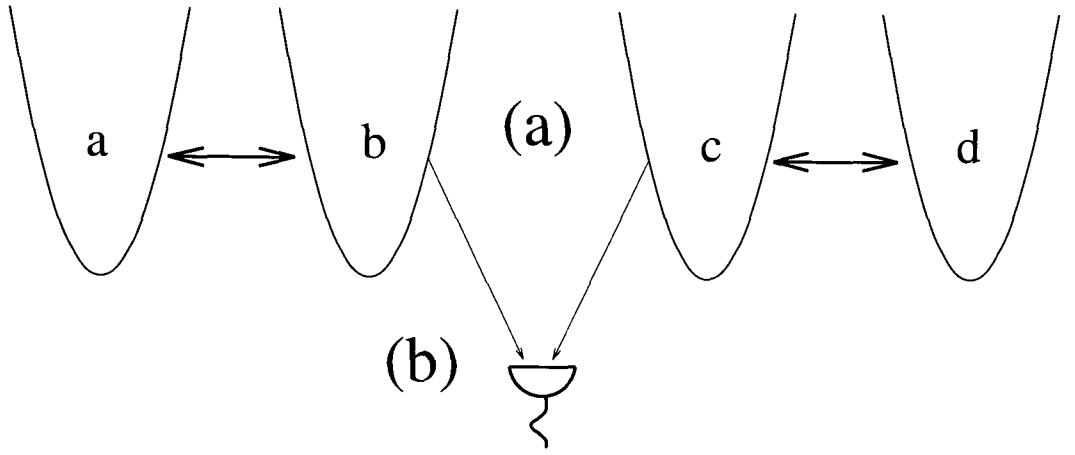

Figure 9.1: The entanglement swapping scheme. (a) Modes a and b are entangled as are modes c and d. (b) An interference pattern is then detected between modes b and c, completely draining both traps.

In the second part of the scheme, we allow atoms to leak out of b (now entangled with a) and c (now entangled with d). We completely drain the two traps and detect all the atoms in both of them in such a way that we do not know which trap a detected atom has come from. We need to be able to measure this number accurately, which limits the number of atoms each condensate can contain to small values. The details of this step can be very general. Any method which measures a spatial or temporal interference pattern in the overlap region will work [39, 47, 48, 84]. We can write this step as the operation

$$\mathcal{O}(p,q)\,|\psi\rangle_1 = \delta_{r,(p+q)}\left[\frac{1}{\sqrt{2}}\left(\hat{b}+\hat{c}\,\mathrm{e}^{i\xi}\right)\right]^{p+q}|\psi\rangle_1, \tag{9.3}$$

where $\hat{b}$ and $\hat{c}$ are annihilation operators for modes b and c respectively, $\delta_{r,(p+q)}$ is the discrete delta function, and r is the outcome of the measurement of the total number of atoms. The phase, ξ, varies stochastically from trial to trial [47] since it has contributions from the position or time of each detection, and these detections are random events. The value of this phase, however, is not important to our scheme. In fact, detecting an interference pattern not only creates a phase, but measures its value, [81], so we could easily correct for it at the end. For this reason and without loss of generality we set $\xi = 0$.

Considering just modes b and c, we get

$$\mathcal{O}(p,q)\ |p\rangle_b|q\rangle_c = \frac{(p+q)!}{\sqrt{p!q!}}\,\delta_{r,(p+q)}\ |0\rangle_b|0\rangle_c. \tag{9.4}$$

Modes b and c have been completely drained and so we will omit these modes from the expression for the total state.

Making the replacements $y = n - p$ and $k = 2n - r$, the final state of modes a and d can be written as

$$|\psi\rangle = \mathcal{N} \sum_{y=y_1}^{y_2} \begin{pmatrix} 2n-k \\ n-y \end{pmatrix}^{1/2} c_{n-y}\, d_{n-k+y}\ |y\rangle_a|k-y\rangle_d, \tag{9.5}$$

where $y_1 = \max(0, k-n)$ and $y_2 = \min(n,k)$. $\mathcal{N}$ is an unimportant normalisation factor which has absorbed the additional factor of $\sqrt{(2n-k)!}$. Modes a and d are now entangled, though they have never directly interacted.

This completes the entanglement swapping protocol. The physical basis of the swapping is the lack of knowledge of the source of the detected atoms. This is also the principle on which a recent proposal for entangling atoms in distant cavities is based [129].

9.3 Entanglement concentration

The fact that entanglement swapping is possible leads us to investigate whether it could be used for entanglement concentration, as indicated in [128]. Such a scheme depends on the choice of initial states (9.1) and (9.2). We investigate the circumstances under which the entanglement of the final state (9.5) may be greater than that of the original state (9.1).

In this case, mode a may be taken to belong to Alice and modes b, c and d to belong to Bob. The detection, a local action on Bob's side, then serves to increase the entanglement between Alice and Bob. Entanglement concentration is thus demonstrated in principle between Alice and Bob, who may not necessarily be far apart in practice.

To compare the entanglement of the initial and final states, (9.2) and (9.5), we will use a standard measure of entanglement for pure states, namely the Von Neumann entropy of one subsystem [117]. For state (9.5), the entanglement is then given by

$$E = -Tr\left\{\rho_a \log \rho_a\right\} = -Tr\left\{\rho_d \log \rho_d\right\}, \tag{9.6}$$

where $\rho_a = Tr_d\{|\psi\rangle\langle\psi|\}$ and $\rho_d = Tr_a\{|\psi\rangle\langle\psi|\}$ respectively denote the reduced density matrices for modes a and d.

The range of possible initial states is limited by the specific practical methods of entangling the initial pairs of condensates. A number of theoretical schemes could be proposed for which the entanglements and measurements are not practical. However, all the operations in our scheme could be performed in the laboratory.

We consider that a and b have been entangled by measuring an interference pattern between them. This is a very natural form of the entanglement and such a state has been widely studied [47, 48, 84] and experimentally observed [39]. For simplicity and convenience, we consider each mode initially to be in a number state with n atoms with identical trap frequencies, ω, and that we detect n atoms (i.e. half of them) in the entanglement process. Such a procedure gives the unnormalised coefficients in (9.1) as

$$c_p = \left(\begin{array}{c} n \\ p \end{array}\right)^{3/2} \mathrm{e}^{-i\zeta p}, \tag{9.7}$$

As above, this result holds for any measurement of an interference pattern between the condensates and ζ can be set to zero without loss of generality.

We would now like to find an experimentally feasible form of the entanglement between modes c and d (held by Bob) that can give rise to purification of the entanglement between Alice's mode a and Bob's mode b.

We know that the final state has the form of (9.5) and for simplicity we take $r = k = n$ (i.e. the final state has the same number of atoms as the initial state). Substituting the coefficients from (9.7), we obtain

$$|\psi\rangle \propto \sum_{y=0}^{n} \left(\begin{array}{c} n \\ y \end{array}\right)^{2} d_y \, |y\rangle_a |n-y\rangle_d. \tag{9.8}$$

We would now like to find the form of the coefficients $\{d_y\}$ such that (9.8) has a flatter number distribution than the initial entanglement between modes a and b,

$$|\psi_{ab}\rangle_1 \propto \sum_{p=0}^{n} \left(\begin{array}{c} n \\ p \end{array}\right)^{3/2} |p\rangle_a |n-p\rangle_b. \tag{9.9}$$

Comparing (9.8) and (9.9), we see that if $\{d_y\}$ had a perfectly flat distribution, the final state would more more peaked (and hence less entangled) than the original. Our scheme would fail in this case. However, if the distribution $\{d_y\}$ were dipped

in the middle, we might be able to concentrate the entanglement. In particular, if

$$d_y = \binom{n}{y}^{-1/2}, \tag{9.10}$$

we would 'break even', in the sense that the final state would be identical to the original. Furthermore, if the distribution $\{d_y\}$ were even more strongly dipped, we should be able to arrange things so that the final state is more entangled than the original. For,

$$d_y = \binom{n}{y}^{-2}, \tag{9.11}$$

the final state (9.8) would be maximally entangled. It's not clear how we could generate an entanglement of this form, instead we look for states (9.2) with dipped number distributions that could be experimentally realised.

We have already seen how entanglements of this form may be created. In Chapter 5 we showed that if number correlated pairs of condensates are Raman (or Josephson) coupled for a quarter cycle, the resulting number distribution is dipped in the middle (see Figure (5.1)). Unfortunately, however, this has a very flat middle section which dominates and, as we saw above, a flat distribution does not allow for entanglement concentration. We need to be able to generate states that are more strongly dipped.

We now outline how an appropriate distribution may be produced. The scheme we describe is interesting in its own right and is very similar to the Schrödinger cat state scheme in Chapter 7. We start by entangling c and d in just the same way as we produced the entanglement between a and b. It is assumed that this process takes place much faster than the evolution due to the nonlinear interactions and so we can ignore the interactions during this time. The system is then allowed to evolve naturally due to the interactions between atoms. We take the modes to have the same interaction strength, U, and assume that there is no interaction between the two modes. Cornish *et al.* [97] have shown how the scattering length may be tuned, which may be useful in a practical implementation of this step. The system is allowed to evolve for time $t = \pi/4U$. The operator for this step is

$$U_{\text{evolve}} = \exp\left[i\frac{\pi}{4}\left(\hat{c}^{\dagger 2}\hat{c}^2 + \hat{d}^{\dagger 2}\hat{d}^2\right)\right], \tag{9.12}$$

and is equivalent to the 'one-axis twisting' described by Kitagawa and Ueda [130].

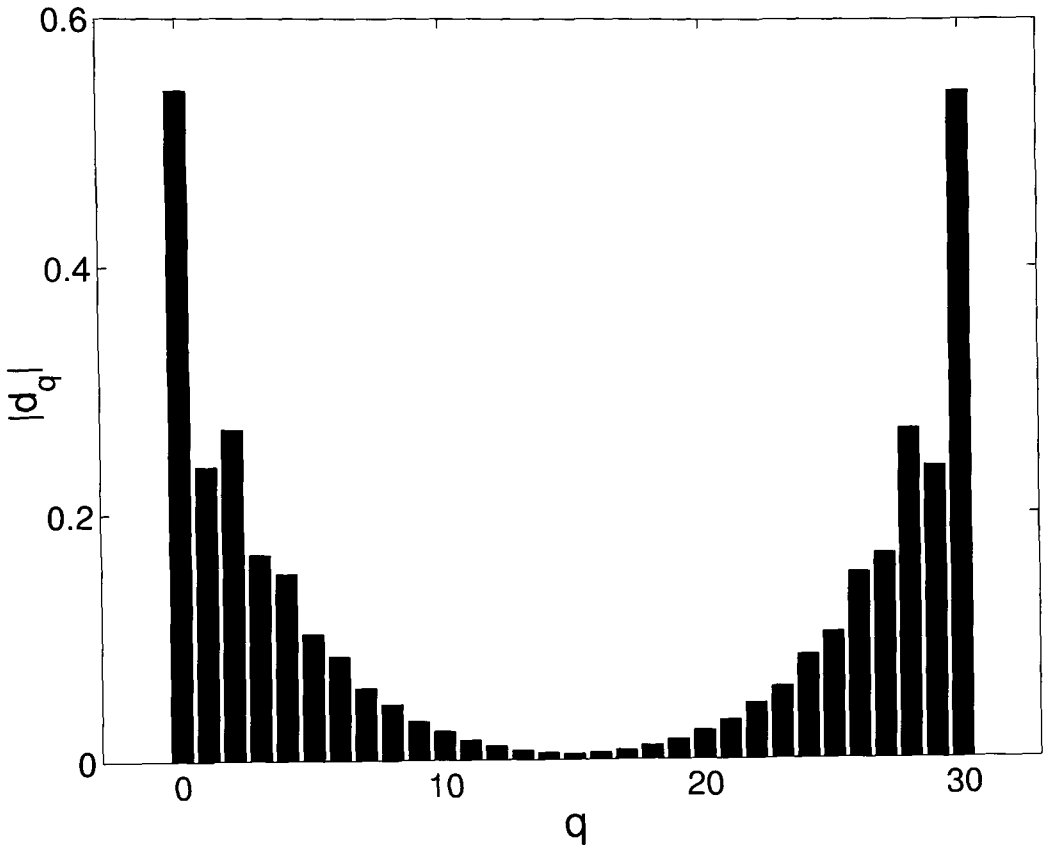

Figure 9.2: Plot of the coefficients $|d_q|$ against q, for $n = 30$ and $\phi = 0.8$.

Next we advance the phase of one condensate by $\phi\pi/2$. This can be achieved by applying a suitable far-detuned light pulse. The state after this step is, ignoring the global phase, is

$$|\psi_{cd}\rangle_1 \propto \sum_{q=0}^{n} \binom{n}{q}^{3/2} e^{i\pi q(q-n-\phi)/2} |q\rangle_c |n-q\rangle_d. \tag{9.13}$$

Finally, we resonantly couple modes c and d (by tunneling through the barrier between the traps) for time $t = \pi/4\Gamma$, where Γ is the strength of the coupling [82], (this Hamiltonian is identical to that generated by Raman coupling [64, 76]). The resulting unitary operator is

$$U_{\text{couple}} = \exp\left[i\frac{\pi}{4}(\hat{c}\,\hat{d}^\dagger + \hat{c}^\dagger\hat{d})\right]. \tag{9.14}$$

Operating on (9.13) gives us the form of (9.2). After some algebra, the unnor-

malised coefficients are given by

$$d_q = \sqrt{q!(n-q)!} \sum_{s=0}^{n} \sum_{t=t_1}^{t_2} \binom{n}{s}^2 \binom{s}{t} \binom{n-s}{q-t} e^{\frac{i\pi}{2}(q-2t)} e^{\frac{i\pi}{2}s(s-n-(\phi-1))}, \quad (9.15)$$

where $t_1 = \max(0, q+s-n)$ and $t_2 = \min(q, s)$. The details of this step are shown in Appendix D. A plot of these coefficients for $n = 30$ and $\phi = 0.8$ is shown in Figure (9.2). We see that this has the form of the number distribution that we require.

As described in the entanglement swapping scheme above, once the two entangled pairs have been created, we can measure an interference pattern between modes b and c, detecting the total number of atoms in both. An expression for the final state is then given by substituting the coefficients given by (9.7) and (9.15) into (9.5). The final state depends on three parameters: the total number of atoms detected, r, the angle ϕ introduced in creating (9.15), and the number of atoms in each entangled pair, n.

In fact, the last parameter should really be the number of atoms in (9.1) and the number of atoms in (9.2). We have set these numbers to be the same for convenience, but they need not be. To simplify calculations further, we will not investigate this n-dependence but will set it to the value $n = 30$ throughout the remainder of this discussion. All the features of the results presented here hold for different values of n and for different n in the two initial entangled pairs. We are not so much interested in presenting the best case of entanglement purification, but rather demonstrating that it is possible. We will, however, examine how the entanglement of (9.5) varies with r and ϕ.

We begin by investigating the optimum value for ϕ. In Figure (9.3), the maximum value of the entanglement of (9.5) that can be achieved for any measurement result, r, is plotted as a function of ϕ. For comparison, the dashed line is the entanglement of the initial state (9.1). We see immediately that the entanglement is purified over a wide range of values of ϕ: $\phi \in [0.47, 0.97]$. This is an important result and demonstrates a means of purifying the entanglement of macroscopic objects. For $n = 30$ the best entanglement of the final state is achieved when $\phi = 0.9$. We now set ϕ to this optimum value and investigate how the entanglement of the final state depends on the outcome of the measurement of the total number of atoms in modes b and c. In particular, we would like to study the range of outcomes that give rise to entanglement purification.

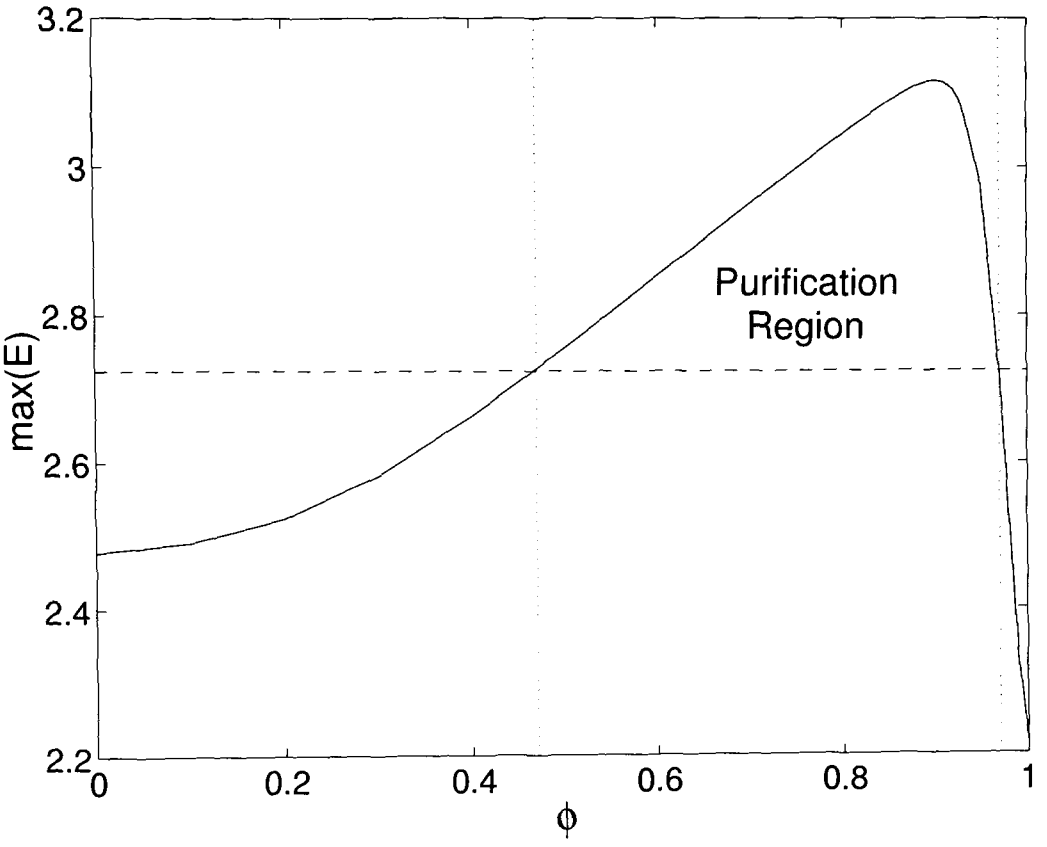

Figure 9.3: The maximum entropy over all possible measurement outcomes, r, of the final state (9.5) as a function of ϕ. The dashed line is the entropy of the initial state (9.1).

In Figure (9.4), we plot E against the total number of atoms remaining in the final state, $k = 2n - r$. We see that the final state is purified if $k \in \{n-1, n, n+1\}$, i.e. the measurement outcome lies in the range $r \in \{n-1, n, n+1\}$. If any other measurement result is obtained, the trial has failed to purify the entanglement and we would need to try again.

A problem that arises is that one would need to accurately know the number of atoms in each entangled pair. This is probably the most severe limitation on carrying out this scheme. However, we have seen in Chapter 6 how it is possible to generate pairs of number correlated condensates. We can make use of this scheme in the present context as follows. We could take a condensate and generate a number correlated pair using the technique outlined in Chapter 6. We could then destructively measure the number of atoms in one of these pairs. This would give us accurate information about the number of atoms in the remaining condensate,

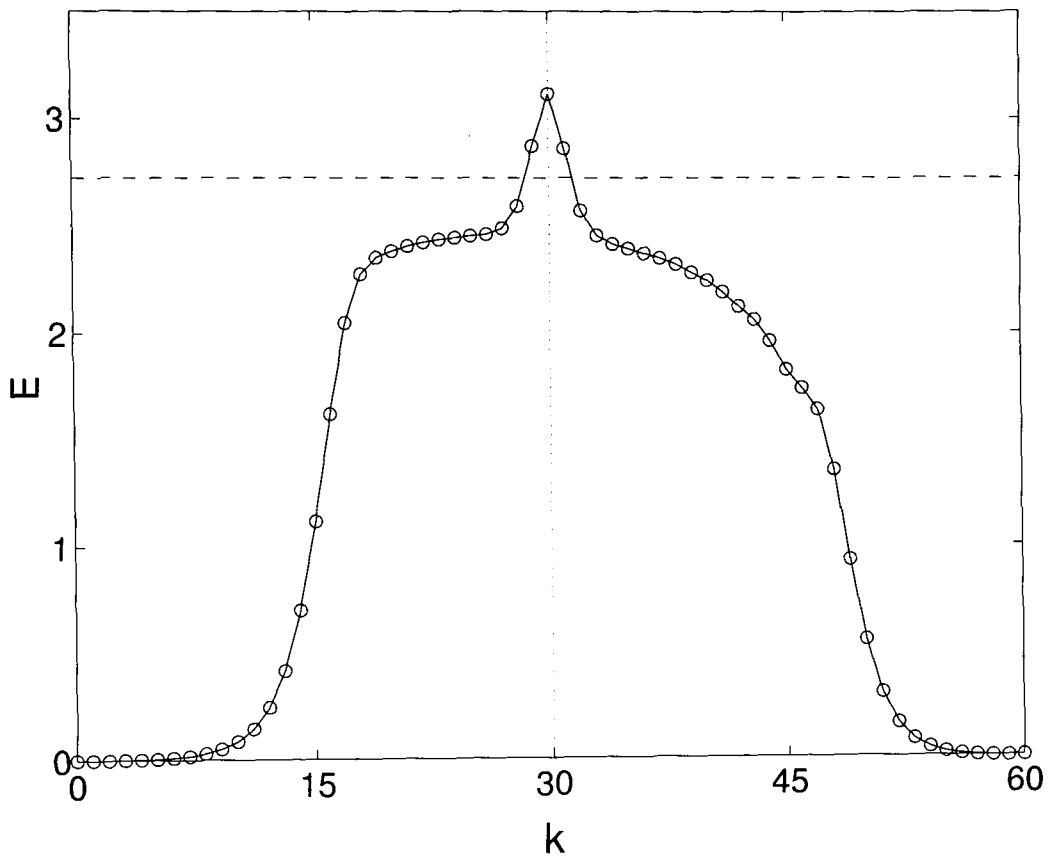

Figure 9.4: Entropy of the final state (9.5) as a function of the total number of atoms in the state, k. The dashed line is the entropy of the initial state (9.1). The entanglement is purified over the range $k \in [n-1, n+1]$, with a maximum for $k = n = 30$.

which we take to be our starting point. The next step is to generate a number correlated pair from this condensate, and then to generate number correlated pairs from each condensate in this pair. The result of all this is that we are left with four condensates which are all number correlated and, since we knew the number of atoms in the original condensate (i.e. the total number of atoms in the system), we know the number of atoms in each mode. This is precisely the starting point we require.

We see from Figure (9.4) that if we were to average over all measurement outcomes, the entanglement would be degraded. However, conditional on a small range of measurement outcomes, it is possible to concentrate the entanglement. This is precisely the idea of entanglement concentration: from a large number of entangled pairs, we can distill a set with enhanced entanglement.

In this chapter, we have not been so much concerned with obtaining the best

possible concentration or indeed with demonstrating a scheme with great practical advantages Rather, the interest lies in the fact that, by demonstrating a feasible scheme for carrying out this protocol, we have shown that entanglement concentration is possible. The ability to manipulate and, in particular, purify the entanglement of macroscopic objects is of fundamental importance. Techniques for manipulating entanglement are progressing rapidly and improved purification schemes should follow. In particular, schemes which could generate maximally entangled condensates would be very desirable. The ability to concentrate the entanglement of Bose condensates suggests that they may be a valuable tool in quantum information experiments.

Chapter 10

Concluding remarks

10.1 Introduction

In this final chapter, we take a step back and provide an overview of the main results of this thesis and how they fit together. We also look ahead to how this work could be extended and discuss some of the exciting developments and practical applications that should soon be within technological reach.

The subject of this thesis, the quantum phase of BECs, has long caused confusion and debate. Sometimes this unease has been due to the fact that it raises difficult and subtle issues such as symmetry breaking. Often, however, it is the result of unclear terminology: for example, how can a number state condensate, which has no phase, be phase coherent? This lack of clarity is not helped by the fact that assumptions, which are valid in one area of BEC theory, can lead to incorrect conclusions in another. For example, while it is valid to assume that the condensate is in a coherent state when studying condensate dynamics, if taken literally, this assumption leads to the incorrect conclusion that a condensate has an absolute phase.

In the early part of this thesis, we set about clarifying these issues and providing a solid platform for our subsequent investigations. The remainder of the thesis extended our understanding of phase and can broadly be divided into four interlinked categories: the properties of the phase of BECs, the relationship between phase and entanglement, schemes for creating specific interesting entanglements, and a comparison of the practical merits of these entanglements. We begin by discussing each of these in turn.

10.2 Main results

Our discussion of the properties and nature of phase began in Chapter 2 where we established some key axioms. We used phase coherence as a definition of BEC and showed that it is a consequence of the atoms all sharing a single macroscopic wave function and does not depend on the quantum state of the condensate. We also showed that absolute phase is a valid concept only for infinite condensates and that all condensates produced in the laboratory must be thought of in terms of relative phase. This relative phase is due to an entanglement between condensate modes and can be created by a measurement.

In Chapter 3, we turned the idea of relative phase on its head, by showing how it is possible to define a phase standard for BECs. A phase reference, against which we can compare the phase of other condensates, allows of us to think of phase as if it were absolute. This is an important result which gives a clear and precise definition to the phase of a condensate. In the following chapter, we showed that phase could arise naturally between coupled condensates due to interactions and loss. Such a scheme does not rely on measurements to create a phase and was used to explain the results of an experimental demonstration of a mode locked atom laser.

The second area we treated was the link between phase and entanglement. This was first introduced in Chapter 2 to explain how measurements could establish a phase. In Chapter 3, we extended this idea to show that once an entanglement has been established, it is robust. This robustness comes in two forms: subsequent measurements of the phase between condensates will give the same result and the existing entanglements are not destroyed when other condensates are entangled with the phase standard. This robustness is the essence of how the phase standard works. We also discussed how entanglements and hence relative phase may be established by coupling condensates. Chapter 5 provided an important insight by demonstrating that different entanglements could lead to different natures of the phase. In particular, we showed that when number correlated pairs are passed through a beam splitter, the resulting state has Heisenberg limited phase. This suggested that the more entangled a state is, the better its phase resolution.

The link between entanglement and phase was further highlighted in Chapter 9, where we discussed a scheme for concentrating the entanglement in a pair of condensates. The improvement in entanglement may be modest, but it serves to demonstrate that entanglement swapping is possible in BECs and that they could

become a valuable tool in quantum information.

Our discussion of the link between phase and entanglement led us to consider schemes for creating specific interesting entanglements. We were interested primarily in creating entangled states that could give the best improvement in practical tasks over states that are not entangled. The two candidates we treated were the Schrödinger cat state and the number correlated state which, when passed through a beam splitter, has the approximate form,

$$|\psi\rangle = \frac{1}{\sqrt{N+1}} \sum_{i=0}^{N} |2i\rangle|2(N-i)\rangle. \tag{10.1}$$

We chose to study these states since they are each commonly referred to in the literature as maximally entangled states. This means that they should have the best possible phase resolution and so should give the best improvement in performance over classical states.

In Chapter 6, we outlined a straightforward scheme to create states of the form of (10.1). The scheme presented relies on coupling condensates with the right balance between the interaction and coupling strengths and should be within current technological capabilities. In Chapter 7 we considered how Schrödinger cat states may be generated in condensates by manipulating their phases. We presented two schemes: one is a simple scheme based on interferometry and the other is a more complex scheme that has the advantage of being relatively robust to loss during the creation process. Interestingly, we found that we could create cat states from number correlated states when there is loss present. The fact that these two states should be able to be created relatively easily is very exciting. Not only do they have great potential in practical applications, but they may provide a valuable tool for studying the nature of measurement and entanglement.

Finally, our fourth area of interest was to compare the merits of these two entangled states. We did this by comparing their performance as the input states to an interferometer and seeing which one could detect the smallest path length difference. For the lossless case, they both delivered the same performance, which is the best possible allowed by quantum mechanics. However, when dissipation was introduced to the system, they differed dramatically. In particular, the cat state was completely destroyed by the loss of a single atom, which severely restricted its practical usefulness. By contrast, the number correlated state was only gently degraded by loss. This is a remarkable result, not just for practical applications (some of which we outline below), but also from a theoretical perspective as it sug-

gests that the number correlated state is more information-rich, or more entangled, than the cat state.

10.3 Proposals for future work

One of the most exciting prospects for practical applications of this work is to investigate how we can make use of the number correlated state (10.1). The fact that this state has Heisenberg limited phase resolution and is relatively robust to loss means that it should be able to be used in a variety of schemes to give greatly enhanced sensitivity over its classical counterparts. We briefly discuss two such possibilities below: an improved frequency standard, and a scheme for making accurate force measurements.

We also discuss how our ability to manipulate phase and entanglement should allow us to create other useful entangled states. Two specific entanglements are highlighted. Finally we suggest how the semiclassical treatment of the dynamics of the number squeezed state, developed in Chapter 6, could be extended to other systems. This is potentially a very powerful technique that could be used to great effect when studying systems such as the Bose-Hubbard model.

10.3.1 Frequency standard

In Chapter 8 we commented on the fact that the favourable phase and robustness properties of the number correlated state may make it useful as a frequency standard or clock.

It was Wineland and co-workers who first proposed that the accuracy of frequency standards could be improved by using entangled states instead of uncorrelated particles [91, 131]. By using a cat state, the frequency resolution can be enhanced by a factor equal to the total number of particles, N. This can be very large for BECs and so the potential gain is considerable. The excitement was short-lived, however, when it was shown that any advantage is lost when there is dissipation [105]. The explanation is that, although cat states have much better phase resolution than uncorrelated particles, they are extremely fragile to loss. Their fleeting existence means that any gain due to the enhanced resolution is lost by the uncertainties introduced by being able to compare frequencies only for short times. Interestingly, these effects precisely cancel. At first sight this might suggest that the uncorrelated limit, in which the accuracy scales as $1/\sqrt{N}$, is a

fundamental limit that cannot be surpassed. This is not the case, however, and Huelga *et al.* [105] have shown that an improvement in the resolution by a factor of $1/\sqrt{e}$ can be achieved by using certain partially entangled states. Although this improvement is relatively modest, it is an important result as it shows that the classical limit can be surpassed. By using number correlated states, however, even better improvements in resolution may be able to be achieved.

The two driving factors of the accuracy of a clock are the phase resolution of the state and how long it can be evolved before being destroyed. Cat states excel in the former criterion but not in the latter and conversely for uncorrelated states. However, as we can see in Figure (8.1), number correlated states do not have the same trade off and excel in both areas. The resolution of the number correlated state is better than the uncorrelated (Gaussian) state and remains so even after a large number of the atoms have been lost. This means that the number correlated state can be evolved for times comparable to the Gaussian state and yet retain better phase resolution throughout. Such a state is therefore the perfect candidate for creating an improved frequency standard. An interesting area of study would be to carefully design a scheme by which this could be put into action.

10.3.2 Force measurements

Closely related to the frequency standard is a scheme for accurately measuring forces. Corney *et al.* have proposed a scheme which makes use of BECs to detect very weak differences in forces such as gravity [132]. The scheme is essentially an interferometer in which the two arms experience slightly different frequency shifts due to the different forces acting on them. Following the precedent set by clock schemes, they realised that the accuracy of such a scheme could also be enhanced by using entangled condensates. However, much like the frequency standard schemes, their attention has focused on cat states.

We propose that better performance may be able to be achieved by using number correlated states. The same advantages should be able to be achieved as for the frequency standard. In particular, the evolution under the influence of the force should be able to take place over a longer time, which will improve the sensitivity of the detector.

Corney *et al.* considered the limitations on the accuracy of their scheme due to interactions and external coupling. They did not, however, consider loss which, due to the fragile nature of cat states, may well be the limiting process. By using

number correlated states instead of cat states, however, the effects of loss should be gentle and the scheme should work in the way originally outlined.

10.3.3 Creating exotic entanglements

Our knowledge of manipulating phase and entanglement provides us with the tools to create other interesting entangled states. There are a lot of exciting prospects and many unexplored avenues. In this section, we suggest two possibilities that are feasible: a maximally entangled superposition of correlated condensates, and four-fold number correlated condensates.

We begin by discussing how a maximally entangled superposition of number correlated condensates may be formed. Our starting point is a single number correlated pair. We have described how such a state can be created in Chapter 6. If we pass this state, $|\psi\rangle = |N\rangle|N\rangle$, through a 50:50 beam splitter, the resulting state can be written approximately as

$$|\psi\rangle = \frac{1}{\sqrt{N+1}} \sum_{i=0}^{N} |2i\rangle|2(N-i)\rangle. \tag{10.2}$$

Assuming N is even, each mode can only have an even number of atoms. If we now take one of these modes, couple it to a vacuum state, and once again carry out the number correlating procedure as outlined in Chapter 6, the resulting state is,

$$|\psi\rangle = \frac{1}{\sqrt{N+1}} \sum_{i=0}^{N} |i\rangle|i\rangle. \tag{10.3}$$

We see that we now have a equally weighted superposition over all number correlated pairs. We don't just have even numbers because all the even pairs have been split in half. This is an interesting state as it is maximally entangled. It may be of great use in teleportation or entanglement swapping schemes for condensates.

Another exotic state that could be studied is a higher order version of the number correlated state. We first suggested this in Chapter 9 as a means of carrying out the entanglement concentration scheme in BECs. This state could be formed by creating a number correlated pair, $|\psi\rangle = |2N\rangle|2N\rangle$, in the now-familiar way and then coupling each of these modes to a vacuum state and number squeezing again. This creates four number correlated condensates,

$$|\psi\rangle = |N\rangle|N\rangle|N\rangle|N\rangle. \tag{10.4}$$

Of course this process could be continued to form a longer chain of condensates all in the same number state. The strong correlations in this state make it a powerful quantum resource. We have seen how it could be useful in entanglement concentration and it would be interesting to study how its potential could be exploited in other practical applications.

10.3.4 Bose-Hubbard model

In Chapter 6, we discussed a method for creating number correlated pairs of BECs. This result is interesting in its own right. However, an intriguing and slightly surprising spin-off is how well we were able to describe this process using a semiclassical model. The system we are dealing with is highly entangled and non-classical and it is not usually possible to describe such systems with semiclassical mean field theory. However, we showed how we could apply it to model the squeezing procedure and predict the timescales accurately. The key was using different trajectories to represent groups of a few superposed terms of the state. By splitting the state up into parts each represented by a unique trajectory, we were able to study the evolution of the distribution. This proved to be a surprisingly accurate and powerful technique.

It would be interesting to see what other systems it could be applied to. Of particular interest is the Bose-Hubbard model [133, 134], which consists of a boson gas hopping through a multidimensional lattice, and is simply a higher order generalisation of the number squeezing scheme. This model is of great interest as it exhibits rich structure including a phase transition from the superfluid to the Mott insulator phase at low temperature. The full model, however, is extremely complicated since it is a quantum mechanical system with many modes on a multidimensional lattice. To make any headway with calculations or understanding, it is therefore crucial to be able to make gross simplifications whilst still retaining the key features of the system.

The behaviour of the Bose-Hubbard model has been investigated by a number of theoretical techniques, from mean field, variational and perturbative approaches, to quantum Monte Carlo techniques. The present technique may add another valuable weapon to the armoury. Semiclassical techniques allow us to describe the vastly complicated quantum state with a few c-numbers. This simplification allows for considerable insight to be gained and it is currently under investigation how this could be done for a lattice of coupled BECs. There may well be many other

entangled systems for which this technique could also be applied and it would be of great interest to investigate these.

10.3.5 Other thoughts

This thesis has progressed from a discussion of the phase of a BEC to issues of entanglement and information. It would be natural for future work to continue to forge links between BEC and quantum information. We have already shown in Chapter 9 a scheme by which the entanglement between a pair of condensates may be concentrated. Such a procedure is crucial for teleportation via noisy channels. The interest lies not so much in the fact that this could be used as a practical scheme, but in the fact that it shows that entanglement concentration in BECs should be possible. Further work could develop improved entanglement concentration schemes, eventually even ones that produce maximally entangled pairs. This work would naturally move towards eventually developing faithful entanglement swapping or teleportation schemes for condensates.

Entanglements play an important part in this discussion: both how to create them and how to quantify them. We have already discussed how work may progress in the former. Quantifying entanglement has received a lot of recent theoretical attention and the theory is well established for two modes [110, 111]. In Chapter 8, we showed how the entanglement of a state could be quantified by testing its performance in an interferometer both in the presence and absence of dissipation. It would be interesting to develop this technique further and, in particular, to see whether it can be generalised to more than two modes. This is something that as of now cannot be done theoretically.

10.4 The last word

During the course of this thesis, we have developed an understanding of quantum phase and entanglement. We have cleared up some conceptual issues and discussed how phase may be defined, created, manipulated, and controlled. We began with very theoretical discussions of issues such as symmetry breaking and have progressed through to practical and useful schemes that could be carried out in the laboratory.

This progression may reflect the interest in the field itself. BECs are a wonderful testing ground for many theories, and since their discovery they have been studied

in their own right. As time goes by, however, it seems BECs will become not only an object of academic interest, but also a valuable tool to be used in various practical schemes. The indications are that one of their main uses will be to create states with useful multiparticle entanglements. This may allow them to be used in quantum information schemes and should allow for a considerable improvement in the accuracy of measurement and other schemes.

The study of phase and entanglement in BECs is a relatively new field of study. However, the signs are good that it is a fertile one and will lead to many exciting developments for quite some time yet. It seems that the excitement generated in 1995 when BECs were first observed in dilute gases is well and truly justified.

APPENDIX A

Derivation of beam splitter outputs

In this appendix, we derive the output from a 50:50 beam splitter for two different input states. We consider a beam splitter with input modes labelled by a and b and output modes labelled by c and d. The beam splitter transformation is given by

$$c = ta + rb \tag{A.1}$$

$$d = ra + tb, \tag{A.2}$$

where t and r are respectively complex transmission and reflection coefficients. Boundary conditions at the surface of the beam splitter yield the following conditions,

$$|t|^2 + |r|^2 = 1 \tag{A.3}$$

$$rt^* + r^*t = 0. \tag{A.4}$$

Without loss of generality, we take t to be real and r to be imaginary. This allows us to parametrise t and r as: $t = \cos(\theta/2)$ and $r = i\sin(\theta/2)$.

We now consider the cases of two different inputs. The first is a number state $|n\rangle$ at mode a and a vacuum state at mode b. This can be written as

$$|n\rangle_a|0\rangle_b = \frac{1}{\sqrt{n!}}\left(a^\dagger\right)^n|0\rangle_a|0\rangle_b. \tag{A.5}$$

We can find the output state simply by transforming the operators into those for modes c and d,

$$\begin{pmatrix} a \\ b \end{pmatrix} = \begin{pmatrix} \cos\frac{\theta}{2} & -i\sin\frac{\theta}{2} \\ -i\sin\frac{\theta}{2} & \cos\frac{\theta}{2} \end{pmatrix} \begin{pmatrix} c \\ d \end{pmatrix}, \tag{A.6}$$

which simply corresponds to a rotation of θ between the input and output modes. This gives

$$a^\dagger = \cos\frac{\theta}{2}\, c^\dagger + i\sin\frac{\theta}{2}\, d^\dagger. \tag{A.7}$$

For a 50:50 beamsplitter, $|r|^2 = |t|^2 = 0.5$, which gives $\theta = \pi/2$. Substituting into (A.7), we can write the output state (A.5) as

$$|\text{out}\rangle = \left[\frac{1}{\sqrt{2}}\left(c^\dagger + id^\dagger\right)\right]^n |0\rangle_c|0\rangle_d. \tag{A.8}$$

Expanding the square brackets using the binomial distribution, we get

$$|\text{out}\rangle = \frac{1}{\sqrt{2^n n!}} \sum_{m=0}^{n} \binom{n}{m} \left(c^\dagger\right)^m \left(id^\dagger\right)^{n-m} |0\rangle_c|0\rangle_d. \tag{A.9}$$

Operating on the kets and rewriting i as $\exp(i\pi/2)$ we get

$$|\text{out}\rangle = \frac{1}{\sqrt{2^n}} \sum_{m=0}^{n} \binom{n}{m}^{1/2} \mathrm{e}^{-im\pi/2} |m\rangle_c|n-m\rangle_d, \tag{A.10}$$

where we have ignored the overall global phase. This is the result shown in Equation (5.5)

The second case we would like to consider is the output from a beam splitter for number correlated inputs. The input state, in this case, can be written as

$$|n\rangle_a|n\rangle_b = \frac{1}{n!}\left(a^\dagger b^\dagger\right)^n |0\rangle_a|0\rangle_b. \tag{A.11}$$

Proceeding as before, we can transform to the output operators,

$$a^\dagger b^\dagger = i\sin\frac{\theta}{2}\cos\frac{\theta}{2}\left(d^\dagger d^\dagger + c^\dagger c^\dagger\right) + \left(\cos^2\frac{\theta}{2} - \sin^2\frac{\theta}{2}\right) c^\dagger d^\dagger. \tag{A.12}$$

This allows us to write the output state for a 50:50 beam splitter as

$$|\text{out}\rangle = \frac{1}{n!}\left[\frac{i}{2}\left(d^\dagger d^\dagger + c^\dagger c^\dagger\right)\right]^n |0\rangle_c|0\rangle_d. \tag{A.13}$$

Expanding the square brackets using the binomial distribution, we get,

$$|\text{out}\rangle = \frac{1}{n!}\sum_{j=0}^{n}\frac{n!}{(n-j)!j!}\left(\frac{i}{2}\right)^{n}(d^{\dagger})^{2j}(c^{\dagger})^{2(n-j)}\,|0\rangle_c|0\rangle_d. \tag{A.14}$$

Ignoring the irrelevant global phase, we can write this as

$$|\text{out}\rangle = \frac{1}{2^n}\sum_{j=0}^{n}\sqrt{\frac{(2n-2j)!}{(n-j)!^2}}\sqrt{\frac{(2j)!}{j!^2}}\,|2(n-j)\rangle_c|2j\rangle_d, \tag{A.15}$$

which is the result shown in Equation (5.9).

Appendix B

Semiclassical equations for coupled condensates

We consider two coupled condensates denoted by the annihilation operators a and b. The Hamiltonian governing this system is

$$H = \omega_a a^\dagger a + \omega_b b^\dagger b + U\left(a^{\dagger 2}a^2 + b^{\dagger 2}b^2\right) + \Gamma\left(a^\dagger b + b^\dagger a\right), \tag{B.1}$$

where $\hbar \equiv 1$, U is the interatomic interaction strength which is assumed to be the same for each mode, Γ is the coupling strength, and ω_a and ω_b are the frequencies of modes a and b respectively.

We can now write down the equations of motion for these two operators. These are given by

$$i\dot{a}(t) = \omega_a a + 2Ua^\dagger a^2 + \Gamma b \tag{B.2}$$

$$i\dot{b}(t) = \omega_b b + 2Ub^\dagger b^2 + \Gamma a \tag{B.3}$$

Next we make the semiclassical approximation which involves replacing the operators with

$$a(t) = \sqrt{N_a(t)}\, \mathrm{e}^{i\theta_a(t)} \tag{B.4}$$

$$b(t) = \sqrt{N_b(t)}\, \mathrm{e}^{i\theta_b(t)}, \tag{B.5}$$

where N_a and N_b correspond to the number of atoms in modes a and b and θ_a and θ_b correspond to the phases of modes a and b respectively. We substitute these

into (B.2) and (B.3) and equate the results with

$$i\frac{\mathrm{d}}{\mathrm{d}t}\left(\sqrt{N_a}\,\mathrm{e}^{i\theta_a}\right) = \frac{i\dot{N}_a}{2\sqrt{N_a}}\,\mathrm{e}^{i\theta_a} - \dot{\theta}_a\sqrt{N_a}\,\mathrm{e}^{i\theta_a} \tag{B.6}$$

$$i\frac{\mathrm{d}}{\mathrm{d}t}\left(\sqrt{N_b}\,\mathrm{e}^{i\theta_b}\right) = \frac{i\dot{N}_b}{2\sqrt{N_b}}\,\mathrm{e}^{i\theta_b} - \dot{\theta}_b\sqrt{N_b}\,\mathrm{e}^{i\theta_b}. \tag{B.7}$$

By then equating the real and imaginary components of each side of each of these equations, we obtain the following four equations

$$\dot{N}_a = 2\Gamma\sqrt{N_a N_b}\,\sin\left(\theta_b - \theta_a\right) \tag{B.8}$$

$$\dot{N}_b = -2\Gamma\sqrt{N_a N_b}\,\sin\left(\theta_b - \theta_a\right) \tag{B.9}$$

$$\dot{\theta}_a = -\omega_a - 2UN_a - \Gamma\sqrt{\frac{N_b}{N_a}}\,\cos\left(\theta_b - \theta_a\right) \tag{B.10}$$

$$\dot{\theta}_b = -\omega_b - 2UN_b - \Gamma\sqrt{\frac{N_a}{N_b}}\,\cos\left(\theta_b - \theta_a\right). \tag{B.11}$$

For convenience, we now define the new quantities of fractional population imbalance,

$$z(t) \equiv \left(N_b(t) - N_a(t)\right)/N, \tag{B.12}$$

where $N = N_a + N_b$ is the total number of atoms and is a constant, and relative phase

$$\phi(t) \equiv \theta_b(t) - \theta_a(t). \tag{B.13}$$

We can write our equations in terms of these relative quantities by taking the differences of (B.8) with (B.9) and (B.10) with (B.11). The resulting equations are

$$\dot{z}(t) = -2\Gamma\sqrt{1 - z^2(t)}\,\sin(\phi(t)) \tag{B.14}$$

$$\dot{\phi}(t) = -\Delta\omega - 2UNz(t) + \frac{2\Gamma z(t)}{\sqrt{1 - z^2(t)}}\,\cos(\phi(t)), \tag{B.15}$$

where $\Delta\omega = (\omega_b - \omega_a)$. These equations are a very useful tool for analysing the dynamics of coupled Bose condensates. If we substitute $\Delta\omega = 0$ and $U = 0$, we recover Equations (4.19) and (4.20). We can obtain Equations (6.8) and (6.9) by making the replacements $\Delta\omega = 0$ and $\phi \to \phi - \pi$, since $\sin(\phi - \pi) = -\sin(\phi)$ and $\cos(\phi - \pi) = -\cos(\phi)$.

Appendix C

Equivalence of Raman coupling and a beam splitter

We consider a beam splitter with input modes labelled by a and b and output modes labelled by c and d. The beam splitter transformation is given by

$$c = ta + rb \tag{C.1}$$

$$d = ra + tb, \tag{C.2}$$

where t and r are respectively complex transmission and reflection coefficients. Boundary conditions at the surface of the beam splitter yield the following conditions,

$$|t|^2 + |r|^2 = 1 \tag{C.3}$$

$$rt^* + r^*t = 0. \tag{C.4}$$

Without loss of generality, we take t to be real and r to be imaginary. This allows us to parametrise t and r as $t = \cos(\theta/2)$ and $r = i\sin(\theta/2)$. This means that the beam splitter transformation is

$$c = \cos\left(\frac{\theta}{2}\right) a + i\sin\left(\frac{\theta}{2}\right) b \tag{C.5}$$

$$d = i\sin\left(\frac{\theta}{2}\right) a + \cos\left(\frac{\theta}{2}\right) b. \tag{C.6}$$

For a 50:50 beam splitter, $\theta = \pi/2$.

Now we consider the form of the resonant Raman coupling operator,

$$U = \exp\left[\frac{1}{2}i\theta\left(a^\dagger b + b^\dagger a\right)\right], \tag{C.7}$$

where $\theta \equiv \Gamma t$, where Γ is the coupling strength and t is the coupling time.

We now investigate how the input mode operators are transformed by this operation,

$$c = U^\dagger a U = \mathrm{e}^{-i\theta\left(a^\dagger b + b^\dagger a\right)}\, a\, \mathrm{e}^{i\theta\left(a^\dagger b + b^\dagger a\right)}. \tag{C.8}$$

If we make use of the operator identity

$$\mathrm{e}^{\xi B} A \mathrm{e}^{-\xi B} = A + \xi[B, A] + \frac{1}{2!}\xi^2[B, [B, A]] + \ldots, \tag{C.9}$$

we can rewrite (C.8) as

$$c = a + i\frac{\theta}{2}b - \frac{1}{2!}\left(\frac{\theta}{2}\right)^2 a - \frac{i}{3!}\left(\frac{\theta}{2}\right)^3 b + \ldots \tag{C.10}$$

$$= \cos\left(\frac{\theta}{2}\right) a + i \sin\left(\frac{\theta}{2}\right) b. \tag{C.11}$$

Similarly,

$$d = i \sin\left(\frac{\theta}{2}\right) a + \cos\left(\frac{\theta}{2}\right) b. \tag{C.12}$$

Comparing (C.11) and (C.12) with (C.5) and (C.6), we see that Raman coupling for time, t, and coupling strength, Γ, is equivalent to passing the two modes through a beam splitter with reflectivity,

$$r = \cos\left(\frac{\Gamma t}{2}\right). \tag{C.13}$$

So, coupling for a quater Raman cycle, $t = \pi/(2\Gamma)$ is equivalent to passing through a 50:50 beam splitter.

Derivation of Equations (7.18) and (9.15)

We wish to find the form of the entangled state

$$|\psi\rangle \propto \sum_{q=0}^{n} \binom{n}{q}^{\zeta} \mathrm{e}^{i\pi q(q-1)/2}\, \mathrm{e}^{-i\pi q m(n+\phi-1)/2}\, |q\rangle|n-q\rangle, \tag{D.1}$$

after passing it through a 50:50 beam splitter. If we set $\zeta = 1/2$ and $m = 0$, we get Equation (7.13). If we set $\zeta = 3/2$ and $m = 1$, we get Equation (9.13). This means that by finding the result of passing (D.1) through a beam splitter we can derive both Equation (7.18) and Equation(9.15).

As discussed in Appendix (A), we can find the effect of the beam splitter by first writing the initial state (D.1) in terms of the input mode operators, a and b,

$$|\psi\rangle \propto \sum_{q=0}^{n} \binom{n}{q}^{\zeta+1/2} \mathrm{e}^{i\eta} \left(a^{\dagger}\right)^{q} \left(b^{\dagger}\right)^{n-q} |0\rangle|0\rangle, \tag{D.2}$$

where $\eta = \pi q\left[q - 1 - m\left(n + \phi - 1\right)\right]/2$. We next transform a and b to the output operators, c and d. Using (A.6) with $\theta = \pi/2$ for a 50:50 beam splitter, we can write (D.2) as

$$|\psi\rangle \propto \sum_{q=0}^{n} \binom{n}{q}^{\zeta+1/2} \mathrm{e}^{i\eta} \left(c^{\dagger} + id^{\dagger}\right)^{q} \left(ic^{\dagger} + d^{\dagger}\right)^{n-q} |0\rangle|0\rangle. \tag{D.3}$$

Next, we expand the operator products using the binomial distribution

$$|\psi\rangle \propto \sum_{q=0}^{n} \binom{n}{q}^{\zeta+1/2} e^{i\eta} \sum_{r=0}^{q} \binom{q}{r} \left(c^\dagger\right)^r \left(id^\dagger\right)^{q-r} \times \sum_{s=0}^{n-q} \binom{n-q}{s} \left(ic^\dagger\right)^s \left(d^\dagger\right)^{n-q-s} |0\rangle|0\rangle. \tag{D.4}$$

Operating on the kets, this state becomes

$$|\psi\rangle \propto \sum_{q=0}^{n}\sum_{r=0}^{q}\sum_{s=0}^{n-q} \binom{n}{q}^{\zeta+1/2} \binom{q}{r} \binom{n-q}{s} e^{i\eta} e^{i\pi(q+s-r)/2} \times \sqrt{(r+s)!(n-r-s)!}\,|r+s\rangle|n-r-s\rangle, \tag{D.5}$$

where we have put $i^{q-r+s} = \exp[i\pi(q-r+s)/2]$. We now make the substitution $t = r + s$

$$|\psi\rangle \propto \sum_{q=0}^{n}\sum_{r=0}^{q}\sum_{t=0}^{n-q+r} \binom{n}{q}^{\zeta+1/2} \binom{q}{r} \binom{n-q}{t-r} e^{i\eta} e^{i\pi(q+t-2r)/2} \times \sqrt{t!(n-t)!}\,|t\rangle|n-t\rangle. \tag{D.6}$$

Finally, we change the order of summation of the second and third sums,

$$\sum_{r=0}^{q}\sum_{t=r}^{n-q+r} \longrightarrow \sum_{t=0}^{n}\sum_{r=r_1}^{r_2}, \tag{D.7}$$

where $r_1 = \max\{0, t+q-n\}$ and $r_2 = \min\{t, q\}$. This allows us to write the final state as

$$|\psi\rangle \propto \sum_{t=0}^{n} C_t\,|t\rangle|n-t\rangle, \tag{D.8}$$

where

$$C_t = \sqrt{t!(n-t)!}\sum_{q=0}^{n}\sum_{r=r_1}^{r_2} \binom{n}{q}^{\zeta+1/2} \binom{q}{r} \binom{n-q}{t-r} e^{i\eta} e^{i\pi(q+t-2r)/2}. \tag{D.9}$$

With this general result, we can now recover the results for the two cases that we are interested in. Substituting $\zeta = 1/2$ and $m = 0$, we get $\eta = \pi q(q-1)/2$ and

recover the result (7.18) for a cat state,

$$C_t = \sqrt{t!(n-t)!}\sum_{q=0}^{n}\sum_{r=r_1}^{r_2}\begin{pmatrix} n \\ q \end{pmatrix}\begin{pmatrix} q \\ r \end{pmatrix}\begin{pmatrix} n-q \\ t-r \end{pmatrix} e^{i\pi(q^2+t-2r)/2}. \tag{D.10}$$

Finally, if we substitute $\zeta = 3/2$, $m = 1$, we get $\eta = \pi q(q-n-\phi)/2$ and recover the result (9.15) for the purification state,

$$C_t = \sqrt{t!(n-t)!}\sum_{q=0}^{n}\sum_{r=r_1}^{r_2}\begin{pmatrix} n \\ q \end{pmatrix}^2\begin{pmatrix} q \\ r \end{pmatrix}\begin{pmatrix} n-q \\ t-r \end{pmatrix} e^{i\pi q(q-n-(\phi-1))/2} e^{i\pi(t-2r)/2}. \tag{D.11}$$

BIBLIOGRAPHY

[1] S. Bose. *Plancks gesetz und lichtquantenhypothese.* Z. Phys. 26, 178 (1924).

[2] A. Einstein. *Quantentheorie des einatomigen idealen gases: Zweite abhandlung.* Sitzungber. Preuss. Akad. Wiss. 1925, 3 (1925).

[3] F. London. *The λ-phenomenon of liquid helium and the Bose-Einstein degeneracy.* Nature 141, 643 (1938).

[4] F. London. *On the Bose-Einstein condensation.* Phys. Rev. 54, 947 (1938).

[5] D. R. Tiley and J. Tilley. Superfluidity and Superconductivity (Adam Hilger, 1990).

[6] I. F. Silvera and J. T. M. Walraven. *Stabilization of atomic hydrogen at low temperature.* Phys. Rev. Lett. 44, 164 (1980).

[7] H. F. Hess, D. A. Bell, G. P. Kochanski, R. A. Cline, *et al.*. *Observation of three-body recombination in spin-polarized hydrogen.* Phys. Rev. Lett. 51, 483 (1983).

[8] M. H. Anderson, J. R. Ensher, M. R. Matthews, C. E. Wieman, and E. A. Cornell. *Observation of Bose-Einstein condensation in a dilute atomic vapor.* Science 269, 198 (1995).

[9] M. H. Anderson, J. R. Ensher, M. R. Matthews, C. E. Wieman, and E. A. Cornell. *Evidence for Bose-Einstein condensation in a dilute atomic vapor.* In Laser Spectroscopy, XII International Conference (edited by M. Inguscio, M. Allegrini, and A. Sasso), p. 3 (World Scientific, 1995).

[10] C. C. Bradley, C. A. Sackett, J. J. Tollett, and R. G. Hulet. *Evidence of Bose-Einstein condensation in an atomic gas with attractive interactions.* Phys. Rev. Lett. 75, 1687 (1995). *ibid.* **79**, 1170 (1997).

[11] K. B. Davis, M.-O. Mewes, M. R. Andrews, N. J. van Druten, *et al.*. *Bose-Einstein condensation in a gas of sodium atoms.* Phys. Rev. Lett. 75, 3969 (1995).

[12] F. Mandl and G. Shaw. Quantum Field Theory (Wiley, 1984).

[13] H.-J. Miesner, D. M. Stamper-Kurn, M. R. Andrews, D. S. Durfee, *et al.*. *Bosonic stimulation in the formation of a Bose-Einstein condensate.* Science 279, 1005 (1998).

[14] D. Jaksch, C. W. Gardiner, K. M. Gheri, and P. Zoller. *Quantum kinetic theory. IV. intensity and amplitude fluctuations of a Bose-Einstein condensate at finite temperature including trap loss.* Phys. Rev. A 58, 1450 (1998).

[15] K. Huang. Statistical Mechanics (John Wiley & Sons, 1963).

[16] M. Abramowitz and I. A. Stegun. Handbook of Mathematical Functions (Dover Publications, Ninth edition, 1970).

[17] V. S. Bagnato, D. E. Pritchard, and D. Kleppner. *Bose-Einstein condensation in an external potential.* Phys. Rev. A 35, 4354 (1987).

[18] N. Bogoliubov. *On the theory of superfluidity.* J. Phys. 11, 23 (1947).

[19] O. Penrose and L. Onsager. *Bose-Einstein condensation and liquid Helium.* Phys. Rev. 104, 576 (1956).

[20] A. Griffin. *Conserving and gapless approximations for an inhomogeneous Bose gas at finite temperatures.* Phys. Rev. B 53, 9341 (1996).

[21] D. S. Jin, M. R. Matthews, J. R. Ensher, C. E. Wieman, and E. A. Cornell. *Temperature-dependent damping and frequency shifts in collective excitations of a dilute Bose-Einstein condensate.* Phys. Rev. Lett. 78, 764 (1997).

[22] D. A. W. Hutchinson, R. J. Dodd, and K. Burnett. *Gapless finite-T theory of collective modes of a trapped gas.* Phys. Rev. Lett. 81, 2198 (1998).

[23] P. O. Fedichev, G. V. Shlyapnikov, and J. T. M. Walraven. *Damping of low-energy excitations of a trapped Bose-Einstein condensate at finite temperatures.* Phys. Rev. Lett. 80, 2269 (1998).

[24] L. P. Pitaevskii. *The problem of the form of the spectrum of elementary excitations of liquid helium II.* Sov. Phys. JETP 12, 155 (1960).

[25] K. Burnett, M. Edwards, and C. W. Clark. *The theory of Bose-Einstein condensation of dilute gases.* Phys. Today 52, 37 (1999).

[26] P. A. Ruprecht, M. J. Holland, K. Burnett, and M. Edwards. *Time-dependent solution of the nonlinear Schrödinger equation for Bose-condensed trapped neutral atoms.* Phys. Rev. A 51, 4704 (1995).

[27] R. J. Dodd, M. Edwards, C. J. Williams, C. W. Clark, *et al.*. *Role of attractive interactions on Bose-Einstein condensation.* Phys. Rev. A 54, 661 (1996).

[28] D. G. Fried, T. C. Killian, L. Willmann, D. Landhuis, *et al.*. *Bose-Einstein condensation of atomic hydrogen.* Phys. Rev. Lett. 81, 3811 (1998).

[29] C. J. Foot. *Laser cooling and trapping of atoms.* Contemp. Phys. 32, 369 (1991).

[30] W. D. Phillips. *Laser cooling and trapping of neutral atoms.* Rev. Mod. Phys. 70, 721 (1998).

[31] S. Chu, L. Hollberg, J. E. Bjorkholm, A. Cable, and A. Ashkin. *Three-dimensional viscous confinement and cooling of atoms by resonance radiation pressure.* Phys. Rev. Lett. 55, 48 (1985).

[32] H. F. Hess. *Evaporative cooling of magnetically trapped and compressed spin-polarized hydrogen.* Phys. Rev. B 34, 3476 (1986).

[33] H. F. Hess, G. P. Kochanski, J. M. Doyle, N. Masuhara, *et al.*. *Magnetic trapping of spin polarized atomic hydrogen.* Phys. Rev. Lett. 59, 672 (1987).

[34] T. W. Hijmans, O. J. Luiten, I. D. Setija, and J. T. M. Walraven. *Optical cooling of atomic hydrogen in a magnetic trap.* J. Opt. Soc. Am. B 6, 2235 (1989).

[35] D. E. Pritchard, K. Helmerson, and A. G. Martin. *Atom traps.* In Atomic Physics 11 (edited by S. Haroche, J. C. Gay, and G. Grynberg), p. 179 (World Scientific, 1989).

[36] T. Walker and P. Feng. In Advances in Atomic, Molecular, and Optical Physics (edited by B. Bederson and H. Walther), p. 125 (Academic Press, San Diego, 1994).

[37] P. W. Anderson. *Considerations on the flow of superfluid Helium.* Rev. Mod. Phys. 38, 298 (1966).

[38] P. W. Anderson. Basic Notions of Condensed Matter Physics (Benjamin-Cummings, 1984).

[39] M. R. Andrews, C. G. Townsend, H.-J. Miesner, D. S. Durfee, *et al.*. *Observation of interference between two Bose-Einstein condensates.* Science 275, 637 (1997).

[40] I. Bloch, T. Hänsch, and T. Esslinger. *Measurement of the spatial coherence of a trapped Bose gas at the phase transition.* Nature 403, 166 (2000).

[41] A. Griffin, D. W. Snoke, and S. Stringari. Bose-Einstein Condensation (Cambridge University Press, 1995).

[42] J. Goldstone. *Field theories with 'superconductor' solutions.* Nuovo Cimento 19, 154 (1961).

[43] M. Holland and J. Cooper. *Expansion of a Bose-Einstein condensate in a harmonic potential.* Phys. Rev. A 53, R1954 (1996).

[44] M. Edwards, P. A. Ruprecht, K. Burnett, R. J. Dodd, and C. W. Clark. *Collective excitations of atomic Bose-Einstein condensates.* Phys. Rev. Lett. 77, 1671 (1996).

[45] D. A. W. Hutchinson, K. Burnett, R. J. Dodd, S. A. Morgan, *et al.*. *Gapless mean-field theory Bose-Einstein condensates.* J. Phys. B 33, 1 (2000).

[46] W. H. Louisell. Quantum Statistical Properties of Radiation (Wiley, 1973).

[47] J. Javanainen and S. M. Yoo. *Quantum phase of a Bose-Einstein condensate with an arbitrary number of atoms.* Phys. Rev. Lett. 76, 161 (1996).

[48] Y. Castin and J. Dalibard. *Relative phase of two Bose-Einstein condensates.* Phys. Rev. A 55, 4330 (1997).

[49] D. T. Pegg and S. M. Barnett. *Unitary phase operator in quantum mechanics.* Europhys. Lett. 6, 483 (1988).

[50] D. T. Pegg and S. M. Barnett. *Phase properties of the quantized single-mode electromagnetic-field.* Phys. Rev. A 39, 1665 (1989).

[51] D. T. Pegg and S. M. Barnett. *On the Hermitian optical phase operator.* J. Mod. Opt. 36, 7 (1989).

[52] S. M. Barnett and P. M. Radmore. Methods in Theoretical Quantum Optics (Oxford University Press, 1997).

[53] A. J. Leggett. *Is 'relative quantum phase' transitive?.* Found. Phys. 25, 113 (1995).

[54] A. J. Leggett. *Broken gauge symmetry in a Bose condensate.* In Bose-Einstein Condensation (edited by A. Griffin, D. W. Snoke, and S. Stringari), p. 452 (Cambridge University Press, 1995).

[55] J. I. Cirac, C. W. Gardiner, M. Naraschewski, and P. Zoller. *Continuous observation of interference fringes from Bose condensates.* Phys. Rev. A 54, R3714 (1996).

[56] B. D. Josephson. *Possible new effects in superconductive tunnelling.* Phys. Lett. 1, 251 (1962).

[57] T. Wong, M. J. Collett, and D. F. Walls. *Interference of two Bose-Einstein condensates with collisions.* Phys. Rev. A 54, R3718 (1996).

[58] M. Naraschewski, H. Wallis, A. Schenzle, J. I. Cirac, and P. Zoller. *Interference of Bose condensates.* Phys. Rev. A 54, 2185 (1996).

[59] H. J. Carmichael. An Open Systems Approach to Quantum Optics (Springer, 1993).

[60] H. M. Wiseman and G. J. Milburn. *Interpretation of quantum jump and diffusion processes illustrated on the Bloch sphere.* Phys. Rev. A 47, 1652 (1993).

[61] J. Ruostekoski and D. F. Walls. *Nondestructive optical measurement of relative phase between two Bose-Einstein condensates.* Phys. Rev. A 56, 2996 (1997).

[62] A. Imamoğlu and T. A. B. Kennedy. *Optical measurements of the condensate phase.* Phys. Rev. A 55, R849 (1997).

[63] J. Javanainen. *Optical detection of the relative phase between two Bose-Einstein condensates.* Phys. Rev. A 54, R4629 (1996).

[64] D. S. Hall, M. R. Matthews, J. R. Ensher, C. E. Wieman, and E. A. Cornell. *Dynamics of component separation in a binary mixture of Bose-Einstein condensates.* Phys. Rev. Lett. 81, 1539 (1998).

[65] H. J. Carmichael, S. Singh, R. Vyas, and P. Rice. *Photoelectric waiting times and atomic state reduction in resonance fluorescence.* Phys. Rev. A 39, 1200 (1989).

[66] J. Dalibard, Y. Castin, and K. Mølmer. *Wave-function approach to dissipative processes in quantum optics.* Phys. Rev. Lett. 68, 580 (1992).

[67] N. Gisin and I. C. Percival. *Wave-function approach to dissipative processes - are there quantum jumps?.* Phys. Lett. A 167, 315 (1992).

[68] N. Gisin and I. C. Percival. *The quantum state diffusion model applied to open systems.* Phys. Phys. A: Math. Gen. 25, 5677 (1992).

[69] E. M. Wright, D. F. Walls, and J. C. Garrison. *Collapses and revivals of Bose-Einstein condensates formed in small atomic samples.* Phys. Rev. Lett. 77, 2158 (1996).

[70] A. Sinatra and Y. Castin. *Phase dynamics of Bose-Einstein condensates: Losses versus revivals.* Eur. Phys. J. D 4, 247 (1998).

[71] D. M. Stamper-Kurn, M. R. Andrews, A. P. Chikkatur, S. Inouye, *et al.*. *Optical confinement of a Bose-Einstein condensate.* Phys. Rev. Lett. 80, 2027 (1998).

[72] B. P. Anderson and M. A. Kasevich. *Macroscopic quantum interference from atomic tunnel arrays.* Science 282, 1686 (1998).

[73] M. R. Matthews, D. S. Hall, D. S. Jin, J. R. Ensher, *et al.*. *Dynamical response of a Bose-Einstein condensate to a discontinuous change in internal state*. Phys. Rev. Lett. 81, 243 (1998).

[74] P. D. Featonby, G. S. Summy, C. L. Webb, R. M. Godun, *et al.*. *Separated-path Ramsey atom interferometer*. Phys. Rev. Lett. 81, 495 (1998).

[75] M.-O. Mewes, M. R. Andrews, D. M. Kurn, D. S. Durfee, *et al.*. *Output coupler for Bose-Einstein condensed atoms*. Phys. Rev. Lett. 78, 582 (1997).

[76] D. S. Hall, M. R. Matthews, C. E. Wieman, and E. A. Cornell. *Measurements of relative phase in two-component Bose-Einstein condensates*. Phys. Rev. Lett. 81, 1543 (1998).

[77] E. W. Hagley, L. Deng, M. Kozuma, J. Wen, *et al.*. *A well-collimated quasi-continuous atom laser*. Science 283, 1706 (1999).

[78] E. M. Wright, T. Wong, M. J. Collett, S. M. Tan, and D. F. Walls. *Collapses and revivals in the interference between two Bose-Einstein condensates formed in small atomic samples*. Phys. Rev. A 56, 591 (1997).

[79] A. Smerzi, S. Fantoni, S. Giovanazzi, and S. R. Shenoy. *Quantum coherent atomic tunneling between two trapped Bose-Einstein condensates*. Phys. Rev. Lett. 79, 4950 (1997).

[80] S. Raghavan, A. Smerzi, S. Fantoni, and S. R. Shenoy. *Coherent oscillations between two weakly coupled Bose-Einstein condensates: Josephson effects, π oscillations, and macroscopic quantum self-trapping*. Phys. Rev. A 59, 620 (1999).

[81] J. A. Dunningham and K. Burnett. *Phase standard for Bose-Einstein condensates*. Phys. Rev. Lett. 82, 3729 (1999).

[82] G. J. Milburn, J. Corney, E. M. Wright, and D. F. Walls. *Quantum dynamics of an atomic Bose-Einstein condensate in a double-well potential*. Phys. Rev. A 55, 4318 (1997).

[83] J. F. Corney and G. J. Milburn. *Homodyne measurements on a Bose-Einstein condensate*. Phys. Rev. A 58, 2399 (1998).

[84] M. W. Jack, M. J. Collett, and D. F. Walls. *Coherent quantum tunneling between two Bose-Einstein condensates*. Phys. Rev. A 54, R4625 (1996).

[85] P. Bouyer and M. A. Kasevich. *Heisenberg-limited spectroscopy with degenerate Bose-Einstein gases*. Phys. Rev. A 56, R1083 (1997).

[86] M. J. Holland and K. Burnett. *Interferometric detection of optical phase shifts at the Heisenberg limit*. Phys. Rev. Lett. 71, 1355 (1993).

[87] T. Kim, O. Pfister, M. J. Holland, J. Noh, and J. L. Hall. *Influence of decorrelation on Heisenberg-limited interferometry with quantum correlated photons*. Phys. Rev. A 57, 4004 (1998).

[88] T. Kim, O. Pfister, M. J. Holland, J. Noh, and J. L. Hall. *Influence of decorrelation on Heisenberg-limited interferometry with quantum correlated photons*. Phys. Rev. A 58, 2617 (1998).

[89] T. Kim, Y. Ha, J. Shin, H. Kim, *et al.*. *Effect of the detector efficiency on the phase sensitivity in a Mach-Zehnder interferometer*. Phys. Rev. A 60, 708 (1999).

[90] M. G. A. Paris. *Entanglement and visibility at the output of a Mach-Zender interferometer*. Phys. Rev. A 59, 1615 (1999).

[91] D. J. Wineland, J. J. Bollinger, W. M. Itano, F. L. Moore, and D. J. Heinzen. *Spin squeezing and reduced quantum noise in spectroscopy*. Phys. Rev. A 46, R6797 (1992).

[92] E. V. Goldstein and P. Meystre. *Phase conjugation of multicomponent Bose-Einstein condensates*. Phys. Rev. A 59, 1509 (1999).

[93] L. Deng, E. W. Hagley, J. Wen, M. Trippenbach, *et al.*. *Four-wave mixing with matter waves*. Nature 398, 218 (1999).

[94] J. A. Dunningham and K. Burnett. *Phase resolution for Bose-Einstein condensates*. Phys. Rev. A 61, 065601 (2000).

[95] J. I. Cirac, M. Lewenstein, K. Mølmer, and P. Zoller. *Quantum superposition states of Bose-Einstein condensates*. Phys. Rev. A 57, 1208 (1998).

[96] D. Gordon and C. M. Savage. *Creating macroscopic quantum superpositions with Bose-Einstein condensates*. Phys. Rev. A 59, 4623 (1999).

[97] S. L. Cornish, N. R. Claussen, J. L. Roberts, E. A. Cornell, and C. E. Wieman. *Stable Rb-85 Bose-Einstein condensates with widely tunable interactions*. Phys. Rev. Lett. 85, 1795 (2000).

[98] E. Schrödinger. Naturwissenschaften 23, 807 (1935).

[99] W. H. Zurek. *Decoherence and the transition from quantum to classical*. Phys. Today 44, 36 (1991).

[100] C. Monroe, D. M. Meekhof, B. E. King, and D. J. Wineland. *A 'Schrödinger cat' superposition state of an atom*. Science 272, 1131 (1996).

[101] C. A. Sackett, D. Kielpinski, B. E. King, C. Langer, *et al.*. *Experimental entanglement of four particles*. Nature 404, 256 (2000).

[102] J. R. Friedman, V. Patel, W. Chen, S. K. Tolpygo, and J. E. Lukens. *Quantum superposition of distinct macroscopic states*. Nature 406, 43 (2000).

[103] J. Ruostekoski, M. J. Collett, R. Graham, and D. F. Walls. *Macroscopic superpositions of Bose-Einstein condensates*. Phys. Rev. A 57, 511 (1998).

[104] J. J. Bollinger, W. M. Ito, D. J. Wineland, and D. J. Heinzen. *Optimal frequency measurements with maximally correlated states*. Phys. Rev. A 54, R4649 (1996).

[105] S. F. Huelga, C. Macchiavello, T. Pellizzari, A. K. Ekert, *et al.*. *Improvement of frequency standards with quantum entanglement*. Phys. Rev. Lett. 79, 3865 (1997).

[106] *Special issue on quantum information*. Phys. World 11 (1998).

[107] D. Bouwmeester, A. Ekert, and A. Zeilinger(Eds.). The Physics of Quantum Information (Springer, 2000).

[108] B. Yurke and D. Stoler. *Generating quantum mechanical superpositions of macroscopically distinguishable states via amplitude dispersion*. Phys. Rev. Lett. 57, 13 (1986).

[109] K. Mølmer and A. Sørenson. *Multiparticle entanglement of hot trapped ions*. Phys. Rev. Lett. 82, 1835 (1999).

[110] V. Vedral, M. B. Plenio, M. A. Rippin, and P. L. Knight. *Quantifying entanglement*. Phys. Rev. Lett. 78, 2275 (1997).

[111] V. Vedral and M. B. Plenio. *Entanglement measures and purification procedures*. Phys. Rev. A 57, 1619 (1998).

[112] C. W. Gardiner. Quantum Noise (Springer-Verlag, 1991).

[113] E. Kreyszig. Advanced Engineering Mathematics (John Wiley & Sons, 1993).

[114] A. K. Ekert. *Quantum cryptography based on Bell's theorem*. Phys. Rev. Lett. 67, 661 (1991).

[115] C. H. Bennett and S. J. Wiesner. *Communication via one- and two-particle operators on Einstein-Podolsky-Rosen states*. Phys. Rev. Lett. 69, 2881 (1992).

[116] C. H. Bennett, G. Brassard, C. Crépeau, R. Jozsa, *et al.*. *Teleporting an unknown quantum state via dual classical and Einstein-Podolsky-Rosen channels*. Phys. Rev. Lett. 70, 1895 (1993).

[117] C. H. Bennett, H. J. Wiesner, S. Popescu, and B. Schumacher. *Concentrating partial entanglement by local operations*. Phys. Rev. A 53, 2046 (1996).

[118] L. Henderson, L. Hardy, and V. Vedral. *Two-state teleportation*. Phys. Rev. A 61, 062306 (2000).

[119] M. Zukowski, A. Zeilinger, M. A. Horne, and A. K. Ekert. *'Event-ready detectors' Bell experiment via entanglement swapping*. Phys. Rev. Lett. 71, 4287 (1993).

[120] D. Bouwmeester, J.-W. Pan, K. Mattle, M. Eibl, *et al.*. *Experimental quantum teleportation*. Nature 390, 575 (1997).

[121] D. Boschi, S. Branca, F. D. Martini, L. Hardy, and S. Popescu. *Experimental realization of teleporting an unknown pure quantum state via dual classical and Einstein-Podolsky-Rosen channels*. Phys. Rev. Lett. 80, 1121 (1998).

[122] A. Furusawa, J. L. Sørenson, S. L. Braunstein, C. A. Fuchs, *et al.*. *Unconditional quantum teleportation*. Science 282, 706 (1998).

[123] J.-W. Pan, D. Bouwmeester, H. Weinfurter, and A. Zeilinger. *Experimental entanglement swapping: Entangling photons that never interacted*. Phys. Rev. Lett. 80, 3891 (1998).

[124] F. Dalfovo, S. Giorgini, L. P. Pitaevskii, and S. Stringari. *Theory of Bose-Einstein condensation in trapped gases.* Rev. Mod. Phys. 71, 463 (1999).

[125] H. Pu and P. Meystre. *Creating macroscopic atomic EPR states from Bose condensates.* quant-ph/0007012 .

[126] L. M. Duan, A. Sørenson, J. I. Cirac, and P. Zoller. *Squeezing and entanglement of atomic beams.* quant-ph/0007048 .

[127] A. Sørenson, L.-M. Duan, I. Cirac, and P. Zoller. *Many-particle entanglement with Bose-Einstein condensates.* quant-ph/0006111 .

[128] S. Bose, V. Vedral, and P. L. Knight. *Purification via entanglement swapping and conserved entanglement.* Phys. Rev. A 60, 194 (1999).

[129] S. Bose, P. L. Knight, M. B. Plenio, and V. Vedral. *Proposal for teleporting of an atomic state via cavity decay.* Phys. Rev. Lett. 83, 5158 (1999).

[130] M. Kitagawa and M. Ueda. *Squeezed spin states.* Phys. Rev. A 47, 5138 (1993).

[131] D. J. Wineland, J. J. Bollinger, W. M. Itano, and D. J. Heinzen. *Squeezed atomic states and projection noise in spectroscopy.* Phys. Rev. A 50, 67 (1994).

[132] J. F. Corney, G. J. Milburn, and W. Zhang. *Weak-force detection using a double Bose-Einstein condensate.* Phys. Rev. A 59, 4630 (1999).

[133] L. Amico and V. Penna. *Dynamical mean field theory of the Bose-Hubbard model.* Phys. Rev. Lett. 80, 2189 (1998).

[134] D. Jaksch, C. Bruder, J. I. Cirac, C. W. Gardiner, and P. Zoller. *Cold bosonic atoms in optical lattices.* Phys. Rev. Lett. 81, 3108 (1998).